University of Cincinnati

Date: 11/7/2017

I, Yeon Jee Suh, hereby submit this original work as part of the requirements for the degree of Doctor of Philosophy in Geology.

It is entitled:

Leaf wax stable isotopes as paleovegetation and paleohydrologic proxies: From a modern calibration study to a paleoclimate application

Student's name: **Yeon Jee Suh**

This work and its defense approved by:

Committee chair: Aaron Diefendorf, Ph.D.

Committee member: Brooke Crowley, Ph.D.

Committee member: Heather Graham, Ph.D.

Committee member: Thomas Lowell, Ph.D.

Committee member: Yurena Yanes, Ph.D.

27994

Leaf wax stable isotopes as paleovegetation and paleohydrologic proxies: From a modern calibration study to a paleoclimate application

A dissertation submitted to the
Graduate School
of the University of Cincinnati
in partial fulfillment of the
requirements for the degree of

DOCTOR OF PHILOSOPHY

in the Department of Geology
of the College of Arts and Sciences

by

Yeon Jee Suh
M.S., Hanyang University, 2011
B.S., De La Salle University, 2007

Dissertation Committee

Dr. Aaron F. Diefendorf, Chair
Dr. Brooke E. Crowley
Dr. Heather Graham
Dr. Thomas V. Lowell
Dr. Yurena Yanes

Abstract

Long-chain leaf wax carbon ($\delta^{13}C_{wax}$) and hydrogen (δD_{wax}) isotopic compositions in geologic archives are important tools for assessing Earth's climate perturbations through time as they record vegetation and hydrologic conditions during plant growth, respectively. Interpreting sedimentary leaf wax isotopes requires modern calibration studies to identify and constrain vegetation and climate controls on leaf waxes and their carbon and hydrogen isotopes. Calibrations have been carried out for numerous sites worldwide to characterize the biological and environmental controls on leaf wax isotopes. However, uncertainties still exist including *i*) seasonal and canopy controls on $\delta^{13}C_{wax}$ values, and *ii*) integration and transport of leaf waxes from catchment to sediment sink. This lack of information confounds interpretations of leaf wax isotopes in geologic archives.

In this dissertation, I present three related research projects that address uncertainties in forest-level $\delta^{13}C_{wax}$ variations to basin-level leaf wax integration to paleoclimate applications. In the first study (Chapter 2), I identified and quantified temporal and canopy variation in *n*-alkane $\delta^{13}C$ values ($\delta^{13}C_{alk}$) from buds to leaves among different tree species in a single temperate deciduous forest. I then constrained how canopy height and openness affect *n*-alkane production and $\delta^{13}C_{alk}$ values. The results from seasonal and canopy variations were then compared to leaf litter $\delta^{13}C_{alk}$ values to verify if canopy leaves dominate the leaf litter as commonly assumed. In the second study (Chapter 3), I constrained controls on integration and transport of leaf waxes from Mississippi River Basin (MRB) catchment to the Gulf of Mexico (GOM) using GIS-enabled mixing model. Spatial distribution of carbon and hydrogen leaf wax isotopes (i.e. isoscapes) were developed in the MRB for the Holocene without human interferences removed. Production and transport parameters such as runoff, net primary productivity (NPP), distance to river mouth, and wax production were weighted to quantify sourcing of leaf waxes, which then were compared to measured values in the Holocene sediments from northeastern GOM (ODP 625B). In the final study (Chapter 4), I utilized the new insights from the modern calibration and isoscape modeling to investigate

water and vegetation changes in the MRB for the last ~150 kyr using the ODP 625B core in the GOM. This time-interval includes Marine Isotope Stage (MIS) 5e, from 130 to 115 kyr, when global average temperatures were 2°C higher than today. I compared vegetation and hydrologic conditions during the MIS 5e to the Holocene, and within MIS 5 (5a-5e). The results were used to infer changes in source and transport of precipitation sources over the MRB in relation to major climatic changes, and how these changes may have controlled terrestrial vegetation composition.

Overall, this dissertation constrains and quantifies $\delta^{13}C_{alk}$ variations within a forest and during transport to marine sediments to bridge the gap between modern and geologic leaf waxes. The results of this dissertation will advance interpretation and application of leaf wax isotope-based proxy and contribute to better understanding of Earth's ecologic and hydrologic responses to global or regional changes in climate conditions.

Acknowledgements

I would like to express my gratitude to the Department of Geology at the University of Cincinnati for giving me the chance to study what and where I wanted to study. While completing my studies, I have grown both academically and personally, met many great people, and visited many amazing places. These experiences and opportunities would not have been possible without the support from the Department of Geology.

I would also like to thank the following funding sources for supporting my research: Ministry of Oceans and Fisheries in South Korea, American Philosophical Society, UC Sigma Xi, Geological Society of America, University of Utah ITCE, and American Chemical Society Petroleum Research. I also thank the East Fork Wildlife Area for forest access and IODP for providing core sediment samples.

My biggest thanks go to my advisor, Dr. Aaron Diefendorf. I deeply thank you for your guidance, patience, and encouragements over the years. Thank you for making me a better scientist. I have to tell you that you are my role model and I truly enjoyed being your student! I also thank my committee members, Dr. Brooke Crowley, Dr. Heather Graham, Dr. Thomas Lowell, and Dr. Yurena Yanes for very helpful and thorough review and comments on my work and my dissertation, for making me think critically and about the big picture, and for the science and non-science conversations with me. I also thank Dr. Gabriel Bowen at the University of Utah for teaching me about spatial isotope analysis. This significantly improved the interpretation of my dissertation research. I am also grateful to Dr. Sangmin Hyun from Korea Institute of Ocean Science and Technology for continued support and interest in my research.

I would like to sincerely thank Erika Freimuth for countlessly revising my writing, and above that, for being such an awesome friend. I am also incredibly grateful to my office family, Janine Sparks, Elizabeth

Bullard, Elizabeth Haussner, Allison Young, and Julia Wise for your kindness, humor, and thoughtfulness. Your love for Asian cuisine, video games, and K-pop made me feel at home. My graduate school and life here in the U.S. have been so much more fun with you guys. I also thank Lindsay Sommer and Doug Sberna for helping me in the field and lab.

I also thank my South Korean friends for cheering me up and being there whenever. I thank my family who has been supportive through the good times and bad. I thank my dad for influencing me to study earth science, my mom for feeding me with love and laughter, my sister for being my second mom, and my brother for praying for me.

Thank you.

Table of Contents

Chapter 1: Introduction

Constraining carbon and water cycling associated with global climate change in the past is key to understanding the future. Long-chain leaf waxes and their carbon ($\delta^{13}C_{wax}$) and hydrogen (δD_{wax}) isotopic compositions in geologic archives provide valuable records of the Earth's past ecology and hydrology, respectively. This is because leaf waxes are produced by most terrestrial higher plants and are well preserved in the rock record providing evidence of biological and environmental conditions of past plants. However, accurate and quantitative interpretation of sedimentary leaf waxes for paleo-applications is limited by i) uncertainties associated with seasonal and canopy height variations in $\delta^{13}C_{wax}$ values within a forest and ii) integration and transport of leaf waxes from fluvial systems to marine sediments. This dissertation aims to address these questions, and apply leaf wax isotopes to resolve paleovegetation and paleohydrologic questions in the midcontinent North America (NA) since the Last Interglacial using marine sediments in the Gulf of Mexico.

Chapter 2 focus on long-chain *n*-alkanes, one of the constituents of leaf waxes, as they are most commonly used as climatic and ecological proxies for the recent and the geologic past (Freeman and Colarusso, 2001; Tipple and Pagani, 2010; Diefendorf et al., 2011; Feakins et al., 2013; Magill et al., 2013). *n*-Alkane $\delta^{13}C$ ($\delta^{13}C_{alk}$) values reflect carbon isotope fractionation in plants during photosynthesis ($\varepsilon_{leaf\text{-}CO2}$ or Δ_{leaf}) and lipid biosynthesis ($\varepsilon_{alk\text{-}leaf}$). Our understanding of the controls on $\varepsilon_{leaf\text{-}CO2}$ are well constrained and vary between photosynthetic pathways, with water availability, species, light intensity and taxonomic group (O'Leary, 1981; Farquhar et al., 1989; O'Leary et al., 1992; Diefendorf et al., 2010; Kohn, 2010; Graham et al., 2014). However, much less is known about $\varepsilon_{alk\text{-}leaf}$, especially how $\varepsilon_{alk\text{-}leaf}$ values vary within a season or within a forest canopy (Lockheart et al., 1997; Li et al., 2016). Also, canopy effects are found to influence leaf biomass $\delta^{13}C$ values within a forest due to light intensity, humidity and soil respired CO_2 (Vogel, 1978; Medina and Minchin, 1980; van der Merwe and Medina, 1991; Hanba et al., 1997; El-Sharkawy and De Tafur, 2007; Graham et al., 2014). However, canopy

effects on *n*-alkane concentration and $\varepsilon_{alk\text{-}leaf}$ values in temperate forest trees is unknown. Therefore, I investigated variation in $\varepsilon_{alk\text{-}leaf}$ values in a temperate forest, both temporally through the growing season and spatially throughout the canopy, to reduce the uncertainty in using $\delta^{13}C_{alk}$ values for reconstructing past changes in vegetation and the carbon cycle. I then compared these temporal and canopy studies to leaf litter samples collected at the end of the growing season to evaluate whether litter reflects mature canopy leaves, as often assumed (e.g. Graham et al., 2014; Diefendorf and Freimuth, 2017).

Despite increasing use of leaf wax isotopic compositions for paleoenvironment reconstructions, knowledge on the processes from production to transportation and burial in the sediments (i.e. taphonomy), that ultimately determine their isotopic composition in sedimentary archives is limited (Galy et al., 2011; Hoffmann et al., 2016; Diefendorf and Freimuth, 2017). In Chapter 3, I investigated the provenance and integration of plant waxes from the largest fluvial system in the United States, the Mississippi River basin (MRB), to the Gulf of Mexico (GOM). I constructed geographic distribution of leaf wax carbon and hydrogen isotopes (i.e. isoscape) using plant isotopic fractionation calibrations (Liu et al., 2006; Smith and Freeman, 2006; Hou et al., 2007a; Diefendorf and Freimuth, 2017). I used different approaches to estimate isotopic fractionations to build leaf wax carbon and hydrogen isoscapes, and discussed advantages and disadvantages of using each approach. I tested changes in leaf wax source and integration by climatic, production (i.e. biomass and wax production), and distance effects in the MRB catchment to the GOM sediments using GIS-based spatial analysis. I compared the modeled values to measured values in ODP 625B core sediments from the northeastern GOM. This chapter constrained where leaf waxes in the GOM are delivered from and what part of vegetation and hydrologic signals are recorded in these biomarkers, which are critical in refining the paleoclimate interpretations both in the GOM (Chapter 4) and other marine sediment sites that integrate plant waxes.

In Chapter 4, this dissertation provides paleovegetation and paleohydrologic records in MRB since the last 150 kyr to the present, including the Last Interglacial or Marine Isotope Stage (MIS) 5e between 130

to 115 kyr, when global average temperature was ac. 2°C warmer than today. There is limited information as to the source, extent and timing of moisture transport and their roles on terrestrial vegetation composition during the MIS 5e in comparison to the Holocene. Prior study results on hydrologic conditions during the MIS 5e are inconsistent within the MRB or have large uncertainties in age of the sediments (Curry and Baker, 2000; Fredlund and Jaumann, 1987; Grüger, 1972; Hall, 1981; Kapp, 1965; Kapp and Gooding, 1964; Ruhe et al., 1974; Swinehart, 1999). To provide more accurate paleo-records of changes in source moisture and vegetation, I analyzed plant waxes and their δD_{wax} and $\delta^{13}C_{wax}$ values preserved in ODP 625B marine sediment core. As I partly understand leaf wax integration processes from the MRB to the GOM based on Chapter 3, I illustrate how to minimize runoff and production biases to gain information about a poorly constrained area for important recent changes in paleovegetation and paleohydrology.

References

Curry, B.B., Baker, R.G., 2000. Palaeohydrology, vegetation, and climate since the late Illinois Episode (~ 130 ka) in south-central Illinois. Palaeogeography, Palaeoclimatology, Palaeoecology 155, 59-81.

Diefendorf, A.F., Freeman, K.H., Wing, S.L., Graham, H.V., 2011. Production of *n*-alkyl lipids in living plants and implications for the geologic past. Geochimica et Cosmochimica Acta 75, 7472-7485.

Diefendorf, A.F., Freimuth, E.J., 2017. Extracting the most from terrestrial plant-derived *n*-alkyl lipids and their carbon isotopes from the sedimentary record: A review. Organic Geochemistry 103, 1-21.

Diefendorf, A.F., Mueller, K.E., Wing, S.L., Koch, P.L., Freeman, K.H., 2010. Global patterns in leaf ^{13}C discrimination and implications for studies of past and future climate. Proceedings of the National Academy of Sciences 107, 5738-5743.

El-Sharkawy, M.A., De Tafur, S.M., 2007. Genotypic and within canopy variation in leaf carbon isotope discrimination and its relation to short-term leaf gas exchange characteristics in cassava grown under rain-fed conditions in the tropics. Photosynthetica 45, 515-526.

Farquhar, G.D., Ehleringer, J.R., Hubick, K.T., 1989. Carbon isotope discrimination and photosynthesis. Annual review of plant biology 40, 503-537.

Feakins, S.J., Levin, N.E., Liddy, H.M., Sieracki, A., Eglinton, T.I., Bonnefille, R., 2013. Northeast African vegetation change over 12 my. Geology 41, 295-298.

Fredlund, G.G., Jaumann, P.J., 1987. Late Quaternary palynological and paleobotanical records from the central Great Plains. Quaternary Environments of Kansas, 167-178.

Freeman, K.H., Colarusso, L.A., 2001. Molecular and isotopic records of C_4 grassland expansion in the late miocene. Geochimica et Cosmochimica Acta 65, 1439-1454.

Galy, V., Eglinton, T., France-Lanord, C., Sylva, S., 2011. The provenance of vegetation and environmental signatures encoded in vascular plant biomarkers carried by the Ganges–Brahmaputra rivers. Earth and Planetary Science Letters 304, 1-12.

Graham, H.V., Patzkowsky, M.E., Wing, S.L., Parker, G.G., Fogel, M.L., Freeman, K.H., 2014. Isotopic characteristics of canopies in simulated leaf assemblages. Geochimica et Cosmochimica Acta 144, 82-

95.

Grüger, E., 1972. Late Quaternary vegetation development in south-central Illinois. Quaternary Research 2, 217IN213-231IN214.

Hall, S.A., 1981. Deteriorated pollen grains and the interpretation of Quaternary pollen diagrams. Review of Palaeobotany and Palynology 32, 193-206.

Hanba, Y.T., Mori, S., Lei, T.T., Koike, T., Wada, E., 1997. Variations in leaf $\delta^{13}C$ along a vertical profile of irradiance in a temperate Japanese forest. Oecologia 110, 253-261.

Hoffmann, B., Feakins, S.J., Bookhagen, B., Olen, S.M., Adhikari, D.P., Mainali, J., Sachse, D., 2016. Climatic and geomorphic drivers of plant organic matter transport in the Arun River, E Nepal. Earth and Planetary Science Letters 452, 104-114.

Hou, J., D'Andrea, W.J., MacDonald, D., Huang, Y., 2007. Evidence for water use efficiency as an important factor in determining the δD values of tree leaf waxes. Organic Geochemistry 38, 1251-1255.

Kapp, R.O., 1965. Illinoian and Sangamon vegetation in southwestern Kansas and adjacent Oklahoma.

Kapp, R.O., Gooding, A.M., 1964. Pleistocene Vegetational Studies in the Whitewater Basin, Southeastern Indiana. The Journal of Geology 72, 307-326.

Kohn, M.J., 2010. Carbon isotope compositions of terrestrial C_3 plants as indicators of (paleo) ecology and (paleo) climate. Proceedings of the National Academy of Sciences 107, 19691-19695.

Li, R., Meyers, P.A., Fan, J., Xue, J., 2016. Monthly changes in chain length distributions and stable carbon isotope composition of leaf n-alkanes during growth of the bamboo Dendrocalamus ronganensis and the grass Setaria viridis. Organic Geochemistry 101, 72-81.

Liu, W., Yang, H., Li, L., 2006. Hydrogen isotopic compositions of *n*-alkanes from terrestrial plants correlate with their ecological life forms. Oecologia 150, 330-338.

Lockheart, M.J., Van Bergen, P.F., Evershed, R.P., 1997. Variations in the stable carbon isotope compositions of individual lipids from the leaves of modern angiosperms: implications for the study of higher land plant-derived sedimentary organic matter. Organic Geochemistry 26, 137-153.

Madigosky, S.R., 2004. CHAPTER 2 - Tropical Microclimatic Considerations A2 - Lowman, Margaret D,

in: Rinker, H.B. (Ed.), Forest Canopies (Second Edition). Academic Press, San Diego, pp. 24-48.

Magill, C.R., Ashley, G.M., Freeman, K.H., 2013. Ecosystem variability and early human habitats in eastern Africa. Proceedings of the National Academy of Sciences of the United States of America 110, 1167-1174.

Medina, E., Minchin, P., 1980. Stratification of $\delta^{13}C$ values of leaves in Amazonian rain forests. Oecologia 45, 377-378.

O'Leary, M.H., 1981. Carbon isotope fractionation in plants. Phytochemistry 20, 553-567.

O'Leary, M.H., Madhavan, S., Paneth, P., 1992. Physical and chemical basis of carbon isotope fractionation in plants. Plant, Cell & Environment 15, 1099-1104.

Ometto, J.P.H.B., Ehleringer, J.R., Domingues, T.F., Berry, J.A., Ishida, F., Y., Mazzi, E., Higuchi, N., Flanagan, L.B., Nardoto, G.B., Martinelli, L.A., 2006. The stable carbon and nitrogen isotopic composition of vegetation in tropical forests of the Amazon Basin, Brazil. Biogeochemistry 79, 251-274.

Ruhe, R.V., Hall, R.D., Canepa, A.P., 1974. Sangamon paleosols of southwestern Indiana, U.S.A. Geoderma 12, 191-200.

Smith, F.A., Freeman, K.H., 2006. Influence of physiology and climate on δD of leaf wax *n*-alkanes from C_3 and C_4 grasses. Geochimica et Cosmochimica Acta 70, 1172-1187.

Swinehart, J.B., 1999. 200,000 years of climate change recorded in eolian sediments of the High Plains of eastern Colorado and western Nebraska. Colorado and Adjacent Areas 1, 71.

Tipple, B.J., Pagani, M., 2010. A 35Myr North American leaf-wax compound-specific carbon and hydrogen isotope record: Implications for C_4 grasslands and hydrologic cycle dynamics. Earth and Planetary Science Letters 299, 250-262.

van der Merwe, N.J., Medina, E., 1991. The canopy effect, carbon isotope ratios and foodwebs in amazonia. Journal of Archaeological Science 18, 249-259.

Vogel, J., 1978. Recycling of carbon in a forest environment. Oecologia Plantarum 13, 89-94.

Chapter 2: Seasonal and canopy height variation in *n*-alkanes and their carbon isotopes in a temperate forest[1]

ABSTRACT

The stable carbon isotopic composition ($\delta^{13}C$) of terrestrial leaf wax components, such as *n*-alkanes ($\delta^{13}C_{alk}$), are used extensively to address questions about past changes in vegetation, climate and the carbon cycle. To interpret sedimentary $\delta^{13}C_{alk}$ values, characterization of the environmental and biological controls on carbon isotopic fractionation during plant metabolism is required, especially for fractionation that occurs during photosynthesis ($\varepsilon_{leaf\text{-}CO2}$ or Δ_{leaf}) and *n*-alkane biosynthesis ($\varepsilon_{alk\text{-}leaf}$). Although much is understood about controls on $\varepsilon_{leaf\text{-}CO2}$, little is known about seasonal or within canopy variation in *n*-alkane composition and $\varepsilon_{alk\text{-}leaf}$. To address the gap, we sampled five common tree species (four angiosperims: *Acer rubrum, Acer saccharum, Sassafras albidum* and *Ulmus americana*; and one gymnosperm: *Juniperus virginiana*) from buds to senescing leaves within a single temperate forest in southwestern Ohio, USA. We measured *n*-alkane concentration, $\delta^{13}C_{alk}$, leaf biomass $\delta^{13}C$ ($\delta^{13}C_{leaf}$), $\delta^{13}C$ of atmospheric CO_2 within the canopy, luminous flux and specific leaf area (SLA). In angiosperms, $\delta^{13}C_{alk}$ values were low in the buds, increased substantially (4 to 6‰) to the highest values in young leaves and then decreased (1 to 3‰) in mature leaves. Seasonal variation in $\delta^{13}C_{alk}$ values generally tracked changes in $\delta^{13}C_{leaf}$, but the fractionation between leaf and *n*-alkane ($\varepsilon_{alk\text{-}leaf}$) was variable, having lower values in buds (−6.7 ± 1.1‰) than in young leaves (−4.9 ± 2.3‰). Later in the growing season, $\varepsilon_{alk\text{-}leaf}$ values stabilized and ranged between −2.5 and −6.5‰, with a mean of −4.3 ± 1.4‰ in angiosperms. Stabilization of $\delta^{13}C_{alk}$ values coincided with settling of SLA and increase on average chain length (ACL). Temporal variation in $\delta^{13}C_{alk}$ values for J. virginiana was ca. 2‰ smaller than angiosperms, and $\varepsilon_{alk\text{-}leaf}$ values slightly increased when *n*-alkane production increased. Its average $\varepsilon_{alk\text{-}leaf}$ value at the end of the

[1] Suh Y.J., Diefendorf A.F., 2017. Seasonal and canopy height variation in *n*-alkanes and their carbon isotopes in a temperate forest. *Accepted*, Organic Geochemistry

growing season was −5.0 ± 0.7‰. We speculate that $\varepsilon_{alk\text{-}leaf}$ variation in both angiosperms and the conifer reflects changes in the source of carbon for plant metabolism as well as the timing of wax synthesis. We also tested canopy effects on *n*-alkane concentration and carbon isotopic fractionation at different heights and extents of canopy closure. *n*-Alkane concentrations were higher at the top of the canopy by 2 to 8 times than in the lower canopy. $\varepsilon_{leaf\text{-}CO2}$ values were more negative in the lower two thirds of the canopy than the upper one third of the canopy by 2 to 4‰ in two species with higher canopy closure. $\varepsilon_{alk\text{-}leaf}$ values did not vary with height and extent of canopy closure. To further explore the link between canopy leaves and leaf litter, we compared $\delta^{13}C_{alk}$ values of mature canopy leaves to those in leaf litter collected during senescence. Values differed by ca. 1‰. The results confirm previous indications that leaf litter $\delta^{13}C_{alk}$ values primarily reflect those of the upper canopy leaves due to not only higher leaf biomass in the upper canopy but also to high *n*-alkane production.

1. Introduction

n-Alkyl lipids, the cuticular wax component of terrestrial plant leaves, include long-chain *n*-alkanes, *n*-alkanoic acids, *n*-alcohols and *n*-esters (e.g. Eglinton et al., 1962; Eglinton and Hamilton, 1967; Jetter et al., 2000). Of these, the *n*-alkanes, and their carbon isotopic composition ($\delta^{13}C_{alk}$), are most commonly used as climatic and ecological proxies for the recent and the geologic past (Diefendorf et al., 2011; Feakins et al., 2013; Freeman and Colarusso, 2001; Magill et al., 2013a; Tipple and Pagani, 2010). $\delta^{13}C_{alk}$ values reflect carbon isotope fractionation in plants during photosynthesis ($\varepsilon_{leaf\text{-}CO2}$ or Δ_{leaf}) and lipid biosynthesis ($\varepsilon_{alk\text{-}leaf}$); therefore, interpreting sedimentary $\delta^{13}C_{alk}$ values requires robust understanding of the factors that control these fractionations. Our understanding of the controls on $\varepsilon_{leaf\text{-}CO2}$ are well constrained and vary between photosynthetic pathways, with water availability, species, light intensity and taxonomic group (Diefendorf et al., 2010; Farquhar et al., 1989; Graham et al., 2014; Kohn, 2010; O'Leary, 1981; O'Leary et al., 1992). $\varepsilon_{leaf\text{-}CO2}$ is calculated using $\delta^{13}C_{leaf}$ values relative to atmospheric CO_2 $\delta^{13}C$ ($\delta^{13}C_{CO2}$ = −8.4‰ in 2014; White et al., 2011) as follows:

$$\varepsilon_{\mathrm{leaf-CO2}} = \Delta_{leaf} = \left(\frac{\delta^{13}\mathrm{C}_{leaf}+1000}{\delta^{13}\mathrm{C}_{atm}+1000} - 1\right) \quad (1)$$

Unlike $\varepsilon_{leaf\text{-}CO2}$ values, much less is known about $\varepsilon_{alk\text{-}leaf}$, which is calculated using the following equation for the lipid of interest (e.g., *n*-alkanes) relative to $\delta^{13}C_{leaf}$ values:

$$\varepsilon_{\mathrm{alk-leaf}} = \left(\frac{\delta^{13}\mathrm{C}_{\mathrm{alk}}+1000}{\delta^{13}\mathrm{C}_{\mathrm{leaf}}+1000} - 1\right) \quad (2)$$

Photosynthetic pathway, elevation, environment and species may be important factors controlling $\varepsilon_{alk\text{-}leaf}$ values (Diefendorf and Freimuth, 2017). For example, the magnitude of $\varepsilon_{alk\text{-}leaf}$ varies between photosynthetic pathways: C_3 graminoids = −6.0 ± 2.0‰, *n* = 7; C_4 graminoids = −9.3 ± 2.1‰, *n* = 24. The

$\varepsilon_{alk\text{-}leaf}$ value also varies with altitude, with lower $\varepsilon_{alk\text{-}leaf}$ in a higher elevation cloud forest than a lowland rainforest (slope = 0.6 ± 0.3‰ km-1, $r^2 = 0.76$, $p < 0.01$, $n = 399$). The range of $\varepsilon_{alk\text{-}leaf}$ values can also be large within a single climate regime. For example, a range of ca. −6 to −13‰ was observed in tropical forests (n = 25 to 58 per site; Wu et al., 2017), and ca. −10‰ in the temperate ecosystem ($n = 32$; Diefendorf et al., 2011). However, we know very little about how $\varepsilon_{alk\text{-}leaf}$ values vary within a season or within a forest canopy (Li et al., 2016; Lockheart et al., 1997).

Limited prior studies reported different magnitudes and controls of seasonal variation in $\delta^{13}C_{alk}$ values between sites and species. For example, Eley et al. (2016) found 8 to 10‰ inter- and intra-species variation in $\delta^{13}C_{alk}$ values of C_3 plants across the growing season in a temperate saltmarsh, while a ca. 2‰ range was observed in C_4 monocots. They found a general increase in $\delta^{13}C_{alk}$ values in summer and attributed this to environmental stressors such as water availability and salinity. Lockheart et al. (1997), on the other hand, found a decrease in $\delta^{13}C$ at the end of the growing season and suggested this was caused by either changes in temperature or a replacement of ablated wax with ^{13}C-depleted carbon. Another study by Li et al. (2016) suggested that seasonal changes in $\delta^{13}C_{alk}$ values of C_3 bamboo and C_4 grass reflect monthly mean temperature and precipitation amount. These various patterns and magnitudes of $\delta^{13}C_{alk}$ complicate the assignment of $\varepsilon_{alk\text{-}leaf}$ values for sedimentary $\delta^{13}C_{alk}$ reconstructions. Further, the focus of these previous studies has been on $\delta^{13}C_{alk}$ values, but additional information is needed to evaluate if these patterns are controlled by changes in $\varepsilon_{leaf\text{-}CO2}$ and/or $\varepsilon_{alk\text{-}leaf}$, and how these are reflected in leaf litter.

Canopy effects also influence $\delta^{13}C_{leaf}$ values within a forest (El-Sharkawy and De Tafur, 2007; Graham et al., 2014; Hanba et al., 1997; Medina and Minchin, 1980; van der Merwe and Medina, 1991; Vogel, 1978). Canopy effects occur in forests with dense canopy cover and have been linked to gradients in light intensity, humidity and soil respired CO_2. Collectively, these variables result in lower canopy leaves having more negative $\delta^{13}C$ values than upper canopy leaves (Madigosky, 2004; Medina and Minchin,

1980; Ometto et al., 2006; Vogel, 1978). Graham et al. (2014) demonstrated that canopy effects are due mainly to changes in light intensity and to a minor extent relative humidity in tropical rainforests. In this study, we examined canopy effects on *n*-alkane concentration and $\varepsilon_{alk\text{-}leaf}$ values in temperate forest trees with different extents of canopy closure, and compared the results with forest floor leaf litter.

Our goal is to understand variation in $\varepsilon_{alk\text{-}leaf}$ values in a temperate forest, both temporally through the growing season and spatially throughout the canopy, so that we can reduce uncertainty in using $\delta^{13}C_{alk}$ values for reconstructing past changes in vegetation and the carbon cycle. The specific questions addressed here are:

- What is the magnitude and timing of $\varepsilon_{alk\text{-}leaf}$ variations over the growing season in temperate forest trees?
- How do *n*-alkane concentrations and $\delta^{13}C_{alk}$ values vary with canopy height and extent of canopy closure?
- Is isotopic variability from season and canopy height reflected in leaf litter?

To answer these questions, we foliage from deciduous angiosperms and an evergreen conifer over the growing season from buds to senescing leaves. We also determined *n*-alkane composition and $\delta^{13}C$ values at different tree heights with varying degree of canopy closure. We then analyzed $\varepsilon_{leaf\text{-}CO2}$ and $\varepsilon_{alk\text{-}leaf}$ values for each collection month and compared these results with leaf litter samples collected at the end of the growing season to evaluate if litter reflects mature canopy leaves, as often assumed (e.g. Diefendorf and Freimuth, 2017; Graham et al., 2014).

2. Methods

2.1. Sample location

Fresh buds and leaves from four deciduous angiosperm and one evergreen gymnosperm species were collected from East Fork Wildlife Area [EF; 39.02°N, 84.09°W, 186 m above sea level (masl)] in southwestern Ohio (USA) from March to October 2014. The mean annual temperature is 12.6 ºC and mean annual precipitation is 1073 mm (Midwestern Regional Climate Center, http://mrcc.isws.illinois.edu/). Monthly precipitation is higher from April to July (98.3 to 106.2 mm) compared with the rest of the year (73.2 to 91.7 mm) (Fig. 1). EF is characterized as a temperate forest that consists mainly of deciduous angiosperm trees and understory shrubs and herbs. *Acer saccharum* (sugar maple) is the most common species in EF, comprising ca. 70% of the trees (Kolbe et al., 2016). Four common tree species were sampled, including *Acer rubrum* (red maple), *Acer saccharum* (sugar maple), *Sassafras albidum* (sassafras) and *Ulmus americana* (American elm). The evergreen conifer *Juniperus virginiana* (red cedar) was also sampled, but is rare within the forest.

2.2. Temporal leaf sampling

Angiosperm buds and leaves were sampled weekly during leaf flush and monthly thereafter, while *J. virginiana* was sampled monthly. The same individuals were repeatedly sampled throughout the growing season. On several collection dates, additional individuals were sampled to compare intra-species variability. Buds and leaves were collected from sun exposed canopy branches using an arborist's sling shot. For *S. albidum*, sampling began after leaf flush and buds were therefore not collected. In EF, buds swelled in April. We therefore refer to buds collected before April as winter buds and refer to swelled buds as late buds. Buds that formed in August and September of 2014 were also sampled and are referred to as summer buds. At least 20 leaves were collected from the same branch of each individual for the

angiosperms and, for the conifer, at least 40 needles were collected through the year from cohorts for the current year (CC hereafter) and additional samples were collected at the same time from the 2013 or prior cohorts (PC hereafter).

2.3. Canopy leaf and air sampling

Maximum tree height varied for each species: 20 m for *A. rubrum*, 18 m for *A. saccharum* and 13 m for *U. americana*. To examine canopy effects, leaves of *A. rubrum, A. saccharum* and *U. americana*, the three most dominant species, were sampled on July 26, 2014 from 1 m above the ground to the top of the canopy at ca. 3 m intervals, with a total of five sampling heights for *A. rubrum* and *A. saccharum*, and four for *U. americana*.

Light intensity was measured using a light meter (LM-8000A) under each sampled tree at 1 m above the ground at 11:00 am as an estimate of canopy closure. Light intensity outside of the forest canopy was on average 11,780 lux. *Acer saccharum* had the highest canopy closure (594 lux or 5.0% of total incoming), followed by *A. rubrum* (1,531 lux or 13.0%) and *U. americana* (5,884 lux or 50.0%). Atmospheric air was also collected at leaf sampling heights on May 13th and August 10th, 2014 using an established method (Knohl et al., 2005) at leaf sampled heights with 3.2 mm i.d. phthalate-free flexible tubing (Tygon E-3603) connected to a KNF air pump (UNMP09). Exetainer vials with butyl rubber septa were purged by inserting the tubing into the vial and flushing with sample air for 5 min inside of a small plastic bag with a small opening to prevent contamination. The tubing was then removed and the vials were quickly capped inside of the bag.

To compare leaf wax concentration and $\delta^{13}C$ values between canopy leaves and leaf litter, litter was collected under the three sampled trees on November 8, 2014. Collection was made by sampling at 5 random locations under the tree crown from within a 625 cm^2 square. Litter samples were visually

inspected to remove any leaves from other species and to remove wood and bark. Litter samples were bulked together from the 5 sampling locations to make one bulk sample for analysis. It is important to note here that it was not possible with our sampling design to exclude leaves from nearby individuals of the same species.

2.4. Specific leaf area

Specific leaf area (SLA), the fresh leaf area divided by its dry mass was measured and is expressed in cm^2/g following Cornelissen et al. (2003). It was measured on 5 to 15 upper canopy leaves and needles free of pathogen or herbivore attack. In the field, sampled leaves were stored in sealed plastic bags with a moist paper towel to prevent dehydration. Leaf area was measured on the same day as collection with a digital scanner and Image-J software (http://imagej.nih.gov/ij). The leaves were then frozen, freeze-dried and weighed.

2.5. Lipid extraction and separation

Freeze-dried leaf material was powdered using a mortar and pestle. Lipids were extracted from powdered leaves (ca. 200 mg) with 20 ml dichloromethane (DCM)/MeOH (2:1, v/v) in round bottomed 40 ml glass vials by sonication with two extraction cycles (30 min each). The total lipid extract (TLE) was saponified with 2.5 ml of 0.5 N KOH in MeOH/H_2O (3:1, v/v) for 2 h at 75°C. After cooling, ca. 3 ml of NaCl in water (5%, w/w) was added to the saponified lipid extract (SLE) and ca. 0.5 ml of 6 N HCl added to acidify the solution to a pH of ca. 1. Hexanes/DCM (4:1, v/v) was used to extract the acidic solution and was subsequently neutralized with $NaHCO_3$/H_2O (5%, w/w) and dried over Na_2SO_4. The SLE was separated into four fractions with 0.5 g of aminopropyl-bonded silica gel in a 6 ml glass solid phase extraction column with gravity. The hydrocarbon fraction was eluted with 4 ml hexanes, ketones were eluted with 8 ml hexanes/DCM (6:1, v/v), alcohols with 8 ml DCM/acetone (9:1, v/v) and acids with 8 ml

of DCM/85% HCO_2H (49:1 v/v).

2.6. Identification and quantification

n-Alkanes were identified using gas chromatography-mass spectrometry (GC-MS; Agilent 7890A-Agilent 5975C mass selective detector, MSD) equipped with flame ion detection (FID) and electron-impact ionization (70 eV). A fused silica column (Agilent J&W DB-5 ms; 30 m, 0.25 mm i.d., 25 μm film thickness) and guard column (Restek Rxi, 5 m, 0.32 mm) were used with He as carrier gas. The oven temperature program was: 60°C (1 min) to 320°C (held 15 min) at 6°C/min. The column effluent was split (1:1) between FID and MSD with a 2 way splitter (Agilent G3180B) at a constant pressure. Compounds were identified using authentic standards, retention times and MS spectra.

As an internal standard, 1,1′-binaphthyl was added to *n*-alkane samples at known concentration prior to quantification. The peak areas were normalized to those for 1,1′-binaphthyl and converted to mass quantities using response curves for the external standard compounds, a mixture of C_7 to C_{40} *n*-alkanes (Sigma Aldrich) analyzed in concentrations ranging from 0.1 to 120 μg/ml. Precision and accuracy were determined by analyzing external standards at 25 μg/ml as unknowns and were 0.17 μg/ml (1σ, $n = 40$) and 0.33 μg/ml (1σ, $n = 40$), respectively. *n*-Alkane concentration was normalized to the mass of dry leaf extracted.

The average chain length ($ACL_{25\text{-}35}$) of *n*-alkanes was calculated using the following equation to convert concentration to weighted chain length numbers following the recommendation of Freeman and Pancost (2014):

$$ACL_{25-35} = \frac{\sum_{i=25}^{35} i[Ci]}{\sum_{i=25}^{35} Ci} \quad (3)$$

2.7. n-Alkane carbon isotope ($\delta^{13}C_{alk}$) analysis

Prior to $\delta^{13}C_{alk}$ analysis, the hydrocarbon fraction was further separated into a saturated and unsaturated fraction by eluting with 4 ml hexanes and 4 ml EtOAc, respectively, on 5% Ag^+ impregnated silica gel. The saturated hydrocarbon fraction was analyzed using a Thermo Trace GC Ultra coupled to a Thermo Fisher Delta V Advantage isotope ratio mass spectrometry (IRMS) instrument, via an Isolink combustion furnace. GC conditions were similar to those above, but with a faster ramp rate (8°C/min). The $\delta^{13}C$ values were determined relative to a reference gas calibrated with a suite of *n*-alkanes of known $\delta^{13}C$ composition (Mix A; *n*-C_{16} to *n*-C_{30}; Arndt Schimmelmann, Indiana University). Carbon isotope values of samples are reported in delta notation relative to Vienna Peedee Belemnite (VPDB) as $\delta^{13}C = [(^{13}R_{sample}/^{13}R_{VPDB}) - 1]$ where $^{13}R = {}^{13}C/{}^{12}C$. Within each run, the precision and accuracy were determined with co-injected internal standards (*n*-C_{38} and *n*-C_{41} alkanes) and were ± 0.30‰ (1σ, $n = 138$) and ± 0.17‰ ($n = 138$), respectively.

2.8. Bulk leaf carbon isotope analysis

An aliquot of the powdered leaf sample (not extracted) was analyzed for $\delta^{13}C_{leaf}$ with a Costech elemental analyzer (EA) interfaced with a Thermo Fisher Delta V Advantage IRMS via a Conflo IV interface. Measured $\delta^{13}C$ values were corrected for sample size dependency and normalized to the VPDB scale with a two point calibration with IAEA calibrated (NBS-19, L-SVEC) in-house standards (−38.26‰ and −11.35‰) (Coplen et al., 2006b). Accuracy and precision, determined by analyzing independent standards across all EA runs, were 0.07‰ (1σ, $n = 60$) and 0.17‰ ($n = 60$), respectively.

2.9. Atmospheric CO_2 carbon isotope ($\delta^{13}C_{CO2}$) analysis

Atmospheric air samples collected in exetainer vials were analyzed for $\delta^{13}C_{CO2}$ using a GasBench II coupled to a Thermo Fisher Delta V Advantage IRMS. $\delta^{13}C_{CO2}$ values were normalized to the VPDB scale with CO_2 produced from reacting NBS-19 and NBS-18 with 100% H_3PO_3 at 25 ºC for 24 h. Precision and accuracy, determined with independent calcite standards, were 0.06‰ (1σ, n = 47) and 0.28‰ (n = 47), respectively. All statistical analyses were performed using JMP Pro 12.0 (SAS Institute Inc, Cary, NC, USA).

3. Results

3.1. Specific leaf area

SLA is often used as an indicator of change in leaf growth rate and as an indicator of the investment in leaf defense (Bongers and Popma, 1990; Hunt and Cornelissen, 1997; Lambers and Poorter, 1992). SLA varied through the growing season and by species (Figs. 2b and 4b; Appendix Table A1). *Acer saccharum* had higher average SLA (259 cm^2/g) than other angiosperm species (*A. rubrum* = 142 cm^2/g; *S. albidum* = 184 cm^2/g; *U. americana* = 172 cm^2/g). In general, SLA increased rapidly after bud burst by ca. 100 to 200 cm^2/g, and reached a maximum value within 2 to 4 weeks. This rapid increase indicates high growth rate in young leaves. Then the values decreased in late May to early June (i.e. 5 to 6 weeks after bud burst) and began to stabilize. Leaf area also increased rapidly by ca. 30 cm^2 after leaf flush over 2 to 5 weeks, and stabilized thereafter (Figs. 2c and 4a). However, in *A. saccharum*, the average leaf area for mature leaves varied considerably (30 to 100 cm^2). In angiosperms, we used the starting point of SLA stabilization in late May to early June as the transition from young leaves to fully matured leaves. Therefore, leaves collected prior to the first week of June are referred to as young leaves and thereafter as

mature leaves. For the conifer, SLA ranged from 28 to 37 cm^2/g, with a mean of 34 ± 3.3 cm^2/g. The values were relatively consistent over the year, but varied slightly with age. CC (i.e. 2014 cohort) had statistically higher SLA (35.2 ± 0.7) than PC (i.e. 2013 or prior cohort; 28.1 ± 0.7) (paired t-test, $p < 0.0001$, Fig 3b).

3.2. n-Alkane concentration and chain length distribution

n-Alkanes exhibited a strong odd-over-even carbon preference, with *n*-C_{29} or *n*-C_{31} alkanes as the most abundant chain length (C_{max}) for angiosperms. *n*-Alkane concentration and chain length distribution varied among species and growth stage (Table 1 and Fig. 2e). For angiosperms, *A. rubrum* produced the most *n*-alkanes both in buds (ca. 300 to 800 μg/g) and leaves (ca. 100 to 800 μg/g), while *S. albidum* had lowest *n*-alkane production (buds = ca. 20 μg/g; leaves = ca. 10 μg/g). Temporally, buds contained ca. 1 to 3 times more long-chain *n*-alkanes than mature leaves. Young leaves had the lowest concentration, and either increased or remained similar in mature leaves. *n*-Alkane concentrations of C_{max} in mature leaves are 802.8 ± 266.9 μg/g for *A. rubrum*, 74.8 ± 36.5 μg/g for *A. saccharum*, 10.8 ± 15.1 μg/g for *S. albidum*, and 126.4 ± 104.8 μg/g for *U. americana*. *n*-C_{29} and *n*-C_{31} in *A. rubrum* and *n*-C_{29} in *A. saccharum* had statistically higher concentrations in mature leaves than in young leaves (paired t-test, $p < 0.05$). By contrast, young and mature leaves had similar *n*-alkane concentrations in *U. americana* and *S. albidum* (paired t-test, $p > 0.05$). ACL ranged from 27.8 to 31.6 in angiosperms with slightly higher average value for buds (29.9 ± 1.2, $n = 9$) than leaves (29.2 ± 0.8, $n = 35$; Fig. 2d). Young leaves had lower ACL (*A. rubrum* = 29.4; *A. saccharum* = 28.9; *U. americana* = 28.3) than mature leaves (*A. rubrum* = 30.0; *A. saccharum* = 30.0; *U. americana* = 29.1) except in *S. albidum* (young leaves = 29.2; mature leaves = 28.4).

In *J. virginiana,* *n*-C_{33} was the C_{max} throughout the year, followed by *n*-C_{35} (Table 1). *J. virginiana* produced a higher amount of *n*-C_{33} (106.6 ± 6.1 μg/g on average) than the angiosperms. *A. rubrum*

produced 80.5 ± 29.8 μg/g of *n*-C_{33} and other angiosperm species had no or low average of *n*-C_{33} (< 29.2 ± 32.7 μg/g) in mature leaves. *n*-Alkane concentrations also varied seasonally and annually between conifer cohorts (i.e. CC and PC). Seasonally, we observed higher concentrations during growing season (Jun-Oct; 99.4 to 207.6 μg/g) than the rest of the year (Nov-May; 7.0 to 86.4 μg/g; Fig. 3d). Both the CC and PC had low concentrations until May 3rd (12.9 to 25.9 μg/g), and increased substantially in June (CC = 207.6 μg/g; PC = 86.4 μg/g). This ca. 4 times increase in *n*-alkane concentrations in June in PC indicates that this species is adding *n*-alkanes to previous years' needles, although to a lesser degree than in the CC (ca. 10 times). In November, the *n*-C_{33} concentration in CC (44.3 μg/g) was a quarter of the concentration measured in June (207.6 μg/g). Inter-annually, average *n*-alkane concentration was significantly higher in CC than in PC (paired t-test, $p < 0.05$). ACL was higher in *J. virginiana* than angiosperm species, ranging from 31.9 to 33.5 and a mean value of 32.9 ± 0.5 (Fig. 3c). CC had slightly higher ACL (33.0 ± 0.4) than PC (32.6 ± 0.7). ACL increased from June to October (33.2 ± 0.2) by ca. 0.6 compared to the other months (mean = 32.6 ± 0.6).

3.3. Temporal changes in $\delta^{13}C_{leaf}$

$\delta^{13}C_{leaf}$ values in angiosperm species varied by growth stage (Fig. 2a). The $\delta^{13}C_{leaf}$ values were lowest in buds over the growing season in all three species: *A. rubrum* (−29.6‰), *A. saccharum* (−30.6‰) and *U. americana* (−30.1‰). As buds swelled prior to leaf flush, $\delta^{13}C_{leaf}$ values increased by 0.9 to 2.6‰ in each species. Leaves flushed on April 19th in *A. rubrum* and *S. albidum*, and April 26th in *A. saccharum* and *U. Americana* (indicated by dotted lines in Fig. 2). Leaf flushing occurred over one to two weeks, depending on the species. Due to the weekly sampling resolution of this study, it is difficult to estimate the exact day or duration of the leaf flush. After leaf flush, $\delta^{13}C_{leaf}$ values in young leaves remained relatively high: −27.1 ± 0.7‰ in *A. rubrum*, −28.7 ± 1.5‰ in *A. saccharum*, −26.0 ± 1.4‰ in *S. albidum*, and −28.3 ± 1.0‰ in *U. americana*. As leaves reached full maturation (i.e. SLA stabilization), average $\delta^{13}C_{leaf}$ values decreased by ca. 1.5 to 2.0‰ becoming significantly lower than young leaves (paired t-test, $p < 0.05$) for

all species except *A. saccharum*; average $\delta^{13}C_{leaf}$ values increased by 0.7‰, for this species but were not statistically different. Average $\delta^{13}C_{leaf}$ values for mature leaves remained relatively consistent until leaf senescence. $\delta^{13}C_{leaf}$ values in mature angiosperm leaves ranged from −30.8 to −24.5‰ with a mean value of −28.5 ± 1.4‰, with slight variations among species (i.e. −29.9 ± 0.5‰ in *U. americana*; −28.5 ± 0.9‰ in *A. rubrum*; −28.0 ± 1.1‰ in *A. saccharum*; −27.9 ± 1.7‰ in *S. albidum*).

For *J. virginiana,* $\delta^{13}C_{leaf}$ values ranged from −29.5 to −26.5‰ over the growing season, which is within the range of $\delta^{13}C_{leaf}$ values in angiosperms (Fig. 3a). CC had relatively consistent $\delta^{13}C_{leaf}$ values throughout the growing season, except for one sampling date in July (−26.9‰), recording the highest value. PC had slightly but significantly lower $\delta^{13}C_{leaf}$ values on average (−28.9 ± 0.2‰) than CC (−27.8 ± 0.2‰; paired t-test, $p < 0.002$).

3.4. Temporal change in $\delta^{13}C_{alk}$ values

Temporal patterns in $\delta^{13}C_{alk}$ values were similar to those in $\delta^{13}C_{leaf}$ values, although the magnitude of change varied with species and/or *n*-alkane homologs (see Section 3.5. for $\varepsilon_{alk\text{-}leaf}$; Fig. 2a). Winter buds had the lowest $\delta^{13}C_{alk}$ values over the growing season (−34.7‰ in *A. rubrum* for *n*-C_{31}, −38.2‰ in *A. saccharum* for *n*-C_{31} and −37.9‰ in *U. americana* for *n*-C_{29}). Values increased before leaf flush by 1.6‰ in *A. rubrum*, 3.6‰ in *A. saccharum* and 2.6‰ in *U. americana*. The young leaves had highest average $\delta^{13}C_{alk}$ values over the growing season (−29.1 ± 0.4‰ in *A. rubrum*; −31.3 ± 1.0‰ in *A. saccharum*; −31.4 ± 3.4‰ in *S. albidum*; −33.5 ± 1.4‰ in *U. americana*). The $\delta^{13}C_{alk}$ values decreased from young to mature leaves for all species, although by differing amounts. *A. rubrum* had the greatest ^{13}C-depletion (3.5‰) from young to mature leaves, and *A. saccharum* had the smallest decrease (1.7‰). Mature angiosperm leaves have $\delta^{13}C_{C31\ alk}$ values ranging from −35.0 to −30.1‰, with a mean of −32.8 ± 1.6‰.

In *J. virginiana*, $\delta^{13}C_{C33\ alk}$ ranged from −34.5 to −31.5‰ with a mean value of −32.9 ± 0.9‰ (Fig. 3a).

Temporal variations in $\delta^{13}C_{alk}$ values were similar to those in $\delta^{13}C_{leaf}$ values. PC had lower $\delta^{13}C_{C33\ alk}$ values (−33.8 ± 0.3‰) than CC (−32.4 ± 0.3‰; paired t-test, $p < 0.004$). The difference was greater in $\delta^{13}C_{C31\ alk}$ values between PC (−35.4 ± 0.6‰) and CC (−32.5 ± 0.5‰; paired t-test, $p < 0.002$). We also observed temporal variation in $\delta^{13}C_{C33\ alk}$ values during the growing season. Spring and summer needles (−32.4 to −31.6‰) had slightly but significantly higher values than those from later in the growing season (Aug-Nov; −33.5 to −32.8‰; paired t-test, $p < 0.008$). A similar decreasing trend in $\delta^{13}C_{alk}$ values of CC from August to November was observed for *n*-C_{31} and *n*-C_{35} alkanes.

3.5. Temporal change in $\varepsilon_{leaf\text{-}CO2}$ values

$\varepsilon_{leaf\text{-}CO2}$ values were calculated using Eq. 1 with a $\delta^{13}C_{CO2}$ value of −8.4‰ for the year 2014 (White et al., 2011). $\varepsilon_{leaf\text{-}CO2}$ values ranged from −22.5‰ to −19.3‰ in buds and −22.6 to −16.2‰ in leaves (Fig. 4c). $\varepsilon_{leaf\text{-}CO2}$ values in buds are −21.0 ± 0.6‰ for *A. rubrum*, −21.6 ± 1.5‰ for *A. saccharum*, −20.9 ± 1.3‰ for *U. americana* (Table 1). Values increased from buds to young leaves by ca. 1 to 2‰ on average (*A. rubrum* = −18.9 ± 0.7‰; *A. saccharum* = −20.5 ± 1.5‰; *S. albidum* = −17.7 ± 1.4‰; *U. americana* = −20.1 ± 1.0‰). The $\varepsilon_{leaf\text{-}CO2}$ values in mature angiosperm leaves ranged from −22.6 to −16.2‰ with an average of −20.3 ± 1.4‰. Average $\varepsilon_{leaf\text{-}CO2}$ values were −20.3 ± 0.9‰ in *A. rubrum*, −19.8 ± 1.1‰ in *A. saccharum*, −19.7 ± 1.7‰ in *S. albidum* and −21.7 ± 0.5‰ in *U. americana*. Average $\varepsilon_{leaf\text{-}CO2}$ values were higher in mature leaves than in young leaves by ca.1 to 2‰ (paired t-test, $p < 0.05$). For *A. saccharum*, mature leaves had 0.7‰ higher average $\varepsilon_{leaf\text{-}CO2}$ values than young leaves, but were not statistically different. In *J. virginiana*, $\varepsilon_{leaf\text{-}CO2}$ values ranged from −21.3 to −18.3‰ with a mean value of −20.0 ± 0.8‰. These values are within the range of $\varepsilon_{leaf\text{-}CO2}$ values for angiosperms. CC had slightly and significantly higher $\varepsilon_{leaf\text{-}CO2}$ values (−19.6 ± 0.5‰) than PC (−20.7 ± 0.4‰; paired t-test, < 0.05).

3.6. Temporal change in $\varepsilon_{alk\text{-}leaf}$ values

$\varepsilon_{alk\text{-}leaf}$ values are calculated using Eq. 2. In angiosperm buds, $\varepsilon_{C29\text{-}leaf}$ values ranged from −8.1 to −5.3‰ with a mean value of −6.7 ± 1.1‰ (Fig. 4d-4e). The values increased in young leaves by ca. −1 to −6 ‰. The rate of increase in $\varepsilon_{C29\text{-}leaf}$ values from buds to leaves varied with species. For example, $\varepsilon_{C29\text{-}leaf}$ values in *A. rubrum* and *A. saccharum* increased from buds to young leaves by 3 to 4‰ in two weeks, while in *S. albidum* and *U. americana*, values increased 3 to 4‰ over a two-month period. In all species, $\varepsilon_{C29\text{-}leaf}$ values increased early in the growing season, but the amount of change varied by species. For example, in *A. saccharum*, average $\varepsilon_{C29\text{-}leaf}$ values decreased slightly from −3.3 ± 1.2‰ in young leaves to −4.5 ± 0.6‰ in mature leaves, while in *U. americana*, values increased slightly from −6.5 ± 1.2‰ in young leaves to −4.3 ± 0.4‰ in mature leaves. In *A. rubrum*, $\varepsilon_{C29\text{-}leaf}$ values remained consistent. The average $\varepsilon_{C29\text{-}leaf}$ value for the angiosperm mature leaves is −4.3 ± 1.1‰. For the conifer, $\varepsilon_{C33\text{-}leaf}$ values ranged from −6.1 to −3.8‰, with a smaller temporal variation (ca. 2‰) than angiosperms (Fig. 4f-4g). $\varepsilon_{C33\text{-}leaf}$ values in CC were ca. −5‰ in May, and then increased slightly in June by 1‰. PC also increased slightly from May (ca. −6‰) to June (ca. −5‰). No statistical difference was found in $\varepsilon_{C33\text{-}leaf}$ values between CC (−4.7 ± 0.4‰) and PC (−5.1 ± 0.7‰; t-test, $p > 0.05$).

3.7. Canopy effects on $\delta^{13}C_{CO2}$, $\delta^{13}C_{leaf}$, $\delta^{13}C_{alk}$ and n-alkane concentration

The $\delta^{13}C_{CO2}$, $\delta^{13}C_{leaf}$, $\delta^{13}C_{alk}$ and *n*-alkane concentrations in *A. rubrum*, *A. saccharum* and *U. americana* at different heights from the ground to the top of the canopy are reported in Fig. 5. $\delta^{13}C_{CO2}$ values at the top of the canopy were −7.4‰ for *A. rubrum,* −7.0‰ for *A. saccharum* and −7.1‰ for *U. americana*. The $\delta^{13}C_{CO2}$ values were consistent across the canopy except at the lowest height (10 cm above ground) for all trees. The $\delta^{13}C_{CO2}$ values at the lowest height were −8.0‰ for *A. rubrum,* −9.7‰ for *A. saccharum* and −9.3‰ for *U. americana*; these values are ca. 0.5 to 2.5‰ lower than those from the upper canopy (Fig. 5a). The $\delta^{13}C_{leaf}$ values were lower below the canopy by 2.8‰ and 3.2‰ than the top canopy in *A.*

rubrum and *A. saccharum*, respectively. *U. americana*, with the lowest canopy closure, did not have any trend in $\delta^{13}C_{leaf}$ values with height (Fig. 5b). The $\delta^{13}C_{alk}$ values showed the same trend as $\delta^{13}C_{leaf}$ values with respect to canopy height and extent of canopy closure (Fig. 5c): higher at the top of the canopy for *A. rubrum* (−29.9‰ for *n*-C_{31}) and *A. saccharum* (−31.9‰ for *n*-C_{31}) than those from ground level (−33.8‰ and −36.1‰, respectively). The reduction in $\delta^{13}C_{alk}$ values in the lower canopy was up to 2.6‰ for *n*-C_{27}, 3.3‰ for *n*-C_{29}, 3.9‰ for *n*-C_{31} and 4.4‰ for *n*-C_{33} in *A. rubrum*. For *A. saccharum*, there was up to 2.7‰ and 4.2‰ decrease below canopy for *n*-C_{29} and *n*-C_{31}, respectively. In *U. americana*, no trend was observed in $\delta^{13}C_{alk}$ values with height. In terms of isotope fractionation, $\varepsilon_{leaf\text{-}CO2}$ values were lower below the canopy (−22.2 to −21.0‰ in *A. rubrum*; −22.9 to −21.6‰ in *A. saccharum*) than at the top of the canopy (−19.2‰ in *A. rubrum*; −18.9 in *A. saccharum*) in two species with high canopy closure (Fig. 5d). No $\varepsilon_{leaf\text{-}CO2}$ trend was observed in *U. americana* with height, the species with higher canopy openness (range = −23.3 to −21.9‰). $\varepsilon_{alk\text{-}leaf}$ values did not show any patterns with height or canopy closure (Fig. 5e). In terms of *n*-alkane concentrations, leaves from the top of the canopy had 2 to 8 times higher concentrations (Fig. 5f; 1,201.7 µg/g for *n*-C_{31} in *A. rubrum*; 40.7 µg/g for *n*-C_{29} in *A. saccharum*; 290.6 µg/g for *n*-C_{29} in *U. americana*) than those from lower heights. ACL remained consistent with height.

3.8. $\delta^{13}C_{leaf}$ and $\delta^{13}C_{alk}$ values in leaf litter

The $\delta^{13}C_{leaf}$ values in litter were highest under *S. albidum* (−27.9‰), followed by *A. rubrum* (−28.8‰), *J. virginiana* (−29.3‰), *A. saccharum* (−29.4‰) and *U. americana* (−30.5‰) (Table 1; Fig. 2; dotted lines in Fig. 5). These isotopic trends among species are most similar to those observed in mature leaves. Difference in $\delta^{13}C_{leaf}$ values between leaf litter and mature leaves was minimal (≤ 0.6‰) except for *A. saccharum* ($\delta^{13}C_{leaf}$ values in mature leaves were 1.4‰ higher than in leaf litter).

Trends in $\delta^{13}C_{alk}$ values among species differed from those in $\delta^{13}C_{leaf}$; values were highest in *A. rubrum* litter (−31.9‰), followed by *A. saccharum* (−34.0‰), *U. americana* (−35.0‰), *S. albidum* (−35.6‰) and

J. virginiana (−36.3‰). We compared $\delta^{13}C_{alk}$ values in leaf litter to mature leaves from the canopy. The difference varied from 0.0 to 3.0‰, with greater offset in longer chains such as *n*-C_{33} for *A. rubrum* (1.3‰), *A. saccharum* (3.0‰) and *J. virginiana* (1.9‰) and *n*-C_{31} for *S. albidum* (2.8‰). For *n*-C_{29}, $\delta^{13}C_{alk}$ offsets between mature leaves and litter were smaller/less than 0.9‰. Average *n*-alkane concentration and ACL in the litter were more comparable to mature leaves than young leaves. The offsets in ACL values between mature leaves and litter ranged from 0 to 0.3.

4. Discussion

4.1. Timing of n-alkane synthesis and concentration change through the growing season

To identify the timing and magnitude of long-chain *n*-alkane synthesis and loss over the growing season, as well as how these factors affected $\delta^{13}C_{alk}$ values, we compared temporal changes in SLA, *n*-alkane concentration and distributions (i.e. ACL) and $\delta^{13}C_{alk}$ values (Figs. 2 and 4; Table A1). A rapid leaf expansion occurred after leaf flush, with leaf area increasing by 162 to 841%, consistent with observations in other studies (Fig. 4b; Hauke and Schreiber, 1998). Rapid leaf expansion was accompanied by low *n*-alkane concentration and ACL (Fig. 2d-2e), indicating that the rate of leaf expansion outpaced the rate of *n*-alkane synthesis in young leaves (Freimuth et al., 2017). Full maturation of leaves, as indicated by SLA stabilization, occurred in late May to early June, which is 5 to 6 weeks after bud burst (indicated by gray bar in Fig. 2 and 4). ACL also did not increase until June, indicating a 5- to 6-week delay in the shift of production to longer chain *n*-alkanes. For *A. saccharum* and *U. americana*, ACL increased further after June; this was mainly due to a decrease in shorter chain-alkanes (Figs. 2-2 and 2-4). A delay in longer-chain leaf wax synthesis has been observed in previous studies (Eglinton and Hamilton, 1967; Freimuth et al., 2017; Hauke and Schreiber, 1998; Li et al., 2016; Piasentier et al., 2000). Jetter et al. (2001) observed during the leaf development of *Prunus laurocerasus*

that leaf wax accumulation rates varied by wax compounds where *n*-alkanes increased after alkyl acetates and alcohols. Jetter et al. (2001) also noted that leaf wax flux rates may be influenced by compound diffusion rates and ontogenetic regulation of wax biosynthesis. In our study, the onset of ACL increase coincided with the timing of leaf maturation, and the rate and duration of ACL increase varied by species. $\delta^{13}C_{leaf}$ and $\delta^{13}C_{alk}$ values also stabilized at the timing of leaf maturation. These results suggest the timing of long-chain *n*-alkane accumulation (and/or loss of shorter-chains) may be related to the rate of leaf development, which in turn varies with (or is influenced by) species and ontogeny.

For the conifer, we observed a large increase in *n*-C_{33} alkane concentrations from May (24.2 µg/g) to June (167.2 µg/g), and values remained consistent until October (Fig. 3d). ACL also increased early in the growing season (Fig. 3c). We attribute the significant increase in *n*-alkanes from June to October to an increase in photosynthetic rate in evergreen conifers during the growing season and subsequent *n*-alkane synthesis (Gordon and Larson, 1968; Troeng and Linder, 1982). Comparing years, we found lower *n*-alkane concentrations in PC (29 ± 33 µg/g) than in CC (107 ± 61µg/g), probably due to either lower *n*-alkane production in previous years than the current year and/or ablation of leaf waxes through time. Our sampling strategy primarily focused on a single growing season, therefore it is difficult to provide a clear explanation for the difference in *n*-alkane concentrations and ACL between the two cohorts. Nevertheless, these results suggest that *n*-C_{33} alkane concentrations in *J. virginiana* can vary across seasons and years with higher production in summer months.

4.2. Control on temporal change in leaf and n-alkane $\delta^{13}C$ values

Winter buds had relatively low $\delta^{13}C_{leaf}$ and $\delta^{13}C_{alk}$ values, which most likely reflects carbon utilized in the previous growing season (Hoch et al., 2013; Tipple et al., 2013). This was confirmed in this study as both average $\delta^{13}C_{leaf}$ and $\delta^{13}C_{alk}$ values of the summer buds were similar to mature leaves (paired t-test, $p > 0.05$). As buds swelled prior to bud burst, $\delta^{13}C_{leaf}$ and $\delta^{13}C_{alk}$ values increased by ca. 3‰ and 4‰,

respectively, compared to the winter buds, and remained high in young leaves (Fig. 2a). This ^{13}C-enrichment toward bud burst may reflect trees utilizing stored carbon reserves for spring growth in expanding leaves (Barbaroux et al., 2003; Hoch et al., 2013; Lacointe et al., 1993), and stored carbon reserves are known to be relatively enriched in ^{13}C (Brüggemann et al., 2011; Cernusak et al., 2009). Therefore, we attribute the higher $\delta^{13}C_{leaf}$ and $\delta^{13}C_{alk}$ values in late buds and young leaves to the utilization of stored carbon for plant metabolism early in the growing season.

On average, $\delta^{13}C_{leaf}$ and $\delta^{13}C_{alk}$ values decreased from young leaves to mature leaves by ca. 1.7‰ and 1.1‰, respectively. A decreasing trend in $\delta^{13}C_{leaf}$ or $\delta^{13}C_{wax}$ values through the growing season has been observed in prior studies, although various explanations for this change have been postulated (Dungait et al., 2010; Flanagan et al., 1997; Garten and Taylor, 1992; Lockheart et al., 1997; Lowdon and Dyck, 1974). Lowdon and Dyck (1974) suggested that $\delta^{13}C_{leaf}$ values may change through the growing season because of seasonal variation in $\delta^{13}C_{CO2}$ values. To test this, we measured upper canopy $\delta^{13}C_{CO2}$ values in May when leaves are sparse and July during maximum canopy closure, and found that the values were higher in July by 0.4 to 0.9‰. Increased $\delta^{13}C_{CO2}$ occurs due to high net photosynthesis during summer months, leaving atmospheric CO_2 relatively enriched in ^{13}C (Boutton, 1991). This seasonal shift in $\delta^{13}C_{CO2}$ is opposite to the observed variation in $\delta^{13}C_{leaf}$ values, which are higher in May and lower in July. Other studies suggested that seasonal changes in temperature influence $\delta^{13}C_{leaf}$ and $\delta^{13}C_{alk}$ values (Li et al., 2016; Lockheart et al., 1997; Mihailova et al., 2015). However, we did not observe any relationship between $\delta^{13}C_{leaf}$ or $\delta^{13}C_{alk}$ values and daily temperature measured at a nearby weather station ($r^2 = 0.1$, $p = 0.1$).

The observed decreasing trend in $\delta^{13}C_{leaf}$ and $\delta^{13}C_{wax}$ values from young to mature leaves may be explained, at least in part, by changes in photosynthetic rates and the carbon source utilized. Photosynthetic rates are known to increase from young to mature leaves (Snider et al., 2009). This is due to lower chlorophyll content, underdeveloped chloroplasts, and limited stomatal and cellular conductance

of CO_2 in young leaves (Choinski Jr et al., 2003; Choinski and Johnson, 1993; Choinski and Wise, 1999; Snider et al., 2009; Woodall et al., 1998). Additionally, as leaves mature, their carbon source will shift from stored carbon to recently biosynthesized carbon. Although we did not measure photosynthetic rate, the observed shift to lower $\delta^{13}C_{leaf}$ and $\delta^{13}C_{alk}$ values may reflect changes in photosynthetic capacity of leaves and the shift from heterotrophic to autotrophic status.

Average $\varepsilon_{alk\text{-}leaf}$ values for mature leaves of deciduous angiosperms were −4.3 ± 1.0‰ (n = 20) for n-C_{29}, −4.3 ± 1.3‰ (n = 17) for n-C_{31}, and −1.9 ± 2.0‰ (n = 7) for n-C_{33} (Fig. 4d). This is within the range of values reported in previous studies (Diefendorf and Freimuth, 2017 and references therein). Slight changes in $\varepsilon_{C29\ alk\text{-}leaf}$ from June to October may indicate some n-alkane replacement, but given the small change in $\varepsilon_{alk\text{-}leaf}$, it appears that if any n-alkanes are added, then $\varepsilon_{alk\text{-}leaf}$ values are remaining constant. This is important for paleo applications as these mature leaves and leaf waxes are the major source of wax that enters geologic archives.

For *J. virginiana*, $\varepsilon_{alk\text{-}leaf}$ values are −4.8 ± 0.7‰ for n-C_{31} and −4.6 ± 0.4‰ for n-C_{33} (Fig. 4f-g), and are similar to those in evergreen gymnosperms from prior studies (Diefendorf and Freimuth, 2017). The production of long-chain n-alkanes in *J. virginiana* increased in June. $\delta^{13}C_{alk}$ values were slightly higher from May to August than from September to November by 1 to 2‰. Prior studies that measured seasonal variations in bulk needle $\delta^{13}C$ values also found higher $\delta^{13}C$ values during spring and a gradual decrease later in the growing season (Brendel et al., 2003; Jäggi et al., 2002). We suggest that the same mechanism responsible in angiosperms is also responsible for these observations in conifers. However, unlike the angiosperms, temporal variation in $\delta^{13}C_{leaf}$ and $\delta^{13}C_{alk}$ values was smaller (ca. 2‰) and the ^{13}C-depletion occurred much later in the growing season. These differences among major plant groups may be attributed to the different growth and carbon allocation strategies used by conifers and angiosperms (Johnson et al., 2012; Meinzer et al., 2013; Mueller et al., 2010).

4.3. Canopy effect on $\delta^{13}C_{leaf}$ and $\delta^{13}C_{alk}$ values and n-alkane concentrations

$\delta^{13}C_{leaf}$ values were more ^{13}C-depleted in the lower two thirds of the canopy and ^{13}C-enriched in the upper one third of the canopy for two species (i.e. *A. rubrum* and *A. saccharum*) with higher canopy closure (Fig. 5b). More negative $\varepsilon_{leaf\text{-}CO2}$ values in the lower canopy may have been caused by lower photosynthetic rates and carbon fixation under lower light availability (Fig. 5c). Further, relative humidity is higher in dense canopy forests, and this may have led to lower $\varepsilon_{leaf\text{-}CO2}$ values in the lower canopy. Light intensity, relative humidity, and $\delta^{13}C_{CO2}$ values have all been suggested to influence $\delta^{13}C_{leaf}$ values within the canopy (Ehleringer et al., 1986; Medina and Minchin, 1980; Ometto et al., 2006; Vogel, 1978; Zimmerman and Ehleringer, 1990). However, Graham et al. (2014) observed no relationship between $\delta^{13}C_{CO2}$ and $\delta^{13}C_{leaf}$ values in tropical rainforest trees and found that light intensity was the greatest control on $\delta^{13}C_{leaf}$ values within the canopy. This was also observed here. $\delta^{13}C_{CO2}$ values were lower only at ground level (−8.8 ± 0.8‰), regardless of the extent of canopy closure, and were consistent above 4 m (−7.7 ± 0.4‰), suggesting that air above 4 m is well mixed, at least at mid-day (Fig. 5a). The air below 4 m is consistent with contributions from soil respired CO_2 that are characterized by low $\delta^{13}C$ values (Pataki et al., 2003).

This study further measured $\delta^{13}C_{alk}$ values to examine $\varepsilon_{alk\text{-}leaf}$ variations within the canopy (Fig. 5d-e). $\delta^{13}C_{alk}$ values broadly followed the trend of $\delta^{13}C_{leaf}$. $\varepsilon_{C29\ alk\text{-}leaf}$ values were very similar at 4 m and above in *U. americana* (range = 0.6‰) and *A. rubrum* (range = 0.2‰), while in *A. saccharum*, the values were more variable through the canopy (range = 2.6‰). Due to differences in the extent of canopy openness and canopy shape of each tree species, microclimate variability such as light penetration and relative humidity may exist within and among trees. Considering that large $\varepsilon_{alk\text{-}leaf}$ values have been observed among species at the same site in previous calibration studies, these differences within the canopy are rather small. Given the consistency in $\varepsilon_{alk\text{-}leaf}$ values measured within the canopy and the similarity to values measured for other species (Diefendorf and Freimuth, 2017), $\delta^{13}C_{alk}$ values can be used to track

$\delta^{13}C_{leaf}$ values as canopy closure indicators, as long as other leaf traits are used to differentiate upper and lower canopy leaves (e.g. Graham et al., 2014).

Within the EF temperate forest, we found 2 to 8 times higher *n*-alkane concentrations at the top of the canopy compared to the understory (Fig. 5f). These results contradict observations from a tropical rainforest where shaded understory leaves had higher *n*-alkane concentrations than the upper canopy (Graham, 2014). This suggests that *n*-alkane concentrations within the canopy vary by forest type. The three most likely mechanisms to explain the higher *n*-alkane concentrations in the upper canopy are 1) higher light intensity in the uppermost canopy leaves, 2) increased water stress, and 3) decreased leaf damage in the upper canopy. Leaves exposed to higher light intensity, which would be expected in the uppermost canopy leaves, are known to have thicker leaf waxes (Giese, 1975; Shepherd and Wynne Griffiths, 2006). This has also been observed in a study where barley leaves were grown in the light and dark. Leaf wax density and deposition rate were 2.5 and 7.5 times greater, respectively, when grown in the light than in the dark (Giese, 1975). Higher photosynthetic rates, associated with higher light intensity, in the uppermost canopy leaves may also result in greater water stress and therefore increased *n*-alkane concentrations may be a mechanism to reduce water loss through the cuticle (Burghardt and Riederer, 2008; Jenks and Wood, 2002; Jetter and Riederer, 2016; Kerstiens, 1996; Reynhardt, 1997; Riederer and Schreiber, 1995; Schreiber, 2006). During leaf collection, we observed that upper canopy leaves were generally healthier. They had less infections and damage than the lower canopy leaves. This agrees with studies that find lower herbivory and photosynthetic tissue damage in the upper canopy (Angulo-sandoval and Aide, 2000; Lowman, 1985; Phillipson and Thompson, 1983; Thomas et al., 2010). Future studies are clearly needed to explore which mechanism (or mechanisms) is responsible and to compare different forest types.

4.4. Implications for the geologic past

Settling of $\delta^{13}C_{alk}$ values in temperate forest trees occurred 5 to 6 weeks after leaf flush. This is consistent with another temperate forest 300 km north of EF (Freimuth et al., 2017). For broadleaf riparian trees on the other hand, *n*-alkane δD values were set in the first 2 to 3 weeks (Kahmen et al., 2011; Tipple et al., 2013), while another riparian *Salix* species took 13 weeks to stabilize (Newberry, 2015). Although the timing and duration of $\delta^{13}C_{alk}$ stabilization vary with species and environment, there has been a consensus on the setting of both δD_{alk} and $\delta^{13}C_{alk}$ values coinciding with timing of leaf maturation in deciduous trees. This means that leaf physiology and environmental conditions that influence plant metabolism during the early growing season may be important for leaf wax formation and settling of $\delta^{13}C_{alk}$ values, and that these values should remain largely consistent thereafter. Therefore, $\delta^{13}C_{alk}$ values from deciduous trees in temperate forests represent a record of carbon isotope fractionation influenced by plant metabolism and environmental conditions during the period of leaf flush to full leaf expansion.

A significant amount of variability in leaf level $\delta^{13}C_{leaf}$ and $\delta^{13}C_{alk}$ values has previously been observed within forests (e.g. Diefendorf and Freimuth, 2017), but this variability is reduced in the sedimentary records. Leaves are integrated from multiple species at an ecosystem level and are deposited in sediments. If their wax components are mixed and time averaged, then this would explain the small range observed in sediments.

To further investigate the link from source to sink, we compared $\delta^{13}C_{alk}$ values in the mature canopy leaves to leaf litter collected under the same trees (Fig. 2 and 5). This provides a test to determine if canopy leaves swamp the leaf litter plant wax. The offset on average $\delta^{13}C_{alk}$ values between mature leaves and leaf litter were 0.1‰ to 1.4‰ (Table 1). These differences are smaller than the $\delta^{13}C_{alk}$ range within the canopy (up to 3.9‰ in *A. rubrum* and 4.2‰ in *A. saccharum*). This would be consistent with the forest floor leaf litter being derived primarily from upper canopy leaves. Thus our study further supports

the notion that leaf wax components in sediments are likely biased towards those of mature leaves from the upper canopy, which makes sense given that *n*-alkane production is the 2 to 8 times greater in the upper canopy. Upper canopies are also known to have higher biomass, production rates and shorter leaf longevity (Brasell et al., 1980; Parker et al., 1989; Reich et al., 1991), and this translates into even greater production of *n*-alkanes in the upper canopy and dominance in sedimentary records. Additionally, leaf litter composition is dominated by the few most abundant species. This is particularly true in temperate forests, which has lower species diversity than tropical habitats (e.g. Burnham, 1989; Burnham and Johnson, 1994; Ellis and Johnson, 2013; Greenwood, 1991). Consequently, the large range of $\delta^{13}C_{alk}$ values that are observed in modern calibration studies may be greatly reduced in sedimentary records. Thus, it is important for modern calibrations to continue to make measurements on upper canopy leaves (e.g., Diefendorf et al., 2010) as they are more relevant for the geologic record. Additionally, in order to assess the extent of canopy closure in forests, this study supports the approach of using $\delta^{13}C_{alk}$ values of individual leaf fossils, combined with other leaf traits, as indicators of leaf canopy position (Graham and Freeman, 2013; Graham et al., 2014).

5. Conclusions

This is the first study to report temporal changes in both $\varepsilon_{leaf\text{-}CO2}$ and $\varepsilon_{alk\text{-}leaf}$ values from buds to leaves at weekly to monthly resolution, and to compare these values to leaf litter. Both $\delta^{13}C_{leaf}$ and $\varepsilon_{leaf\text{-}CO2}$ values changed through the growing season as buds developed into fully mature leaves. These changes reflect a shift in the source of carbon from stored reserves to recently photosynthesized carbon. $\delta^{13}C_{alk}$ values stabilized in the mature leaf stage, coinciding with SLA stabilization and an increase in ACL. This suggests that $\delta^{13}C_{leaf}$ and $\delta^{13}C_{alk}$ values reflect environment and plant physiologic conditions during leaf development, but that these values remain largely consistent once the leaf has matured.

Canopy effects on $\varepsilon_{leaf\text{-}CO2}$ and $\varepsilon_{alk\text{-}leaf}$ values were examined in trees with different extent of canopy closure. As observed in other studies, $\varepsilon_{leaf\text{-}CO2}$ values were lowest at the ground level (greatest fractionation) and highest at the top of the canopy (least fractionation), largely due to variable photosynthetic rates and relative humidity. $\varepsilon_{alk\text{-}leaf}$ values on the other hand did not vary appreciably in relation to height. However, we observed large changes in the concentration of leaf waxes within the canopy. The uppermost canopy leaves had up to 8 times higher *n*-alkane concentrations than observed in the lower canopy. We speculate that leaves have higher *n*-alkane concentrations in the uppermost canopy in response to high light intensity, to limit water loss in the most photosynthetically active leaves, and possibly due to decreased leaf damage.

Given that the upper canopy has higher biomass and *n*-alkane concentrations, and combined with paleobotany literature that suggest a bias towards upper canopy leaves in leaf litter, the *n*-alkanes of leaf litter are likely biased towards upper canopy leaves. This is further supported by the small offsets in $\delta^{13}C_{alk}$ values (< 1.5‰) between leaf litter and mature canopy leaves measured in this study.

Acknowledgements

We thank S. Feakins and an anonymous reviewer for helpful comments that improved this study. Thanks to E. Freimuth for comments on earlier versions of the manuscript. We also thank K. Kim and D. Sberna for assistance in field sampling. We are grateful to East Fork Wildlife Area for sampling permissions. Portions of the research were supported by the US National Science Foundation (EAR-1229114) and by the Ministry of Oceans and Fisheries, South Korea (K-IODP). Acknowledgement is made to the Donors of the American Chemical Society Petroleum Research Fund for partial support of the research (PRF # 51787-DNI2). We also acknowledge support from the Lewis and Clark Fund from the American Philosophical Society to Y.J.S.

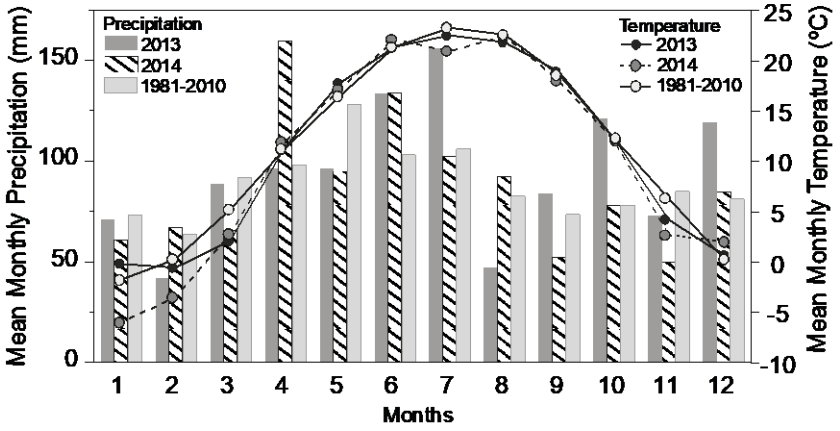

Figure 1. Mean monthly precipitation (mm; bars) and mean monthly temperature (°C; lines) in southwestern Ohio, USA for 2013, 2014 and a 30 yr average (1981-2010; Midwestern Regional Climate Center, cli-MATE; http://mrcc.isws.illinois.edu/CLIMATE/).

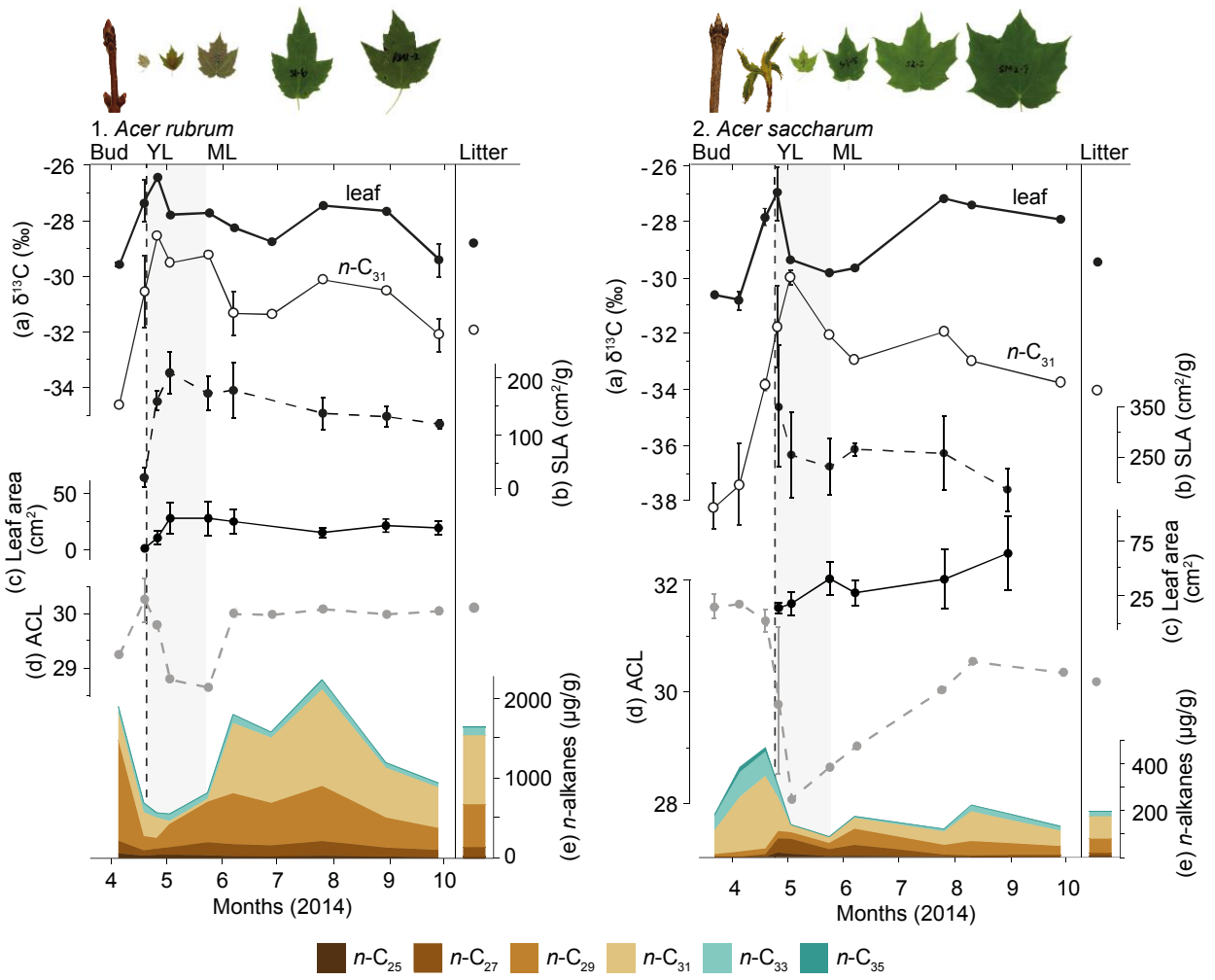

Figure 2. Temporal variation in (a) $\delta^{13}C$ values of leaf biomass (‰; closed circle) and *n*-alkanes (‰; open circle), (b) specific leaf area (SLA, cm^2/g; dashed black line), (c) leaf area (cm^2; black line), (d) average chain length (ACL; dashed gray line) and (e) *n*-alkane concentrations from *n*-C_{25} to *n*-C_{35} (µg/g dry leaf) in (1) *A. rubrum*, (2) *A. saccharum*, (3) *S. albidum*, (4) *U. americana* collected in 2014 from East Fork Wildlife Area, southwestern OH, USA. Dotted vertical line indicates timing of bud burst (*A. rubrum* and *S. albidum* = April 19, 2014; *A. saccharum* and *U. americana* = April 26, 2014). Sample types are indicated from bud to leaves (YL = young leaves; ML = mature leaves) and leaf litter. Transition from YL to ML is determined by the timing of SLA stabilization (See text). Gray bar indicates leaf development period in YL. Note different scales for *n*-alkane concentration.

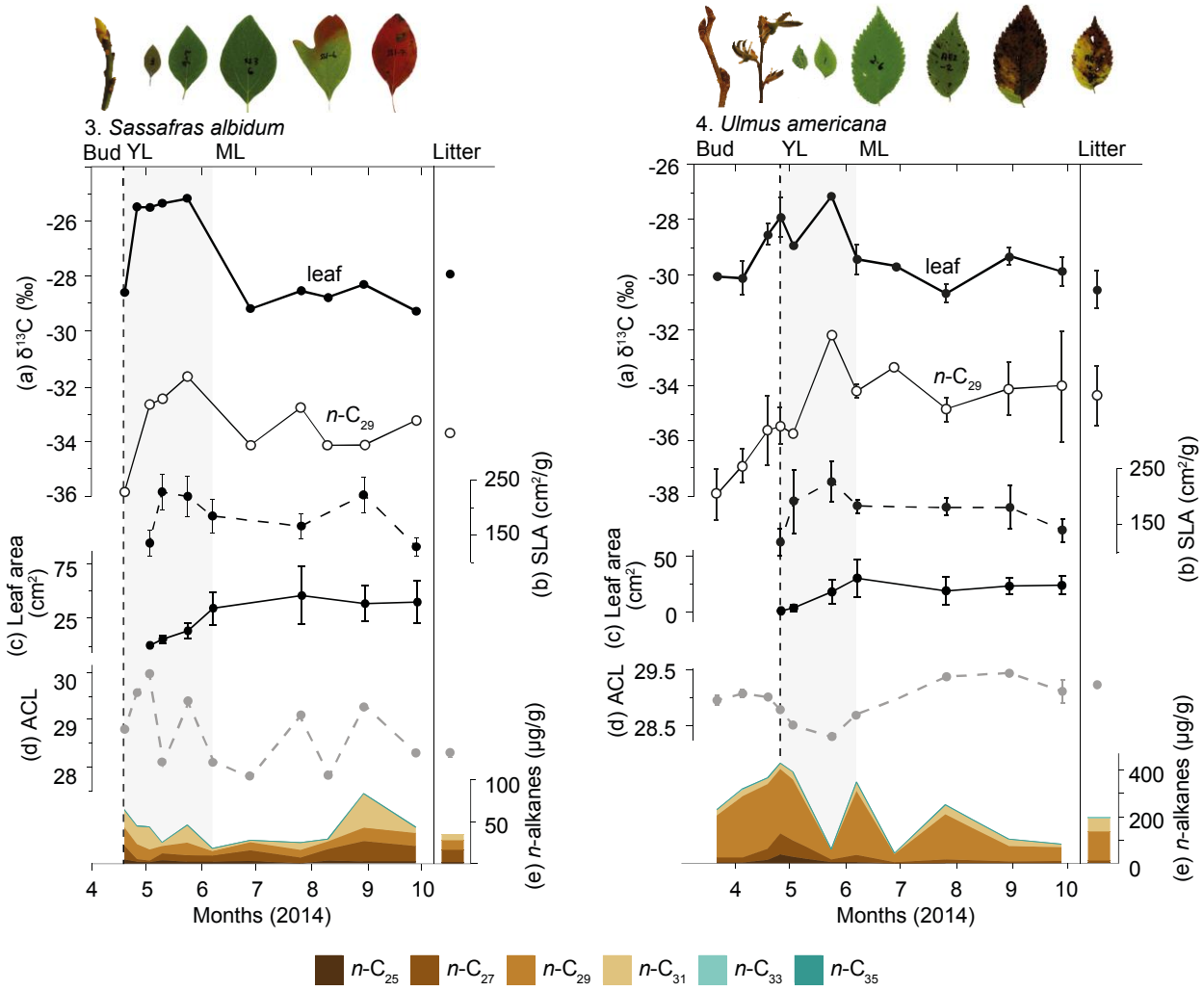

Figure 2. continued

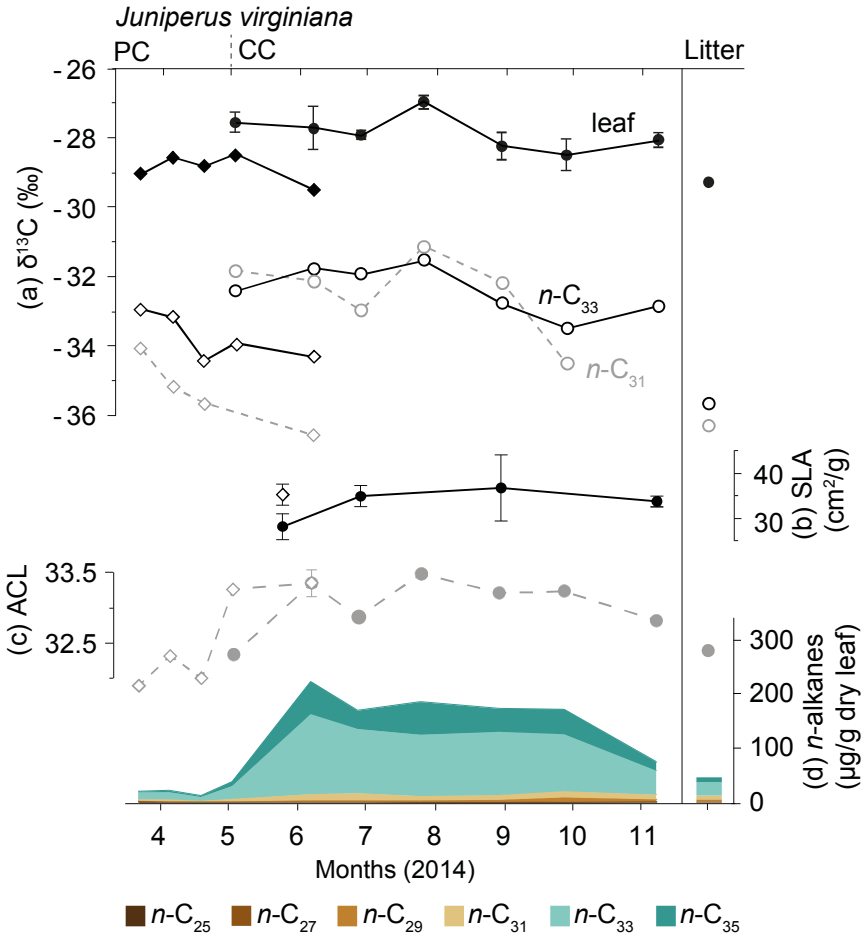

Figure 3. Temporal variation in (a) δ^{13}C values of leaf biomass (‰; closed circle) and *n*-alkanes (‰; open circle), (b) specific leaf area (SLA, cm^2/g), (c) average chain length (ACL, dashed gray line) and (d) *n*-alkane concentrations from *n*-C_{25} to *n*-C_{35} (µg/g dry leaf) for *J. virginiana* collected in 2014 from East Fork Wildlife Area, southwestern OH, USA. Diamonds and circles indicate needle samples from the current year cohort (CC) and prior year cohort (PC), respectively. Litter data are presented on the right.

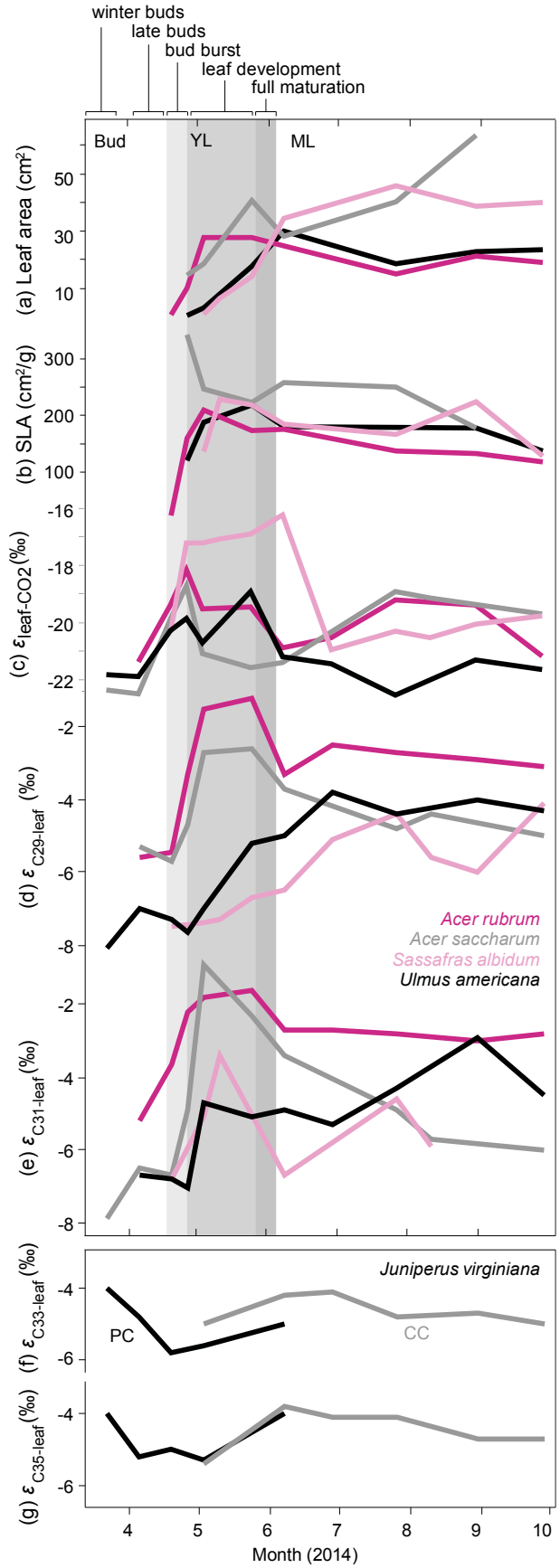

Figure 4. Temporal variation in (a) leaf area (cm^2), (b) specific leaf area (SLA, cm^2/g) (c) $\varepsilon_{leaf\text{-}CO2}$ (‰), (d) $\varepsilon_{C29\ alk\text{-}leaf}$ (‰), (e) $\varepsilon_{C31\ alk\text{-}leaf}$ (‰) in angiosperms; (f) $\varepsilon_{C33\ alk\text{-}leaf}$ (‰) and (g) $\varepsilon_{C35\ alk\text{-}leaf}$ (‰) in the conifer (*J. virginiana*) collected in 2014 from East Fork Wildlife Area, southwestern OH, USA. Leaf growth stages are indicated from buds to young leaves (YL) and mature leaves (ML). Timing of winter buds, late buds, bud burst (*A. rubrum* and *S. albidum* = April 19, 2014; *A. saccharum* and *U. americana* = April 26, 2014), leaf development and full maturation are indicated. CC = cohorts from current year; PC = cohorts from prior years.

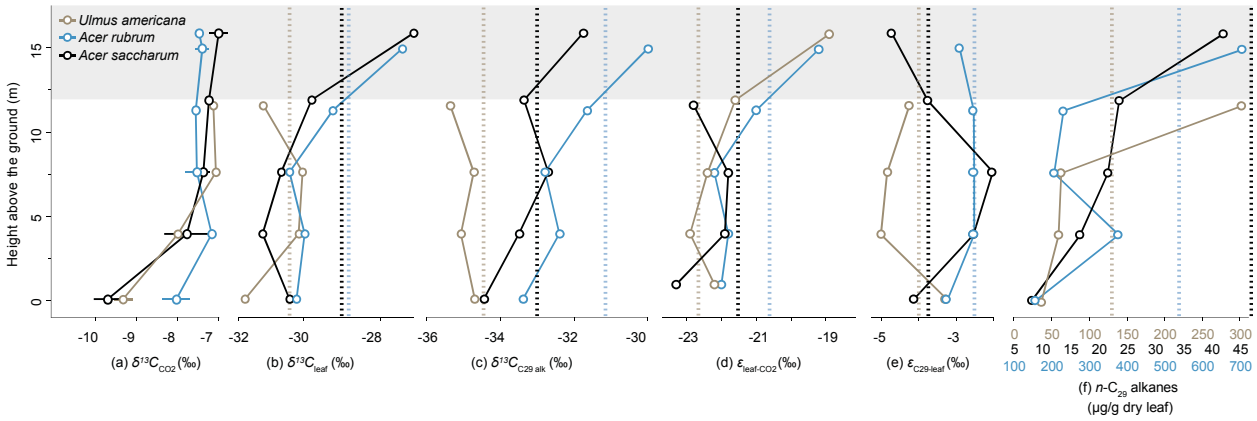

Fig. 5. Canopy effects on (a) carbon isotopic composition of atmospheric CO_2 ($\delta^{13}C_{CO2}$, ‰) in August 10, 2014, with error bars indicating standard deviation of duplicate samples, (b) $\delta^{13}C_{leaf}$ (‰), (c) $\delta^{13}C_{C29\ alk}$ (‰), (d) $\varepsilon_{leaf\text{-}CO2}$ (‰; calculated using the $\delta^{13}C_{CO2}$ value of −8.4‰ $_{CO2}$ for 2014; (White et al., 2011)), (e) $\varepsilon_{C29\text{-}leaf}$ (‰) and (f) *n*-alkane concentration (μg/g dry leaf) at different heights above ground (m) in *A. rubrum* (tree height 20 m), *A. saccharum* (18 m) and *U. americana* (13 m) collected in July 26, 2014 from East Fork Wildlife Area, Southwestern Ohio, USA. *A. saccharum* had the highest canopy closure (5.0% light penetration), followed by *A. rubrum* (13.0%) and *U. americana* (50.0%; See text for more information). Dotted vertical lines indicate results for leaf litter of each species collected in November 8th, 2014. The gray bar indicates the upper canopy.

Table 1. Mean and standard deviation of *n*-alkane concentration (μg/g dry leaf), average chain length (ACL), $\delta^{13}C_{leaf}$ (‰), $\varepsilon_{leaf\text{-}CO2}$ (‰), $\delta^{13}C_{alk}$ (‰), and $\varepsilon_{alk\text{-}leaf}$ (‰), for *A. rubrum*, *A. saccharum*, *J. virginiana*, *S. albidum*, and *U. americana* by growth stage from buds to leaves and litter collected over the growing season 2014 in East Fork Wildlife area, Southwestern OH, USA.

Species (≤ n)	*n*-Alkane concentration (μg/g dry leaf)					ACL	$\delta^{13}C_{leaf}$ (‰)	$\varepsilon_{leaf\text{-}CO2}$ (‰)	$\delta^{13}C_{alk}$ (‰)					$\varepsilon_{alk\text{-}leaf}$ (‰)				
	n-C_{27}	*n*-C_{29}	*n*-C_{31}	*n*-C_{33}	*n*-C_{35}				*n*-C_{27}	*n*-C_{29}	*n*-C_{31}	*n*-C_{33}	*n*-C_{35}	*n*-C_{27}	*n*-C_{29}	*n*-C_{31}	*n*-C_{33}	*n*-C_{35}
Acer rubrum																		
Bud (2)	116.9 (58.5)	754.8 (705.8)	292.0 (66.5)	84.4 (8.5)		29.5 (0.4)	−29.2 (0.6)	−21.0 (0.6)	−34.5 (0.3)	−35.0 (0.0)	−33.9 (1.1)	−33.8 (1.9)		−5.5 (0.4)	−6.0 (0.6)	−4.9 (0.5)	−4.7 (1.3)	
YL[a] (5)	98.2 (43.0)	254.6 (185.6)	131.2 (200.7)	89.4 (34.8)		29.4 (0.9)	−27.1 (0.7)	−18.9 (0.7)	−30.5 (0.7)	−29.7 (0.9)	−29.1 (0.4)	−28.2 (0.4)		−3.5 (1.4)	−2.6 (1.5)	−2.1 (0.5)	−1.2 (0.4)	
ML[b] (4)	134.7 (34.7)	498.2 (174.3)	802.8 (266.9)	80.5 (29.8)		30.0 (0.0)	−28.5 (0.9)	−20.3 (0.9)	−31.5 (0.6)	−31.3 (1.1)	−31.2 (0.8)	−29.7 (1.3)		−3.2 (0.2)	−2.9 (0.3)	−2.8 (0.1)	−1.4 (0.6)	
Sbud[c] (1)	212.6	5792.3	1450.2	345.4		29.5	−28.0	−19.8		−31.8	−32.2	−32.6			−3.8	−4.3	−4.7	
Litter (1)	122.9	535.9	871.1	95.5		30.1	−28.8	−20.6	−31.6	−31.2	−31.9	−31.0		−2.8	−2.5	−3.2	−2.2	
Acer saccharum																		
Bud (7)	4.9 (4.3)	19.8 (8.1)	217.5 (106.3)	90.9 (25.3)	13.7 (8.0)	31.5 (0.1)	−29.8 (1.5)	−21.6 (1.5)		−34.9 (1.4)	−36.6 (1.8)	−35.9 (2.0)			−5.5 (0.3)	−7.0 (0.8)	−6.3 (0.8)	
YL (5)	52.3 (19.3)	28.9 (1.8)	67.8 (66.5)	15.8 (27.4)	1.5 (2.5)	28.9 (0.9)	−28.7 (1.5)	−20.5 (1.5)	−32.7 (0.4)	−31.9 (0.4)	−31.3 (1.0)	−29.1 (1.6)		−4.1 (1.4)	−3.3 (1.2)	−2.7 (2.1)	−0.4 (3.2)	
ML (3)	18.3 (19.8)	52.4 (15.6)	74.8 (36.5)	15.4 (9.6)	0.2 (0.4)	30.0 (0.7)	−28.0 (1.1)	−19.8 (1.1)	−32.6	−32.4 (0.7)	−32.9 (0.7)	−31.4 (2.6)		−3.1	−4.5 (0.6)	−5.0 (1.2)	−3.0 (4.4)	
Sbud (1)	2.0	33.9	94.3	77.6	6.2	31.5	−29.5	−21.3		−32.5	−34.6	−34.0			−3.1	−5.2	−4.6	
Litter (1)	14.5	60.8	96.5	20.1	0.0	30.2	−29.4	−21.2		−33.1	−34.0	−34.4			−3.8	−4.7	−5.1	
Juniper virginiana																		
NN[d] (7)	1.0 (0.3)	3.5 (2.4)	10.7 (3.6)	106.6 (61.1)	39.4 (29.3)	33.0 (0.4)	−27.8 (0.5)	−19.6 (0.5)		−31.4	−32.5 (0.7)	−32.4 (0.4)	−32.2 (0.5)			−4.8 (0.7)	−4.7 (0.4)	−4.4 (0.5)
PN[e] (5)	0.6 (0.2)	1.1 (0.5)	3.8 (2.7)	29.2 (32.7)	12.1 (17.4)	32.6 (0.7)	−28.9 (0.4)	−20.7 (0.4)			−35.4 (0.9)	−33.8 (0.7)	−33.4 (0.7)			−6.6 (0.9)	−5.1 (0.7)	−4.7 (0.7)
Litter (1)	1.6	3.5	7.1	24.8	8.6	32.4	−29.3	−21.1			−36.3	−35.7	−34.9			−7.3	−6.6	−5.8
Sassafras albidum																		
YL (5)	7.5 (5.8)	15.5 (5.0)	19.0 (8.6)			29.2 (0.8)	−26.0 (1.4)	−17.7 (1.4)	−33.2 (1.8)	−33.1 (1.8)	−31.4 (3.4)			−7.2 (0.3)	−7.2 (0.4)	−5.1 (1.7)		
ML (6)	14.0 (6.6)	10.9 (4.0)	10.8 (15.1)			28.4 (0.7)	−27.9 (1.7)	−19.7 (1.7)	−32.8 (1.3)	−33.2 (1.3)	−32.8 (1.7)			−4.8 (1.0)	−5.3 (0.9)	−5.7 (1.0)		
Sbud (1)	8.5	15.6	5.5			28.5	−27.8	−19.6	−34.5	−34.6	−34.5			−6.9	−7.0	−6.9		
Litter (1)	14.5	11.5	7.0			28.3	−27.9	−19.7	−31.3	−33.7	−35.6			−3.5	−6.0	−7.9		
Ulmus americana																		
Bud (4)	31.7 (12.7)	238.4 (43.8)	25.2 (1.3)	1.6 (2.2)		28.9 (0.2)	−29.1 (1.3)	−20.9 (1.3)	−36.4 (1.2)	−36.4 (0.9)	−35.6 (0.9)			−7.9 (0.3)	−7.6 (0.5)	−7.1 (0.6)		
YL (4)	77.2 (67.8)	212.6 (150.4)	19.4 (17.2)	0.3 (0.5)		28.3 (0.2)	−28.3 (1.0)	−20.1 (1.0)	−33.9 (1.6)	−34.6 (2.1)	−33.5 (1.4)			−5.8 (0.7)	−6.5 (1.2)	−5.4 (0.9)		
ML (4)	13.1 (10.9)	126.4 (104.8)	23.7 (14.9)	1.9 (1.3)		29.1 (0.2)	−29.9 (0.5)	−21.7 (0.5)	−34.6 (1.1)	−34.0 (0.7)	−34.2 (1.1)	−34.6 (0.7)		−4.5 (0.9)	−4.3 (0.4)	−4.4 (0.9)		
Sbud (1)	19.5	314.3	29.7	2.0		29.1	−29.1	−20.9	−35.3	−34.8	−34.1			−6.4	−5.9	−5.2		
Litter (1)	10.2	123.8	54.6	5.1		29.4	−30.5	−22.3		−34.4	−35.0				−4.0	−4.6		

[a]Young leaves; [b]mature leaves; [c]summer buds; [d]2014 cohorts; [e]2013 and prior cohorts.

Appendix 1

Table A1. Species, dates, growth stages, and mean specific leaf area (SLA; cm^2/g) of leaves collected from the southwestern OH, USA in 2014.

Species	Date	Growth stages	*n*	Mean SLA (cm^2/g)	Std Dev of SLA
A. rubrum	4/19/2014	YL	30	22.3	19.0
A. rubrum	4/26/2014	YL	17	160.4	17.1
A. rubrum	5/3/2014	YL	18	209.8	37.9
A. rubrum	5/24/2014	YL	18	173.7	30.7
A. rubrum	6/7/2014	ML	15	178.7	49.9
A. rubrum	7/26/2014	ML	10	137.7	28.8
A. rubrum	8/30/2014	ML	20	132.1	17.9
A. rubrum	9/28/2014	ML	10	118.3	7.4
A. saccharum	4/26/2014	YL	5	343.6	119.1
A. saccharum	5/3/2014	YL	12	246.7	84.5
A. saccharum	5/24/2014	YL	18	273.2	88.8
A. saccharum	6/7/2014	ML	14	234.0	30.2
A. saccharum	7/26/2014	ML	11	250.7	73.9
A. saccharum	8/30/2014	ML	20	205.3	46.5
J. virginiana	5/24/2014	CN[c]	12	35.2	2.3
J. virginiana	5/24/2014	PN[d]	12	28.1	2.8
J. virginiana	6/28/2014	PN	12	34.8	2.3
J. virginiana	8/30/2014	PN	12	36.7	7.3
J. virginiana	11/8/2014	PN	12	33.7	1.2
S. albidum	5/3/2014	YL	18	135.6	24.2
S. albidum	5/10/2014	YL	6	228.9	32.2
S. albidum	5/24/2014	YL	18	220.8	37.3
S. albidum	6/7/2014	ML	14	185.0	30.7
S. albidum	7/26/2014	ML	12	166.4	23.0
S. albidum	8/30/2014	ML	10	224.0	32.5
S. albidum	9/28/2014	ML	23	128.8	16.5
U. americana	4/26/2014	Yla	5	116.3	23.1
U. americana	5/3/2014	YL	12	188.1	55.9
U. americana	5/24/2014	YL	17	223.4	35.4
U. americana	6/7/2014	ML[b]	15	180.0	11.8
U. americana	7/26/2014	ML	20	178.5	15.4
U. americana	8/30/2014	ML	21	178.1	38.7
U. americana	9/28/2014	ML	13	136.8	20.4

[a] Young leaves

[b] Mature leaves

[c] needles formed in 2014

[d] needles formed in 2013 & prior years

References

Angulo-sandoval, P., Aide, T.M., 2000. Effect of plant density and light availability on leaf damage in *Manilkara bidentata* (Sapotaceae). Journal of Tropical Ecology 16, 447-464.

Barbaroux, C., Bréda, N., Dufrêne, E., 2003. Distribution of above-ground and below-ground carbohydrate reserves in adult trees of two contrasting broad-leaved species (*Quercus petraea* and *Fagus sylvatica*). New Phytologist 157, 605-615.

Bongers, F., Popma, J., 1990. Leaf characteristics of the tropical rain forest flora of Los Tuxtlas, Mexico. Botanical Gazette 151, 354-365.

Boutton, T.W., 1991. Stable carbon isotope ratios of natural materials: II. Atmospheric, terrestrial, marine, and freshwater environments A2 - Coleman, David C. In: Fry, B. (Ed.), Carbon Isotope Techniques. Academic Press, pp. 173-185.

Brasell, H., Unwin, G., Stocker, G., 1980. The quantity, temporal distribution and mineral-element content of litterfall in two forest types at two sites in tropical Australia. The Journal of Ecology, 123-139.

Brendel, O., Handley, L., Griffiths, H., 2003. The $\delta^{13}C$ of Scots pine (*Pinus sylvestris* L.) needles: spatial and temporal variations. Annals of Forest Science 60, 97-104.

Brüggemann, N., Gessler, A., Kayler, Z., Keel, S., Badeck, F., Barthel, M., Boeckx, P., Buchmann, N., Brugnoli, E., Esperschütz, J., 2011. Carbon allocation and carbon isotope fluxes in the plant-soil-atmosphere continuum: a review. Biogeosciences 8, 3457-3489.

Burghardt, M., Riederer, M., 2008. Cuticular transpiration. Biology of the Plant Cuticle 23, 292-309.

Burnham, R.J., 1989. Relationships between standing vegetation and leaf litter in a paratropical forest: implications for paleobotany. Review of Palaeobotany and Palynology 58, 5-32.

Burnham, R.J., 1994. Paleoecological and floristic heterogeneity in the plant-fossil record; an analysis based on the Eocene of Washington. United States Geological Survey Bulletin 2085-B, pp. 1-36.

Cernusak, L.A., Tcherkez, G., Keitel, C., Cornwell, W.K., Santiago, L.S., Knohl, A., Barbour, M.M., Williams, D.G., Reich, P.B., Ellsworth, D.S., Dawson, T.E., Griffiths, H.G., Farquhar, G.D., Wright, I.J., 2009. Why are non-photosynthetic tissues generally ^{13}C enriched compared with leaves in C_3

plants? Review and synthesis of current hypotheses. Functional Plant Biology 36, 199-213.

Choinski Jr, J., Ralph, P., Eamus, D., 2003. Changes in photosynthesis during leaf expansion in Corymbia gummifera. Australian Journal of Botany 51, 111-118.

Choinski, J.S., Johnson, J.M., 1993. Changes in photosynthesis and water status of developing leaves of *Brachystegia spiciformis* Benth. Tree Physiology 13, 17-27.

Choinski, J.S., Wise, R.R., 1999. Leaf growth development in relation to gas exchange in *Quercus marilandica* Muenchh. Journal of Plant Physiology 154, 302-309.

Coplen, T.B., Brand, W.A., Gehre, M., Gröning, M., Meijer, H.A.J., Toman, B., Verkouteren, R.M., 2006. New guidelines for $\delta^{13}C$ measurements. Analytical Chemistry 78, 2439-2441.

Cornelissen, J., Lavorel, S., Garnier, E., Diaz, S., Buchmann, N., Gurvich, D., Reich, P., Ter Steege, H., Morgan, H., Van Der Heijden, M., 2003. A handbook of protocols for standardised and easy measurement of plant functional traits worldwide. Australian Journal of Botany 51, 335-380.

Diefendorf, A.F., Freeman, K.H., Wing, S.L., Graham, H.V., 2011. Production of *n*-alkyl lipids in living plants and implications for the geologic past. Geochimica et Cosmochimica Acta 75, 7472-7485.

Diefendorf, A.F., Freimuth, E.J., 2017. Extracting the most from terrestrial plant-derived *n*-alkyl lipids and their carbon isotopes from the sedimentary record: A review. Organic Geochemistry 103, 1-21.

Diefendorf, A.F., Mueller, K.E., Wing, S.L., Koch, P.L., Freeman, K.H., 2010. Global patterns in leaf ^{13}C discrimination and implications for studies of past and future climate. Proceedings of the National Academy of Sciences 107, 5738-5743.

Dungait, J.A., Docherty, G., Straker, V., Evershed, R.P., 2010. Seasonal variations in bulk tissue, fatty acid and monosaccharide $\delta^{13}C$ values of leaves from mesotrophic grassland plant communities under different grazing managements. Phytochemistry 71, 415-428.

Eglinton, G., Gonzalez, A.G., Hamilton, R.J., Raphael, R.A., 1962. Hydrocarbon constituents of the wax coatings of plant leaves: A taxonomic survey. Phytochemistry 1, 89-102.

Eglinton, G., Hamilton, R.J., 1967. Leaf epicuticular waxes. Science 156, 1322-1335.

Ehleringer, J.R., Field, C., Lin, Z.-f., Kuo, C.-y., 1986. Leaf carbon isotope and mineral composition in

subtropical plants along an irradiance cline. Oecologia 70, 520-526.

El-Sharkawy, M.A., De Tafur, S.M., 2007. Genotypic and within canopy variation in leaf carbon isotope discrimination and its relation to short-term leaf gas exchange characteristics in cassava grown under rain-fed conditions in the tropics. Photosynthetica 45, 515-526.

Eley, Y., Dawson, L., Pedentchouk, N., 2016. Investigating the carbon isotope composition and leaf wax *n*-alkane concentration of C_3 and C_4 plants in Stiffkey saltmarsh, Norfolk, UK. Organic Geochemistry 96, 28-42.

Ellis, B., Johnson, K.R., 2013. Comparison of leaf samples from mapped tropical and temperate forests: Implications for interpretations of the diversity of fossil assemblages. Palaios 28, 163-177.

Farquhar, G.D., Ehleringer, J.R., Hubick, K.T., 1989. Carbon isotope discrimination and photosynthesis. Annual Review of Plant Biology 40, 503-537.

Feakins, S.J., Levin, N.E., Liddy, H.M., Sieracki, A., Eglinton, T.I., Bonnefille, R., 2013. Northeast African vegetation change over 12 my. Geology 41, 295-298.

Flanagan, B.L., Cook, S.C., Ehleringer, R.J., 1997. Unusually low carbon isotope ratios in plants from hanging gardens in southern Utah. Oecologia 111, 481-489.

Freeman, K.H., Colarusso, L.A., 2001. Molecular and isotopic records of C_4 grassland expansion in the late Miocene. Geochimica et Cosmochimica Acta 65, 1439-1454.

Freeman, K.H., Pancost, R.D., 2014. Biomarkers for terrestrial plants and climate. In: Turekian, H.D., Holland, K.K. (Eds.), Treatise on Geochemistry. second ed. Elsevier, pp. 395-416.

Freimuth, E.J., Diefendorf, A.F., Lowell, T.V., 2017. Hydrogen isotopes of *n*-alkanes and *n*-alkanoic acids as tracers of precipitation in a temperate forest and implications for paleorecords. Geochimica et Cosmochimica Acta 206, 166-183.

Garten, C.T., Taylor, G.E., 1992. Foliar $\delta^{13}C$ within a temperate deciduous forest: spatial, temporal, and species sources of variation. Oecologia 90, 1-7.

Giese, B.N., 1975. Effects of light and temperature on the composition of epicuticular wax of barley leaves. Phytochemistry 14, 921-929.

Gordon, J.C., Larson, P.R., 1968. Seasonal course of photosynthesis, respiration, and distribution of ^{14}C in young *Pinus resinosa* trees as related to wood formation. Plant Physiology 43, 1617-1624.

Graham, H., Freeman, K., 2013. Fossil leaves and fossil leaf *n*-alkanes: reconstructing the first closed canopied rainforests. American Geophysical Union Fall Meeting 2013 Abstracts #PP34B-02.

Graham, H.V., 2014. Molecular and Isotopic Indicators of Canopy Closure in Ancient Forests and the Effects of Environmental Gradients on Leaf Alkane Expression. The Pennsylvania State University. pp. 1-206

Graham, H.V., Patzkowsky, M.E., Wing, S.L., Parker, G.G., Fogel, M.L., Freeman, K.H., 2014. Isotopic characteristics of canopies in simulated leaf assemblages. Geochimica et Cosmochimica Acta 144, 82-95.

Greenwood, D.R., 1991. The Taphonomy of Plant Macrofossils, the Processes of Fossilization. Belhaven Press, London, pp. 141-169.

Hanba, Y.T., Mori, S., Lei, T.T., Koike, T., Wada, E., 1997. Variations in leaf $\delta^{13}C$ along a vertical profile of irradiance in a temperate Japanese forest. Oecologia 110, 253-261.

Hauke, V., Schreiber, L., 1998. Ontogenetic and seasonal development of wax composition and cuticular transpiration of ivy (*Hedera helix* L.) sun and shade leaves. Planta 207, 67-75.

Hoch, G., Siegwolf, R.T., Keel, S.G., Korner, C., Han, Q., 2013. Fruit production in three masting tree species does not rely on stored carbon reserves. Oecologia 171, 653-662.

Hunt, R., Cornelissen, J., 1997. Components of relative growth rate and their interrelations in 59 temperate plant species. New Phytologist 135, 395-417.

Jäggi, M., Saurer, M., Fuhrer, J., Siegwolf, R., 2002. The relationship between the stable carbon isotope composition of needle bulk material, starch, and tree rings in *Picea abies*. Oecologia 131, 325-332.

Jenks, M., Wood, A., 2002. Critical issues with the plant cuticle's function in drought tolerance. Biochemical and Molecular Responses of Plants to the Environment, 97-127.

Jetter, R., Riederer, M., 2016. Localization of the transpiration barrier in the epi-and intracuticular waxes of eight plant species: water transport resistances are associated with fatty acyl rather than alicyclic

components. Plant Physiology 170, 921-934.

Jetter, R., Schäffer, S., Riederer, M., 2000. Leaf cuticular waxes are arranged in chemically and mechanically distinct layers: evidence from *Prunus laurocerasus* L. Plant, Cell & Environment 23, 619-628.

Jetter, R., Stefanie, S., xe, ffer, 2001. Chemical composition of the *Prunus laurocerasus* leaf surface. Dynamic changes of the epicuticular wax film during leaf development. Plant physiology 126, 1725-1737.

Johnson, D.M., McCulloh, K.A., Woodruff, D.R., Meinzer, F.C., 2012. Hydraulic safety margins and embolism reversal in stems and leaves: why are conifers and angiosperms so different? Plant Science 195, 48-53.

Kahmen, A., Dawson, T.E., Vieth, A., Sachse, D., 2011. Leaf wax *n*-alkane δD values are determined early in the ontogeny of *Populus trichocarpa* leaves when grown under controlled environmental conditions. Plant, Cell & Environment 34, 1639-1651.

Kerstiens, G., 1996. Diffusion of water vapour and gases across cuticles and through stomatal pores presumed closed. In: Kerstiens, G. (Ed.), Plant cuticles: an integrated functional approach. Bios Scientific Publishers, Oxford, UK, pp. 121–134.

Knohl, A., Werner, R.A., Brand, W.A., Buchmann, N., 2005. Short-term variations in $\delta^{13}C$ of ecosystem respiration reveals link between assimilation and respiration in a deciduous forest. Oecologia 142, 70-82.

Kohn, M.J., 2010. Carbon isotope compositions of terrestrial C_3 plants as indicators of (paleo) ecology and (paleo) climate. Proceedings of the National Academy of Sciences 107, 19691-19695.

Kolbe, S.E., Miller, A.I., Cameron, G.N., Culley, T.M., 2016. Effects of natural and anthropogenic environmental influences on tree community composition and structure in forests along an urban-wildland gradient in southwestern Ohio. Urban Ecosystems 19, 915-938.

Lacointe, A., Kajji, A., Daudet, F.-A., Archer, P., Frossard, J.-S., Saint-Joanis, B., Vandame, M., 1993. Mobilization of carbon reserves in young walnut trees. Acta Botanica Gallica 140, 435-441.

Lambers, H., Poorter, H., 1992. Inherent variation in growth rate between higher plants: a search for physiological causes and ecological consequences. Advances in Ecological Research 23, 187-261.

Li, R., Meyers, P.A., Fan, J., Xue, J., 2016. Monthly changes in chain length distributions and stable carbon isotope composition of leaf *n*-alkanes during growth of the bamboo *Dendrocalamus ronganensis* and the grass *Setaria viridis*. Organic Geochemistry 101, 72-81.

Lockheart, M.J., Van Bergen, P.F., Evershed, R.P., 1997. Variations in the stable carbon isotope compositions of individual lipids from the leaves of modern angiosperms: implications for the study of higher land plant-derived sedimentary organic matter. Organic Geochemistry 26, 137-153.

Lowdon, J.A., Dyck, W., 1974. Seasonal variations in the isotope ratios of carbon in maple leaves and other plants. Canadian Journal of Earth Sciences 11, 79-88.

Lowman, M.D., 1985. Temporal and spatial variability in insect grazing of the canopies of five Australian rainforest tree species. Australian Journal of Ecology 10, 7-24.

Madigosky, S.R., 2004. CHAPTER 2 - Tropical Microclimatic Considerations A2 - Lowman, Margaret D. In: Rinker, H.B. (Ed.), Forest Canopies (Second Edition). Academic Press, San Diego, pp. 24-48.

Magill, C.R., Ashley, G.M., Freeman, K.H., 2013. Ecosystem variability and early human habitats in eastern Africa. Proceedings of the National Academy of Sciences 110, 1167-1174.

Medina, E., Minchin, P., 1980. Stratification of $\delta^{13}C$ values of leaves in Amazonian rain forests. Oecologia 45, 377-378.

Meinzer, F.C., Woodruff, D.R., Eissenstat, D.M., Lin, H.S., Adams, T.S., McCulloh, K.A., 2013. Above- and belowground controls on water use by trees of different wood types in an eastern US deciduous forest. Tree Physiology 33, 345-356.

Mihailova, A., Abbado, D., Kelly, S.D., Pedentchouk, N., 2015. The impact of environmental factors on molecular and stable isotope compositions of *n*-alkanes in Mediterranean extra virgin olive oils. Food Chemistry 173, 114-121.

Mueller, K.E., Diefendorf, A.F., Freeman, K.H., Eissenstat, D.M., 2010. Appraising the roles of nutrient availability, global change, and functional traits during the angiosperm rise to dominance. Ecology

Letters 13, E1-E6.

Newberry, S.L., 2015. *n*-Alkane biosynthetic hydrogen isotope fractionation is not constant throughout the growing season in the riparian tree *Salix viminalis*. Geochimica et Cosmochimica Acta 165, 75-85.

O'Leary, M.H., 1981. Carbon isotope fractionation in plants. Phytochemistry 20, 553-567.

O'Leary, M.H., Madhavan, S., Paneth, P., 1992. Physical and chemical basis of carbon isotope fractionation in plants. Plant, Cell & Environment 15, 1099-1104.

Ometto, J.P.H.B., Ehleringer, J.R., Domingues, T.F., Berry, J.A., Ishida, F., Y., Mazzi, E., Higuchi, N., Flanagan, L.B., Nardoto, G.B., Martinelli, L.A., 2006. The stable carbon and nitrogen isotopic composition of vegetation in tropical forests of the Amazon Basin, Brazil. Biogeochemistry 79, 251-274.

Parker, G.G., O'Neill, J.P., Higman, D., 1989. Vertical profile and canopy organization in a mixed deciduous forest. Plant Ecology 85, 1-11.

Pataki, D.E., Ehleringer, J.R., Flanagan, L.B., Yakir, D., Bowling, D.R., Still, C.J., Buchmann, N., Kaplan, J.O., Berry, J.A., 2003. The application and interpretation of Keeling plots in terrestrial carbon cycle research. Global Biogeochemical Cycles 17(1), 1-14.

Phillipson, J., Thompson, D.J., 1983. Phenology and intensity of phyllophage attack on *Fagus sylvatica* in Wytham Woods, Oxford. Ecological Entomology 8, 315-330.

Piasentier, E., Bovolenta, S., Malossini, F., 2000. The *n*-alkane concentrations in buds and leaves of browsed broadleaf trees. The Journal of Agricultural Science 135, 311-320.

Reich, P., Uhl, C., Walters, M., Ellsworth, D., 1991. Leaf lifespan as a determinant of leaf structure and function among 23 Amazonian tree species. Oecologia 86, 16-24.

Reynhardt, E., 1997. The role of hydrogen bonding in the cuticular wax of *Hordeum vulgare* L. European Biophysics Journal 26, 195-201.

Riederer, M., Schreiber, L., 1995. Waxes: the transport barriers of plant cuticles. The Oily Press: Dundee, Scotland, pp. 131-156.

Schreiber, L., 2006. Characterisation of polar paths of transport in plant cuticles. In: Riederer, M., Müller,

C. (Eds.), Biology of the plant cuticle. Annual Plant Reviews. Blackwell Publishing, pp. 280–291.

Shepherd, T., Wynne Griffiths, D., 2006. The effects of stress on plant cuticular waxes. New Phytologist 171, 469-499.

Snider, J.L., Choinski, J.S., Wise, R.R., 2009. Juvenile *Rhus glabra* leaves have higher temperatures and lower gas exchange rates than mature leaves when compared in the field during periods of high irradiance. Journal of Plant Physiology 166, 686-696.

Thomas, S.C., Sztaba, A.J., Smith, S.M., 2010. Herbivory patterns in mature sugar maple: variation with vertical canopy strata and tree ontogeny. Ecological Entomology 35, 1-8.

Tipple, B.J., Berke, M.A., Doman, C.E., Khachaturyan, S., Ehleringer, J.R., 2013. Leaf-wax *n*-alkanes record the plant-water environment at leaf flush. Proceedings of the National Academy of Sciences 110, 2659-2664.

Tipple, B.J., Pagani, M., 2010. A 35Myr North American leaf-wax compound-specific carbon and hydrogen isotope record: Implications for C_4 grasslands and hydrologic cycle dynamics. Earth and Planetary Science Letters 299, 250-262.

Troeng, F., Linder, S., 1982. Gas exchange in a 20-year-old stand of Scots pine, I. Net photosynthesis of current and one-year-old shoots within and between seasons. Physiologia Plantarum 54, 7-14.

van der Merwe, N.J., Medina, E., 1991. The canopy effect, carbon isotope ratios and foodwebs in amazonia. Journal of Archaeological Science 18, 249-259.

Vogel, J., 1978. Recycling of carbon in a forest environment. Oecologia Plantarum 13, 89-94.

White, J., Vaughn, B., Michel, S., 2011. Stable isotopic composition of atmospheric carbon dioxide (^{13}C and ^{18}O) from the NOAA ESRL carbon cycle cooperative global air sampling network, 1990–2012, Version: 2013-04-05. University of Colorado, Institute of Arctic and Alpine Research (INSTAAR). ftp. cmdl. noaa. gov/ccg/co2c13/flask/event/,(last access 21 September 2012).

Woodall, G., Dodd, I., Stewart, G., 1998. Contrasting leaf development within the genus Syzygium. Journal of Experimental Botany, 79-87.

Wu, M.S., Feakins, S.J., Martin, R.E., Shenkin, A., Bentley, L.P., Blonder, B., Salinas, N., Asner, G.P.,

Malhi, Y., 2017. Altitude effect on leaf wax carbon isotopic composition in humid tropical forests. Geochimica et Cosmochimica Acta 206, 1-17.

Zimmerman, J.K., Ehleringer, J.R., 1990. Carbon isotope ratios are correlated with irradiance levels in the Panamanian orchid *Catasetum viridiflavum*. Oecologia 83, 247-249.

Chapter 3: Using GIS-based isoscapes and isotope mixing models to explore controls on leaf wax integration and transport from the Mississippi River Basin to the Gulf of Mexico

ABSTRACT

Understanding the fate of terrestrial leaf waxes during transport from source to sink is important for accurate interpretation of paleo-records and constraining carbon and water cycling. However, there is limited knowledge of processes and controls on leaf wax integration and transport in catchments with various vegetation and climatic conditions. This study constrained climatic and ecologic controls on leaf wax transport and integration from the Mississippi River Basin (MRB), the largest river in the U.S., to the Gulf of Mexico (GOM). We first developed geographic representation of *n*-alkane carbon ($\delta^{13}C_{alk}$) and hydrogen (δD_{alk}) isotopic compositions (i.e. isoscapes) using plant isotope fractionation calibrations from North America or similar climate regions. Then, the isoscapes were weighted by area of the vegetation (*area model*), runoff (*runoff model*), net primary productivity (NPP model), and *n*-alkane production (*production model*) by *n*-alkane homologues to constrain their influences on leaf wax sourcing using linear mixing models. We also combined NPP and leaf wax production to test the total wax biomass controls (*NP model*) on wax integration. The total wax biomass was combined with runoff to consider both transport and productivity (*RNP model*). The modeled results were compared to measured leaf wax isotope values in sediments from the northeastern GOM (ODP 625B). The *area models* could not capture the strong C_3 signals found in measured values in sediments. *Runoff*, *NPP*, and *production models* predicted a slightly higher leaf wax export from C_3 forested areas than the *area models*. The two combination models, *NP* and *RNP models*, better matched with the measured values, especially the latter model, suggesting that both runoff and productivity affect wax integration and transport. Between chain lengths, *n*-C_{29} alkanes consistently underestimated grassland contribution, while *n*-C_{31} was more sensitive to grasses. The *n*-C_{33} alkanes showed highest sensitivity to the grassland due to their high production in

grasses. We also observed reduced vegetation effects on ε_{app} values due not only to opposing trends of grassland ε_{app} values and deuterium enrichment, but also to export bias towards more humid forested areas. The results confirmed that leaf wax export is not spatially uniform and therefore runoff and productivity have to be taken into account when interpreting sedimentary leaf wax records.

1. Introduction

Long-chain *n*-alkanes are one of the epicuticular leaf wax constituents produced by terrestrial higher plants with a primary role of protecting leaves from water loss, bacterial and fungal pathogens and UV light sorption (Domínguez et al., 2011; Eglinton et al., 1962; Kunst et al., 2005). These high-molecular-weight *n*-alkanes possess information on a plant's growth environment. For example, carbon ($\delta^{13}C_{alk}$) and hydrogen (δD_{alk}) isotopic compositions of *n*-alkanes mainly reflect vegetation (C_3 vs. C_4 plants) and plant source water δD values (i.e. precipitation; δD_p), respectively (Rieley et al., 1991; Sachse et al., 2004). *n*-Alkanes are transported, deposited, and preserved in geologic archives such as continental, lake, and marine sediments, and provide evidence of past ecological and hydrologic change. Therefore, geologic leaf wax isotopes have been used to address a wide range of inquiries such as reconstructing rainfall changes (Niedermeyer et al., 2014), explaining global warmth (Pagani et al., 2006), or strength of monsoonal moisture inflow (Schefuß et al., 2005).

Despite increasing use of leaf wax isotopic compositions for paleoenvironment reconstructions, the processes from production to transportation and burial in the sediments (i.e. taphonomy), which ultimately determine their isotopic composition in sedimentary archives is poorly understood (Diefendorf and Freimuth, 2017; Galy et al., 2011; Hoffmann et al., 2016). In temperate forests, leaf wax signals may be dominated by canopy leaves of C_3 angiosperm trees as they have high biomass and *n*-alkanes production (e.g. Burnham, 1989; Burnham and Johnson, 1994; Diefendorf et al., 2011; Ellis and Johnson, 2013; Suh and Diefendorf, 2017; Greenwood, 1991; Parker et al., 1989), although variations exist in tropical forests (Graham et al., 2014). Several studies measured leaf wax isotopic compositions in lacustrine sediments from a wide range of climate zones and vegetation types, and found that *n*-alkanes were also dominated by angiosperm trees even in sites with high grassland distribution (Garcin et al., 2014; Sachse et al., 2012; Seki et al., 2010). These prior studies suggest that grasses are under-represented in lacustrine sediments due to differences in transport efficiency and leaf wax productivity between

grasses and trees, which also varies with alkane chain length. For example, angiosperms produce more *n*-C_{29} than C_4 grasses, while most C_4 grasses produce more *n*-C_{33} alkanes than angiosperm trees (Diefendorf et al., 2011; Rommerskirchen et al., 2006; Vogts et al., 2009). Further, plant biomass or net primary productivity (NPP) varies with climatic and environmental variables such as precipitation, temperature, evapotranspiration and soil nutrient content (Cramer et al., 1999; Lieth, 1975; McGuire et al., 1992; Saugier et al., 2001).

In fluvial systems, productivity (i.e. NPP and wax production) alone cannot explain leaf wax transport and integration. Erosion is known to control the amount of river flow and sediment transport (Garzanti et al., 2007; Just et al., 2014). Erosion is related to precipitation and topography, and they vary spatially and temporally, therefore terrigenous inputs from different parts of a drainage basin may not be uniform (Hoffmann et al., 2016; Just et al., 2014). Prior studies also observed replacement of leaf waxes along fluvial systems in response to changing vegetation zones and climate, indicating that *n*-alkanes from vegetation upstream get swamped by more local vegetation inputs (Galy et al., 2011; Galy et al., 2008; Ponton et al., 2014). Moreover, during transit, organic matter can undergo degradation, reworking, hydrodynamic soring by size, density and shape, and mixing with allochthonous carbon sources (Aller et al., 2008; Bianchi et al., 2004; Blair and Aller, 2012; Goñi et al., 1997; Pearson and Eglinton, 2000; Tao et al., 2016). However, these prior studies do not extend to marine sediments, which are commonly used to reconstruct terrestrial vegetation and hydrology (Bird et al., 1995; Freeman and Colarusso, 2001; Pagani et al., 2000; Tipple and Pagani, 2010). Understanding controls on leaf wax provenance and modification in fluvial systems to marine sediments is important for informed interpretation of river-influenced marine sedimentary records.

Therefore, in this study, we investigated the provenance and integration of plant waxes from the largest fluvial system in the United States, the Mississippi River Basin (MRB) to the Gulf of Mexico (GOM). We constructed geographic distribution of leaf wax carbon and hydrogen isotopes (i.e. isoscapes) for the

potential natural vegetation cover (ISLSCP II; Ramankutty and Foley, 2010) under current climate (1986-1995) without human activities, and mid-Holocene vegetation (i.e. 7 to 5 kyr; Cotton et al., 2016) using plant isotopic fractionation calibrations (Diefendorf and Freimuth, 2017; Hou et al., 2007a; Liu et al., 2006; Smith and Freeman, 2006). We used different approaches to estimate isotopic fractionations to build leaf wax carbon and hydrogen isoscapes, and discussed advantages and disadvantages of using each approach. We tested the relative influence of changes in leaf wax source and integration by climate and productivity on $\delta^{13}C_{alk}$ and δD_{alk} values in fluvial and marine sediments using GIS-based spatial analysis. Because modern samples of water and sediments in the MRB are significantly affected by anthropogenic activities (Zhuang et al., 2014), we compared the modeled results to the Holocene-age sediments spanning from 9 to 3 kyr in ODP 625B core from the northeastern GOM. This study results helps constrain where leaf waxes in the GOM originate and what part of vegetation and hydrologic signals are recorded in these biomarkers. Such information will be critical in refining paleoclimate interpretations both in the GOM and other marine settings that integrate plant waxes.

2. Method

2.1. Study site

2.1.1. Mississippi River basin

The MRB is the largest drainage system in the United States; it drains approximately 41% of the conterminous US from Rocky to Appalachian mountains (Kammerer, 1987). The MRB consists of five major sub-basins: 1) Ohio-Tennessee River basin, 2) Upper MRB, 3) Missouri River basin, 4) Arkansas-Red River basin, and 5) Lower MRB (Fig. 1A). Under current climate conditions, the Ohio River has the largest mean annual discharge (~8,000 m^3/s), followed by the Upper Mississippi River (~5000 m^3/s),

Missouri River (~2000 m^3/s), and Arkansas-Red River (~1,500 m^3/s) (USGS). The mean annual precipitation (MAP) increases from west to east in MRB ranging from ca. 200 to 1800 mm with an average of ca. 800 mm (Fig. 1C; http://prism.oregonstate.edu). The mean annual temperature (MAT) ranges from ca. 0°C to 20°C (average MAT of 10°C), with higher temperatures towards the south and lower temperatures in the northwestern MRB (http://prism.oregonstate.edu).

The vegetation in MRB mirrors the west to east increase in moisture availability with grasslands in the west and deciduous and mixed forests in the east (Harrington and Harman, 1991). Ramankutty and Foley (2010) predicted global potential vegetation cover in the absence of human activities for the present-day climate (Fig. 1B). Their map indicates that natural vegetation in the MRB consists of grassland (55%), temperate deciduous forest (TDF; 23%), temperate needleleaf evergreen forest (TNEF; 6%), mixed forest (MF; 6%), shrubland (6%), boreal evergreen forest (BEF; 2%) and tundra (< 1%). From this potential vegetation map, we determined C_3 and C_4 grassland composition using a temperature crossover approach (Still et al., 2003), which suggests that C_3 grasses occupies 26% while C_4 grasses covers 29% of the MRB. Another study by Cotton et al. (2016) independently determined a similar extent of C_4 grasses during the mid-Holocene (31%) based on $\delta^{13}C$ values of bison and mammoth tissues.

2.2. n-Alkane carbon isoscape construction

We used the geographic information systems (GIS) software ArcMap 10.5 to develop isoscape maps. The GIS workflow is illustrated in Figure 2. $\delta^{13}C_{alk}$ values reflect atmospheric CO_2 $\delta^{13}C$ ($\delta^{13}C_{CO2}$) values and carbon isotope fractionation in plants during photosynthesis (Δ_{leaf} or $\varepsilon_{leaf\text{-}CO2}$) and lipid biosynthesis ($\varepsilon_{alk\text{-}leaf}$). We used pre-industrial $\delta^{13}C_{CO2}$ value of −6.5‰ (Tipple et al., 2010). The Δ_{leaf} values vary primarily with photosynthetic pathways and mean annual precipitation (MAP) among C_3 plants (Diefendorf et al., 2010; Farquhar et al., 1989; Graham et al., 2014; Kohn, 2010; O'Leary, 1981; O'Leary et al., 1992). Plants using the C_3 photosynthetic pathway, have larger Δ_{leaf} values, while C_4 pathway plants have smaller Δ_{leaf}

values (Farquhar et al., 1989). The magnitude of $\varepsilon_{alk\text{-}leaf}$ varies between photosynthetic pathways and major plant types (i.e. angiosperms and gymnosperms).

First, we need a vegetation cover map to assign carbon isotope fractionations. There are different approaches to estimate vegetation cover (i.e. modeled or reconstructed), and $\delta^{13}C$ values can be assigned by biome or as a function of other parameters, like precipitation. Additionally, grasslands can have variable amounts of C_3 and C_4 grasses within this biome. Rather than settling on one approach, we chose two very different methods to assign $\delta^{13}C$ values and to estimate C_4 grassland distribution in the MRB. The first approach, the *biome-based isoscape* utilizes a ISLSCP II Potential Natural Vegetation Cover by Ramankutty and Foley (2010). This map represents biome distribution for modern climate (1986-1995) in the absence of human activities. It is estimated using a simple algorithm to correct contemporary satellite data for cropland inventory (Ramankutty and Foley, 1999). We assigned Δ_{leaf} values to each biome based on a modern survey (Appendix Table A1; Diefendorf et al., 2010; Lloyd and Farquhar, 1994). To predict C_4 vegetation within the grassland biome, we incorporated the temperature crossover relationship of Still et al. (2003) that predicts when C_4 grasses outcompete C_3 grasses. When pCO_2 is constant, this relationship is based solely on temperature. As such, this model results in binary C_3 and C_4 vegetation assignments for each grid cell within the grassland biome. Plant $\delta^{13}C$ values were then converted to $\delta^{13}C_{alk}$ values using *n*-alkane biosynthetic fractionation factors ($\varepsilon_{alk\text{-}leaf}$) for the most dominant plant type (i.e. angiosperm trees, C_3 grasses and C_4 grasses) and chain lengths (Table A2).

The second approach, the *MAP-based isoscape* (Section 2.2; Fig. 3F), we used spatial C_4 plant distribution data for the North America for the mid-Holocene from Cotton et al. (2016). Their $\%C_4$ map is estimated based on the relationship between climate and C_3-C_4 plant distribution, determined from classification and regression tree analysis using $\delta^{13}C$ values of bison and mammoth tissues and climatic variables. We used this dataset since it is derived from geologic archives with high spatial resolution in $\delta^{13}C$ values for the time period that we can compare to the GOM sediment results. This approach does not

use biome geography; instead it incorporates grassland paleovegetation from the mid-Holocene (Cotton et al., 2016) to assign $\%C_3$ and $\%C_4$ composition. This approach is also not binary; it reflects a continuum of C_3 and C_4 abundance. The MRB boundary shapefile (USGS) was used to extract $\%C_4$ raster data of the basin. For C_3 plant covered regions, Δ_{leaf} values were estimated using the MAP-Δ_{leaf} relationships from Diefendorf et al. (2010). Then leaf $\delta^{13}C$ values were converted to $\delta^{13}C_{alk}$ values using $\varepsilon_{alk\text{-}leaf}$ values assigned by the most dominant plant type (i.e. angiosperm trees, C_3 grasses and C_4 grasses) as well as by three *n*-alkane chain lengths (*n*-C_{29}, *n*-C_{31}, and *n*-C_{33}). For both isoscapes, we used Δ_{leaf} and ε_{alk} values for only angiosperms as they produce *n*-alkanes in higher abundance and dominate sedimentary records than other plant types (Diefendorf et al., 2011; Garcin et al., 2014; Sachse et al., 2012). We used standard deviations of Δ_{leaf} and $\varepsilon_{alk\text{-}leaf}$ values to propagate uncertainties at the basin-level. These uncertainties are ± 2.7‰ for *n*-C_{29}, ± 2.4‰ for *n*-C_{31}, ± 2.1‰ for *n*-C_{33}.

2.3. n-Alkane hydrogen isoscape construction

The δD_{alk} values reflect mean annual precipitation δD values (δD_p; Fig. 1E) and apparent fractionation (ε_{app}) between δD_p and *n*-alkanes (Sachse et al., 2012). The ε_{app} values reflect biosynthetic fractionation during plant metabolism including lipid biosynthesis, and have been found to vary by vegetation type, largely between grasses ($C_3 = -177 \pm 17$‰; $C_4 = 155 \pm 10$‰) and trees (-130 ± 13‰) (Hou et al., 2007b; Liu et al., 2006; Smith and Freeman, 2006). However, several studies reported relatively constant ε_{app} values in sediments or soils across a wide climatic range suggesting a canceling of low ε_{app} values in grasslands by leaf water D-enrichment with relative humidity (RH) (Feakins and Sessions, 2010; Hou et al., 2008; McInerney et al., 2011). To constrain effects of vegetation on ε_{app} values in MRB, we developed two isoscape models for δD_{alk}. First, *biome-based isoscape* model uses ε_{app} values assigned by biome and grassland C_3 and C_4 composition. Second, the *RH-based isoscape* model incorporates effects of RH on the D-enrichment in grasses (McInerney et al., 2011; Smith and Freeman, 2006). The long-term RH raster data was taken from http://www.esrl.noaa.gov/psd/. We used the potential vegetation cover map by

Ramankutty and Foley (2010) with C_4 grassland boundary determined by temperature crossover approach. We used 30-year average δD_p values (Bowen, 2014) and mean ε_{app} values by biomes, photosynthetic pathways, and chain lengths (*n*-C_{27}, *n*-C_{29}, and *n*-C_{31}) measured from plants in the U.S. or in similar climate regions (Table A1; Liu et al., 2006; Smith and Freeman, 2006; Hou et al., 2007). We did not model *n*-C_{33} alkanes due to insufficient modern calibrations. We used standard deviations of ε_{app} values to propagate uncertainties at basin-level: ± 14.2‰ for *n*-C_{29} and ± 13.8‰ for *n*-C_{31}.

2.4. Parameters weighted mixing models using GIS

To constrain controls on leaf wax integration in the MRB, we used weighted mixing models for the following parameters: area, runoff, NPP, and leaf wax production. We refer to each model as *area model*, *runoff model*, *NPP model*, and *production model*, respectively. We combined NPP and leaf wax production to estimate the total leaf wax biomass, and this is referred to as *NP model*. As leaf wax biomass alone cannot explain the transport processes, we combined the total leaf wax biomass and runoff, and this is called as *RNP model*. As a total, we have sex mixing models for two $\delta^{13}C_{alk}$ isoscapes from *n*-C_{29} to *n*-C_{33}, and two δD_{alk} isoscapes from *n*-C_{27} to *n*-C_{31}.

The number of grid cells that correspond to each vegetation are weighed in the *area model*s. For the *runoff models*, we used 30-year MAP at 4 km resolution (Fig. 1C; PRISM) as a first-order approximation of runoff. For the *NPP models*, we used the NPP data that are estimated by applying the Carnegie-Ames-Stanford Approach terrestrial carbon model to satellite data and surface climatology by Imhoff et al. (2004). We transformed their post-urban NPP to pre-urban NPP by replacing urban and peri-urban areas with average post-urban NPP values calculated for non-urban lands within a 3-km radius of the urban cell (Fig. 1D). For the *n*-alkane *production model*, average *n*-alkane concentrations of major plant types were used from a recent review paper by Diefendorf and Freimuth (2017; Table A4 and Fig. 3A-3B). These measurements are based on modern plant leaves, and high variations are observed within the same growth

forms and photosynthetic pathways. Consequently, quantifying the production bias using these data may not be proper. However, higher *n*-C_{33} alkane production in C_4 grasses, and higher *n*-C_{29} alkanes in trees has been consistently observed (Rommerskirchen et al., 2006; Vogts et al., 2009). Therefore, weighting average production values will allow us to explore general patterns and variations in *n*-alkane integration by different homologues. For the combination models, we combined the parameters by multiplying them prior to weighting. The parameters are then weighted to carbon and hydrogen isoscapes to predict $\delta^{13}C$ and δD values at the basin-level using the following mixing model:

$$\delta_{weighted} = \frac{\sum_{i=1}^{n} C_i \delta_i}{\sum_{i=1}^{n} C_i} \quad (1)$$

where C_i represents values of the controls in each grid cell, δ_i is the isotope value assigned to each grid cell and n is the number of grid cells.

2.5. Holocene leaf waxes from ODP 625B core

We measured $\delta^{13}C_{alk}$ and δD_{alk} values in three Holocene sediment samples from the northeastern GOM (ODP core 625B; 28.83°N, 87.16°W; indicated by yellow dot in Fig. 1) near the MR discharge point. This core was retrieved during the Ocean Drilling Program (ODP) Leg 100 in 1985. The core site is about 200 km away from the MR delta and at 889 m water depth (Rabinowitz et al., 1985). Three radiocarbon dates have been obtained for the upper 100 cm and they correspond to the Holocene (^{14}C age: 1-2 cm = 1,970 ± 25 yr; 50-51 cm = 5,300 ± 30 yr; 98-100 cm = 10,600 ± 40 yr; Limoges et al., 2014). Based on estimated sedimentation rates calculated using the three published ^{14}C dates, our three samples correspond to 3.1 (21-23 cm), 6.7 (57-59 cm), and 9.5 kyr (80-82 cm) (Table 2).

Sediment samples were freeze-dried and powdered using a Spex ball mill. Lipids were extracted from ca.

20 g of powdered sediment using an accelerated solvent extractor (ASE; Dionex 350) with dichloromethane (DCM)/methanol (MeOH) (2:1, v/v) at ~7.6 mpa (~1100 psi) and 100 ºC for three extraction cycles. The total lipid extract was then base saponified to cleave fatty esters with 2.5 ml of 0.5 N KOH in MeOH/H_2O (3:1, v/v) for 2 h at 75°C. After cooling the saponified lipid extract (SLE) to room temperature, ~3 ml of NaCl in water (5%, w/w) was added and was acidified by adding ~0.5 ml of 6 N HCl to a pH of ~1. The acidic solution was extracted using Hexane/DCM (4:1, v/v). The saponified lipids were then neutralized with $NaHCO_3$/H_2O (5%, w/w) and dried with Na_2SO_4. We separated the SLE into acid and neutral fractions with 0.5 g of aminopropyl (Supelco Supelclean LC-NH_2). The neutral fraction was eluted with 4 ml 2:1 DCM/IPA.

n-Alkanes were analysed using an Agilent 7890A GC-MS and flame ion detection (FID) interfaced to an Agilent 5975C quadrupole mass selective detector (MSD) with electron-impact ionization (70 eV). Compounds were separated on a fused silica capillary column (Agilent J&W DB-5 ms; 30 m, 0.25 mm ID, 25-µm film thickness) and a 5 m guard column (Restek Rxi, 5 m, 0.32 mm) was used with helium as the carrier gas. The oven started at 60°C initially for 1 min and was increased to 320°C at 6°C/min, and a final hold of 15 min. The column effluent was split (1:1) between the FID and MSD with a 2-way splitter (Agilent G3180B) at a constant pressure (182 Pa). Compounds were identified using authentic standards, library databases (NIST 2008 and Wiley 2009), spectral library, and retention times.

Prior to quantification, all samples were diluted in hexane with an internal standard, 1,1′-binaphthyl, at 25 µg/ml. The compound peak areas were normalized to those of 1,1′-binaphthyl and converted to concentrations using response curves of an in-house mixture of *n*-alkanes at concentrations ranging from 0.5 to 100 µg/ml. Compound concentrations were normalized to the mass of dry sediment extracted. Precision and accuracy were determined by analyzing *n*-alkane standards at 25 µg/ml and were 0.85 µg/ml (1σ, n = 46) and -0.13 µg/ml (1σ, n = 46), respectively.

Prior to $\delta^{13}C_{alk}$ and δD_{alk} analysis, the hydrocarbon fraction was separated into a saturated and unsaturated fraction by eluting with 4 ml hexanes and 4 ml ethyl acetate, respectively, using 5% silver nitrate impregnated silica gel. *n*-Alkanes were further separated from unresolved complex mixture (UCM) by urea adduction. *n*-Alkanes were analyzed using Thermo Trace GC Ultra coupled to a Thermo Electron Delta V Advantage IRMS instrument, via an isolink combustion reactor for $\delta^{13}C$ at 1100°C and pyrolysis reactor for δD at 1420°C. GC conditions were similar to the above, but with a faster ramp rate (8°C/min). The H_3^+ factor was tested daily and averaged 4.9 ppm mV^{-1} during the period of analysis. The $\delta^{13}C$ and δD values of the compounds were determined relative to a reference gas calibrated with Mix A5 standards (*n*-C_{16} to *n*-C_{30}; Arndt Schimmelmann, Indiana University) that were run every 5 to 10 samples (see Polissar and D'Andrea, 2014). $\delta^{13}C$ and δD values of the samples are reported in delta notation relative to the standard VPDB and VSMOW/VSLAP, respectively, following Coplen et al. (2006a) and Coplen (2011). Precision and accuracy of $\delta^{13}C$ analyses are 0.1 ‰ (n = 78) and −0.1‰ (n = 78), respectively. For δD values, the long term standard deviation for the A5 standards was 4.1‰ (1σ, n = 33).

3. Results

3.1. n-Alkane isoscapes of the MRB

Table 3 summarizes $\delta^{13}C_{alk}$ values for *biome-* and *MAP-based isoscapes* for different parameters weighted models from *n*-C_{29} to *n*-C_{33} alkanes. In *biome-based isoscape*, the basin mean $\delta^{13}C_{alk}$ values ranged from ca. −34‰ to −19‰, without much variations between chain lengths (Figure 3C). The $\delta^{13}C_{alk}$ values in the southeastern forested areas such as needleleaf evergreen forest and temperate and mixed forests ranged between −34‰ and −31‰, while grasslands had values from −30‰ (C_3) to −19‰ (C_4). In the *MAP-based isoscape*, $\delta^{13}C_{alk}$ values ranged from ca. −34‰ to −23‰, without significant variations between chain lengths (Fig. 3D). The southeastern forests had $\delta^{13}C_{alk}$ values around ca. −33‰ to −32‰, while

western grasslands had values from ca. −29‰ to −23‰. The overall spatial patterns were similar between the *biome-* and *MAP-based isoscapes*, but variations occurred in some biomes. In forested areas, offsets less than 2‰ were observed between the two isoscapes, while C_3 grasslands had offsets less than 3‰. This is because the Δ_{leaf} values predicted based on MAP were ca. 1 to 2‰ lower in C_3 forests, and 1 to 3‰ higher in C_3 grasslands than those in *biome-based isoscapes*. The offsets were greater in C_4 grasslands (ca. 4 to 5‰) and northcentral grasslands (ca. −4 to −5‰). This is mainly because *biome-based isoscape* uses discrete and binary assignment, while *MAP-based isoscape* has a continuous and fractional assignment of vegetation and isotopic compositions. In reality, C_3 and C_4 plants may co-exist in varying abundance, and therefore the *biome-based isoscape* may overestimate C_4 distribution.

δD_{alk} values in the *biome-based isoscape* ranged from −304‰ to −124‰ for *n*-C_{27}, −304‰ to −136‰ for *n*-C_{29}, and −310‰ to −134‰ for *n*-C_{31} (Fig. 4A; Table 3). These δD_{alk} values reflect both δD_p values and ε_{app} values. δD_p values in the MRB primarily vary with latitudes ranging from −10‰ near the GOM to −133‰ in northwest, with a basin mean of −50‰. The biomes in lower latitudes such as southeastern forested areas and southwestern C_4 grasslands receive precipitation that has average δD_p values around −35‰ (EWMF = −37‰, TDF = −32‰, MF = −40‰, C_4 grassland = −38‰). The boreal forests, C_3 grasslands, and shrublands in the northwest have mean annual δD_p values that are significantly lower than the south: −122‰, −71‰, and −94‰, respectively. Lower ε_{app} values in C_3 and C_4 grasslands (i.e. ε_{C29} for C_3 = −178‰ and C_4 = −155‰) may have further decreased δD_{alk} values in the northwestern MRB. Relatively higher δD_p and ε_{app} values in forested area (ε_{C29} = −130‰) may have increased δD_{alk} values in the southeastern MRB. For the *RH-based isoscape*, δD_{alk} values were similar except in the western grasslands that increased by up to ca. 50‰ compared to the *biome-based isoscape* (Fig. 3H).

3.2. Parameter weighted mixing models for the MRB

3.2.1. Area models

Table 3 and Figures 5 and 6 illustrates basin mean $\delta^{13}C_{alk}$ and δD_{alk} values by different parameters weighted mixing models by isoscapes and chain lengths. The basin mean $\delta^{13}C_{alk}$ values in *area models* using *biome-based isoscapes* were −27.3 ± 5.2‰ for *n*-C_{29}, −27.5 ± 5.6‰ for *n*-C_{31}, and −27.6 ± 6.1‰ for *n*-C_{33}. The *MAP-based isoscapes* predicted slightly lower values (< 1‰) than the *biome-based isoscapes*: −27.9 ± 3.5‰ for *n*-C_{29}, −28.1 ± 3.7‰ for *n*-C_{31}, and −28.1 ± 4.2‰ for *n*-C_{33}. The basin mean δD_{alk} values in *area models* using *biome-based isoscapes* were −197.1 ± 38.6‰ for *n*-C_{27}, −197.6 ± 37.8‰ for *n*-C_{29}, and −198.0 ± 41.6‰ *n*-C_{31}. The *RH-based isoscapes* estimated ca. 10‰ higher δD_{alk} values than the *biome-based isoscapes*: −187.3‰ for *n*-C_{27}, −188.5‰ for *n*-C_{29}, and −186.4‰ for *n*-C_{31}. For both $\delta^{13}C_{alk}$ and δD_{alk}, there was no much variation between chain lengths.

3.2.2. Runoff models

There is a spatial variation in runoff within the MRB as shown in Figure 1C. The southeastern MRB has a MAP greater than 1,000 mm, while the northwestern MRB has a MAP of lower than 500 mm. By biome, the MAP is higher in forested areas (EMWF = 1,206 mm; TDF = 1,179 mm; MF = 1,070 mm) than in grasslands (C_3 grassland = 526 mm; C_4 grassland = 767 mm). In percentages, 60% of the rainfall in the MRB occurs in forested areas, and grasslands receive 19% of the total rainfall. The basin mean $\delta^{13}C_{alk}$ values by *runoff models* are ca. −28‰ for *biome-based* and ca. −29‰ for *MAP-based isoscapes*. These values are 0.4‰ to 0.9‰ more negative than the *area models*. Between chain lengths, *n*-C_{33} alkanes had slightly more negative $\delta^{13}C_{alk}$ values than *n*-C_{29} or *n*-C_{31} alkanes by 0.1-0.2‰. For hydrogen isotopes, the basin mean δD_{alk} values are ca. −186‰ for the *biome-based isoscape* and −180‰ for the *RH-based isoscapes*. The *runoff models* produced slightly more positive δD_{alk} values than the *area models* by ca. 12‰ on average (Fig. 6).

3.2.3. Net primary productivity models

NPP is the amount of carbon produced by ecosystems (Imhoff et al., 2004). NPP is higher in the southeastern forests (> 3×10^{11} g C) and lower in western grasslands (< 2×10^{11} g C; Fig. 1D). For example, TNEF, TDF, and MF have average NPP between 4.1×10^{11} to 4.8×10^{11} g C, while C_3 and C_4 grasslands have 2.0×10^{11} to 2.8×10^{11} g C. In percentage, forests yield 59% of the total NPP in the MRB, while grasslands generated 19% of the NPP. The *NPP modeled* mean $\delta^{13}C_{alk}$ values are ca. −28‰ for the *biome-based isoscape*, and −29‰ for the *MAT-based isoscape*. Between chain lengths, variations were less than 1‰. These *NPP modeled* $\delta^{13}C_{alk}$ values are ca. 0.5‰ and 0.7‰ lower than the *area models.* The mean δD_{alk} values in *NPP models* are ca. −186 ‰ for the *biome-based isoscape*, and ca. −180‰ for the *RH-based isoscape*. No significant variations were observed between chain lengths. These weighted models predicted ca. 12‰ more positive than those in *area models*.

3.2.4. Leaf wax production models

Leaf wax production varies by plant types and chain lengths (Diefendorf et al., 2011; Rommerskirchen et al., 2006; Vogts et al., 2009). For example, trees produce ca. 2 to 3 times higher *n*-C_{29} concentrations (207 ± 455 µg/g leaf) than grasslands (C_3 grasses = 81 ± 84 µg/g leaf; C_4 grasses = 56 ± 48 µg/g leaf; Fig. 3C). However, C_4 grasses produce twice as many *n*-C_{33} alkanes on average (108 ± 122 µg/g leaf) than trees (60 ± 455 µg/g leaf). Unlike other models, $\delta^{13}C_{alk}$ values in *production models* varied significantly by chain lengths. For *biome-based isoscapes*, $\delta^{13}C_{alk}$ values were −29.4‰ for *n*-C_{29}, −28.2‰ for *n*-C_{31}, and −25.7‰ for *n*-C_{33} alkanes. For *MAP-based isoscapes*, $\delta^{13}C_{alk}$ values were −29.6‰ for *n*-C_{29}, −28.1‰ for *n*-C_{31}, and −27.4‰ for *n*-C_{33} alkanes. Compared to the *area models*, $\delta^{13}C_{alk}$ values of *n*-C_{29} and *n*-C_{31} alkanes either did not change much or decreased by ≤ 2‰, while *n*-C_{33} alkanes increased by ≤ 2‰. For the δD_{alk} values, *production models* predicted −188.6‰ for *n*-C_{27}, −186.4‰ for *n*-C_{29}, and −201.7‰ for *n*-C_{31} for *biome-based isoscapes*. Whereas, *RH-based isoscapes* predicted −181.5‰ for *n*-C_{27}, −182.3‰ for *n*-C_{29}, and −189.9‰ for *n*-C_{31}. *n*-C_{31} Alkanes had consistently lower δD_{alk} values than the other chain

lengths. Compared to the *area models*, *n*-C_{27} and *n*-C_{29} alkanes were higher in *production models* by ca. 10‰, and lower by ca. 4‰ in *n*-C_{33} alkanes.

3.2.5. Multiple parameters weighted models

We combined NPP and leaf wax production to estimate the total leaf wax biomass (*NP model*). This model predicts that 67% of the *n*-C_{29} alkanes in MRB is produced in southeastern forests and 26% from grasslands (C_3 = 13%; C_4 = 14%). For *n*-C_{31} and *n*-C_{33} alkanes, total wax biomass from grasses is higher than the *n*-C_{29} alkanes. For example, grasses produce 48% and 59% of the total wax production in the MRB for *n*-C_{31} and *n*-C_{33} alkanes, respectively. The $\delta^{13}C_{alk}$ values for *NP models* in *biome-based isoscapes* were −29.9‰ for *n*-C_{29}, −28.5‰ for *n*-C_{31}, and −26.3‰ for *n*-C_{33}. For the *MAP-based isoscapes*, $\delta^{13}C_{alk}$ values were −30.4‰ for *n*-C_{29}, −28.7‰ for *n*-C_{31}, and −28.1‰ for *n*-C_{33}. These values are ca. 1-3‰ lower than those in *area models*, while *n*-C_{33} alkanes were ca. 2‰ higher than *area models*. The mean δD_{alk} values in *NP models* in *biome-based isoscapes* were −178.3‰ for *n*-C_{27}, −174.7‰ for *n*-C_{29}, and −186.8‰ for *n*-C_{31}. For the RH-based isoscapes, δD_{alk} values were −174.1‰ for *n*-C_{27}, −172.5‰ for *n*-C_{29}, and −179.5‰ for *n*-C_{31}. These values are ca. 10 to 20‰ higher than those in *area models*.

We combined the runoff and total leaf wax biomass: *RNP models*. The RNP models predict that leaf wax production and export from southeastern forests consist of 78% for *n*-C_{29}, 60% for *n*-C_{31}, and 51% for *n*-C_{33}, whereas the contribution from grasslands are 19% for *n*-C_{29}, 37% for *n*-C_{31}, and 46% for *n*-C_{33}. The *n*-C_{29} alkanes had lowest $\delta^{13}C_{alk}$ values (*biome-based* = −30.3‰, *MAP-based* = −31.0‰), followed by *n*-C_{31} (*biome-based* = −29.1‰, *MAP-based* = −29.6‰), and *n*-C_{33} (*biome-based* = −27.3‰, *MAP-based* = −29.0‰). For δD_{alk} values, *RNP models* for *biome-based isoscapes* predicted −170.4‰ for *n*-C_{27}, −166.7‰ for *n*-C_{29}, and −174.3‰ for *n*-C_{31}. to −165.8‰. For the *RH-based isoscapes*, δD_{alk} values are −168.0‰ for *n*-C_{27}, −165.8‰ for *n*-C_{29}, −170.3‰ for *n*-C_{31}. These δD_{alk} values by *RNP models* are ca. 20 to 30‰ higher than those in *area models*.

3.3. Leaf wax isotopic compositions in 625B core during the Holocene

$\delta^{13}C_{alk}$ and δD_{alk} values measured in the 625B core are summarized in Table 2. Average $\delta^{13}C_{alk}$ values for the Holocene are −31.3 ± 0.7‰ for *n*-C_{29}, −30.2 ± 1.0‰ for *n*-C_{31}, and −28.1 ± 0.3‰ for *n*-C_{33}. Only ca. 1 to 2‰ variations were observed among depths. *n*-C_{33} alkanes have consistently higher $\delta^{13}C_{alk}$ values than the other homologues by ca. 1-3‰. Average δD_{alk} values were −176.8 ± 5.5‰ for *n*-C_{27}, −174.1 ± 3.9‰ for *n*-C_{29}, −174.0 ± 3.3‰ for *n*-C_{31}, and −160.0 ± 5.9‰ for *n*-C_{33}. Values were consistent among depths (less than ca. 10‰). These measured $\delta^{13}C_{alk}$ and δD_{alk} values in sediments matched better with those in *NP* and *RNP models*, and had highest offsets with *area models*.

4. Discussion

4.1. n-Alkane carbon isoscape modeling of the MRB

There are many challenges in modeling the spatial variability in leaf and leaf wax $\delta^{13}C$ values at regional scales, especially for systems with complex climate and ecosystem distributions. One of the largest complicating factors is predicting the location of biomes and then how to assign $\delta^{13}C$ values to the biome or to allow $\delta^{13}C$ to vary as a function of other parameters, like precipitation. Additionally, grasslands pose another challenge due to the variable amounts of C_3 and C_4 grasses within this biome. Rather than settling on one approach, we chose two different methods to assign $\delta^{13}C$ values (i.e. *biome-based* and *MAP-based* Δ_{leaf}) and to estimate C_4 grassland distribution (i.e. temperature crossover and proxy-based reconstruction) in the MRB (Fig. 2).

We chose these two approaches because each has significant advantages and disadvantages. The *biome-*

based isoscape has the advantage of being able to use paleoclimate paleobiogeographic models (e.g., BIOME4; Kaplan et al., 2003; Prentice et al., 2011), which allow this approach to be used into the past with little modification. Additionally, paleoprecipitation is not required. The disadvantages are that this approach does not capture the spatial variability of leaf $\delta^{13}C$ values as a function of precipitation. The second approach, MAP-based isoscape has the advantage of being able to use robust grassland $\%C_3$ and $\%C_4$ vegetation maps for the mid-Holocene (Cotton et al., 2016) that we can compare to measured values in sediments. However, this approach requires paleoprecipitation estimates and these are known to have high uncertainties.

Considering their differences, it is rather remarkable that except for a slight difference in $\%C_4$ in the northern Great Plains, the two isoscapes agreed so well in terms of isotopic compositions (e.g. basin mean $\delta^{13}C_{C29}$ for *biome-based* = −27‰, and for *MAP-based* = −28‰; Fig. 3C and 3D), plant composition and water availability. For the C_3 vegetation, we observed slight differences in the $\delta^{13}C_{C29}$ values between the *biome-* and *MAP-based* approaches. For example, $\delta^{13}C_{C29}$ values differed on average by < 2‰ for the forested biomes. The *Biome-based isoscape* had $\delta^{13}C_{C29}$ values ranging from −34 to −31‰, while the *MAP-based isoscape* had values ranging from −33 to −31‰. However, a few locations had notable offsets (> 5%) between the two approaches, such as in C_3 and C_4 vegetation boundaries. We attribute these disagreements to the location and nature of vegetation boundaries. The *biome-based models* have sharp boundaries between biomes, while *MAP-based models* have a continuous distribution.

For grasslands, we expected to see large variations in $\delta^{13}C_{alk}$ values given the importance of C_3 and C_4 composition. Indeed, the *MAP-based isoscape* model predicted greater areal extent of C_4 grasslands in the northern Great Plains than the *biome-based isoscape* model (Fig. 3). This is largely driven by temperature differences between the cooler pre-industrial climate compared to the generally warmer mid-Holocene (Cotton et al., 2016; Mayewski et al., 2004) and the binary nature of the *biome-based isoscape model*. This results in an offset between the two approaches of ~ 4-5‰. In the *MAP-based isoscape*, the C_3 and

C_4 grasses coexist and therefore grassland $\delta^{13}C_{alk}$ values are lower (ca. −24‰) than in the *biome-based isoscape* (−19‰). The *MAP-based isoscape* will be more ecologically correct, as a grid cell is likely to have heterogenous than homogenous vegetation, and often have complex and patchy geographic distributions (Cerling et al., 2011; Magill et al., 2013b). This is true of the Great Plains, where C_4 plants are more dominant in the south and decrease to the north.

4.2. n-Alkane hydrogen isoscape modeling of the MRB

Latitude and elevation are the major controls on δD_p values in the North America and for the MRB (Bowen and Revenaugh, 2003; Bowen and Wilkinson, 2002; Gat, 1996). Intrusion of cold Arctic airmasses from high latitudes and continental effects also contribute to geographic variation in δD_p values (Bowen and Revenaugh, 2003; Bowen and Wilkinson, 2002). The mean annual δD_p values in the MRB vary from ca. −130‰ to −10‰ under current climate, with higher values near the GOM and progressively decreasing to the north (Fig. 1E).

Overall, the geographic pattern of δD_{alk} values was similar to that in δD_p values, having higher δD_p values in southeastern forests and lower δD_{alk} values towards northwest (Fig. 4A-4C). These patterns are largely driven by δD_p, but are modified by the change in ε_{app} values for different biomes (C_3 grasses = −178 ± 17‰; C_4 grasses = −55 ± 10‰, trees = −130 ± 13‰). The main difference between the *biome-* and *RH-based isoscapes* is that ε_{app} values in grasslands change as a function of RH in *RH-based isoscapes* due to soil evaporation (Smith and Freeman, 2006). As almost half of the MRB is occupied with forestlands in the Holocene, variation in ε_{app} as a function of RH was rather minimal and resulted in a basin mean difference of ca. 10 to 20‰ between the two isoscapes. Since vegetation and source may change through time in the MRB, the grasses and evaporative enrichment effects on ε_{app} may become more important, and this could be true in basins that have more grass cover (Polissar and Freeman, 2010).

4.3. Controls on leaf wax integration from the catchment to the GOM

The MRB covers almost half of the US, where climate and vegetation varies spatially. Therefore, we do not expect a spatially uniform integration of leaf waxes from the entire catchment to the GOM. To evaluate leaf wax sourcing, we performed linearly weighted mixing models of area, runoff, NPP, and wax production, and their combinations. Quantifying the effects of each parameter and evaluating the model performance is challenging. A simple approach would be to analyze the suspended sediment load in MRB rivers. However, this is unlikely to be useful today given the heavy agricultural usage and modification of the rivers within the MRB (Zhang and Schilling, 2006). Instead, we took the approach of comparing our models to a few Holocene age sediment intervals from the GOM. This provides a simple evaluation of our model results to sediments that capture an integrated leaf wax record of the MRB.

The measured $\delta^{13}C_{alk}$ values in the Holocene 625B core sediments were −30.3‰ for *n*-C_{29}, −30.2‰ for *n*-C_{31}, and −28.2‰ for *n*-C_{33}. These measured values had highest offsets from the *area models* for *n*-C_{29} and *n*-C_{31} (offsets = ~3‰; Fig. 5 and 6; Table 2). The *area models* were weighted by the Holocene vegetation composition: ca. 26% C_3 grasslands, ca. 30% C_4 grasslands, and ca. 36% C_3 forests. The ~3‰ ^{13}C-depletion in measured values compared to *area models* translates to ~20% reduction in C_4 grasses in the MRB. This means that using a simple mixing model for sedimentary $\delta^{13}C_{alk}$ values may not predict an accurate areal distribution of C_4 plants for *n*-C_{29} and *n*-C_{31}. For *n*-C_{33} alkanes, $\delta^{13}C$ values between measured and *area models* were similar (offset = < 0.5‰), suggesting that *n*-C_{33} alkanes are more sensitive indicators of grassland.

The *runoff* and *NPP models* predicted $\delta^{13}C_{alk}$ values between −29‰ to −28‰. The forested areas in the MRB experience 60% of the total runoff and NPP, and therefore these models predicted a slightly higher leaf wax export from southeastern forested areas, which have lower $\delta^{13}C_{alk}$ values, compared to *area models*. *Production models* predicted an increase in grassland-derived leaf wax integration with chain

lengths (Fig. 5). For example, C_3 forests produce 3 to 4 times more *n*-C_{29} alkanes, similar *n*-C_{31} alkanes, and lesser *n*-C_{33} alkanes than grasses (Diefendorf and Freimuth, 2017). However, these single parameter weighted models still could not capture the strong C_3 signals observed in the ODP 625B core sediments.

The combination models such as *NP* and *RNP models* predicted ca. 1 to 3‰ more negative $\delta^{13}C_{alk}$ values than the *area models*, and matched better with the measured values in sediments (offset = < 1‰) (Fig. 5 and 6). The *RNP models* matched best with the measured values, these results confirm that both runoff and leaf wax biomass may influence their contribution to the marine sediments (Hoffmann et al., 2016; Kirby et al., 2013). There were consistent patterns in modeled values. All models predicted higher integration of leaf waxes from C_3 forestland except when the wax production is considered for *n*-C_{31} and *n*-C_{33} alkanes (Fig. 7). This may be due to each model not being completely independent. For example, higher precipitation favors C_3 plant growth and results in higher NPP, contributing to more negative $\delta^{13}C_{alk}$ values in the sediments. The C_3 tree contribution decreased with chain length, when wax production was taken into account. The *n*-C_{31} and *n*-C_{33} alkanes predicted higher leaf wax integration from grasslands.

The basin mean δD_{alk} values for *area models* is ca. −198‰ for *biome-based isoscape* and ca. −188‰ for *RH-based isoscape*. The offsets between chain lengths were less than 2‰. The *runoff*, *NPP*, and *production models* estimated ca. 10 to 15‰ more positive values than the *area models* (Fig. 5; Table 3), and matched better with measured δD_{alk} value than *area models*. Similar to the $\delta^{13}C_{alk}$ results, models predicted higher leaf wax export from the southeastern forested regions, where δD_{alk} values are higher. The models by *RH-based isoscapes* consistently predicted slightly higher mean δD_{alk} values compared to *biome-based isoscapes*, but only by ca. 5‰ when runoff, NPP, and production are weighted. This small offset between the two isoscapes in *runoff*, *NPP*, and *production models* indicate that leaf water enrichment effects on ε_{app} values due to soil evaporation in the Great Plains is reduced due to preferential sourcing of C_3 trees in sediments that have higher productivity and transport efficiency.

Higher representation of C_3 trees in lake sediments have been documented in several studies based on leaf wax $\delta^{13}C$ values along a wide climatic gradient including grasslands (Garcin et al., 2014; Sachse et al., 2012; Seki et al., 2010). This study further supports under-representation of grasslands in marine sediments especially for *n*-C_{29} and *n*-C_{31} alkanes. Due to the higher contribution of leaf waxes from C_3 forests, vegetation effects on ε_{app} in grasslands is reduced, and thereby produce a good correlation with δD_p values. These results provide important implications for interpreting geologic sediments, especially in marine sediments with high fluvial influence. Such information is important for understanding the source area and assigning ε_{app} values for δD_p reconstructions for more quantitative hydrologic interpretations. Due to the lack of meta-data for ε_{app} values in *n*-C_{33} alkanes, we were not able to model the sensitivity of sourcing bias in δD_{C33} values. The average measured δD_{C33} value was −160‰, which is ca. 10‰ more D-enriched than *n*-C_{29} and *n*-C_{31}, and may indicate that *n*-C_{33} alkanes are likely derived more from the southern Great Plains, which is dominated by C_4 grasslands.

4.4. Paleo implications using n-alkanes as paleovegetation and paleohydrologic proxies

At the forest-level, integration of plant organic matter may be biased towards plants with higher biomass, leaf wax production and transport efficiency (e.g. Burnham, 1989; Burnham and Johnson, 1994; Ellis and Johnson, 2013; Suh and Diefendorf, 2017; Greenwood, 1991). In surface lake sediments, leaf waxes were also biased towards angiosperm trees due to their higher production and transport (Garcin et al., 2014; Sachse et al., 2012; Seki et al., 2010). This study further expanded the investigation of the controls on leaf wax integration and transport into marine sediments using mixing models. Measured $\delta^{13}C_{alk}$ values in GOM sediments suggested a strong C_3 signal in marine sediment $\delta^{13}C_{alk}$ records, and our models matched measured values best when runoff and leaf wax biomass were combined. These results confirm that leaf wax export to the GOM is not spatially equal. We also found higher wax export from forested areas based on δD_{alk} values. Further, vegetation effects on δD_{alk} values were minor as a whole basin not only due to

opposing trend in low ε_{app} and leaf water D-enrichment in grasslands but also of integration and transport bias of leaf waxes towards forested areas. The results have important implications to more accurate interpretations of paleovegetation and paleohydrology of the source region. We need to take into account possible source bias due to runoff, productivity and distance especially in sites with high fluvial influence and dynamic vegetation and climate. In sites with low grassland-derived leaf wax export, this proxy may only reflect paleoenvironment of forested areas. Compared to *n*-C_{29} and *n*-C_{31} alkanes, we observed less integration bias in *n*-C_{33} alkanes. We therefore recommend using *n*-C_{33} alkanes to minimize production or source bias and better represent C_4 grassland signals.

Transport processes can vary over geologic timescales. For example, during the Last Glacial, climate and vegetation has changed in North America as well as the basin geometry and river discharge with expansion of Laurentide Ice sheets (Teller, 1990; Wickert, 2016). The northern conifer vegetation zones migrated southward, replacing deciduous angiosperms (Watts, 1970). Grasslands contracted, and climate was in general humid during the Last Glacial in the MRB, and humid climate would reduce vegetation effects on δD_{alk} values. During deglaciation, meltwater discharge increased in the MRB and may have delivered higher amounts of terrigenous organic matter to the GOM (Broecker et al., 1989). These changes in vegetation composition and runoff through time and space should be taken into account in paleo-interpretations as they would influence the spatial distribution of leaf waxes and isotopic compositions in sediments. Other climatic changes such as seasonality or storms may also influence leaf wax delivery to sediments. For example, storms and episodic runoff can increase sediment delivery from coastal areas into marine sediment, and this may influence leaf wax records, depending on the intensity and duration of the event and temporal resolution of the sediments (Ponton et al., 2014).

5. Conclusion

This study explored the how vegetation area, runoff, net primary productivity (NPP), and leaf wax production influence leaf wax integration and transport from the Mississippi River Basin (MRB) to the Gulf of Mexico (GOM) using linearly weighted mixing models. First, carbon and hydrogen leaf wax isoscapes were developed for the MRB by using different approaches for estimating $\%C_4$ and assigning isotopic fractionations for each vegetation type. These isoscapes were weighted by area, runoff, NPP, and wax production to determine spatial variations in leaf wax export to the GOM, and resulting leaf wax isotopic compositions of GOM sediments. The modeled values were then compared to measured values in the GOM sediments. The *runoff*, *NPP*, and *production models* estimated/predicted higher C_3 signals (ca. 0.5 to 1‰ ^{13}C-depletion) than *area models* due to higher leaf wax exports from forested areas, but still could not capture the strong C_3 signals in the measured values. Combination models such as *NP* and *RNP models* predicted values similar to the measured values, confirming that both runoff and productivity may influence leaf wax integration and transport into marine sediments. *n*-C_{33} alkanes integrates higher C_4 grassland-derived leaf waxes than *n*-C_{29} and *n*-C_{31} alkanes due to higher production of *n*-C_{33} alkanes in C_4 grasses. Similar patterns were observed in δD_{alk} values. *Runoff*, *NPP*, and *production models* predicted higher leaf wax export from southeastern forested areas than other regions in the MRB drainage. We also examined vegetation effects on δD_{alk} values by comparing isoscapes with ε_{app} values by plant types, or as a function of relative humidity in grasslands. The isotopic offsets between isoscapes due to vegetation effects were ca. 10 to 20‰, but decreased to < 5‰ when these isoscapes were weighted by runoff, productivity. The results suggest that vegetation effects are reduced not only due to the canceling of low ε_{app} values by leaf water D-enrichment, but also integration bias towards C_3 angiosperm trees in southeastern MRB. We therefore conclude that runoff, productivity and distance should be taken into account when interpreting leaf wax isotope records in sedimentary records with high fluvial influence.

Acknowledgement

We thank Jennifer Cotton for providing the raw data to be used in this paper. Thanks goes to the ITCE and the University of Utah for supporting this project. We also thank Ministry of Oceans and Fisheries, South Korea (K-IODP) for partial support of this research.

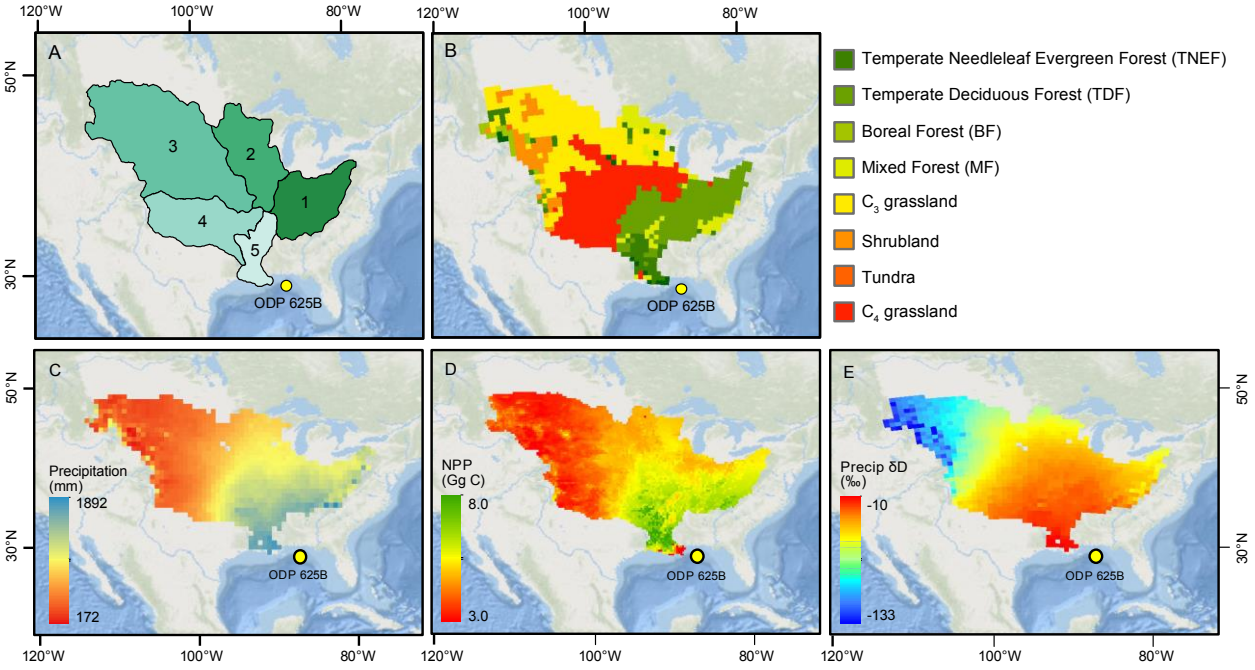

Figure 1. (A) A map of Mississippi River Basin (MRB) and sub-basins 1) Ohio-Tennessee River basin, 2) Upper Mississippi River basin, 3) Missouri River basin, 4) Arkansas-Red River basin, and 5) Lower Mississippi River Basin, (B) biomes in MRB by Ramankutty and Foley (2010) for current climate without human activities, (C) 30-year mean annual precipitation (MAP; mm; PRISM), (D) pre-human net primary productivity (Gg C; modified from Imhoff et al., 2004) and (E) 30-year average MAP δD values (‰; Bowen, 2014).

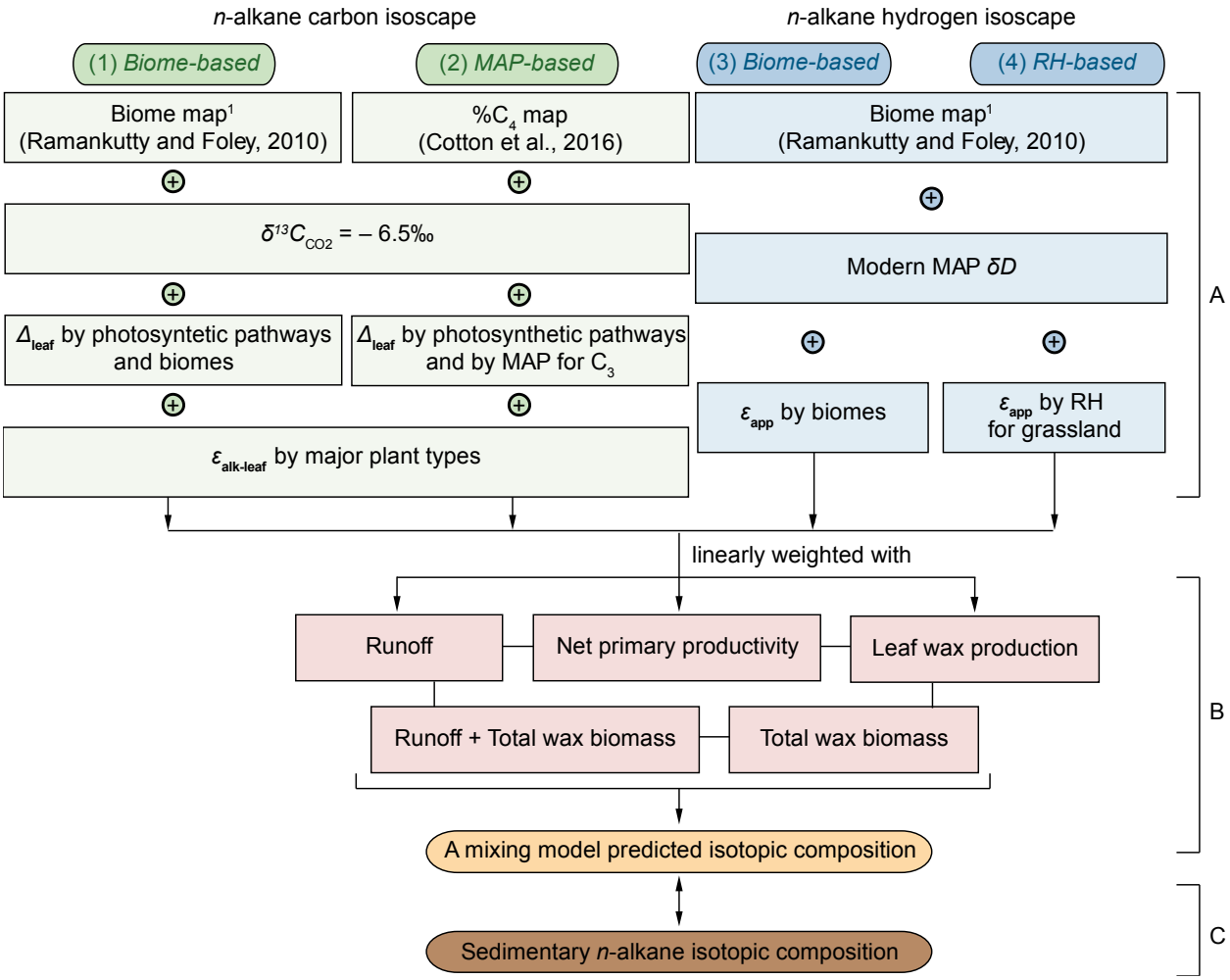

Figure 2. A GIS workflow of creating *n*-alkane carbon (green; *biome-* and *MAP-based*) and hydrogen (blue; *biome-based*, *RH-based*) isoscapes (A), and weighted parameters such as runoff, net primary productivity (NPP), leaf wax production, total wax biomass (NPP + wax production), and runoff + total wax biomass (B) to quantify their effects on *n*-alkane integration and transport from the Mississippi River Basin to the Gulf of Mexico. The modeled results were compared to measured values in sediments from the Gulf of Mexico (C; ODP 625B).

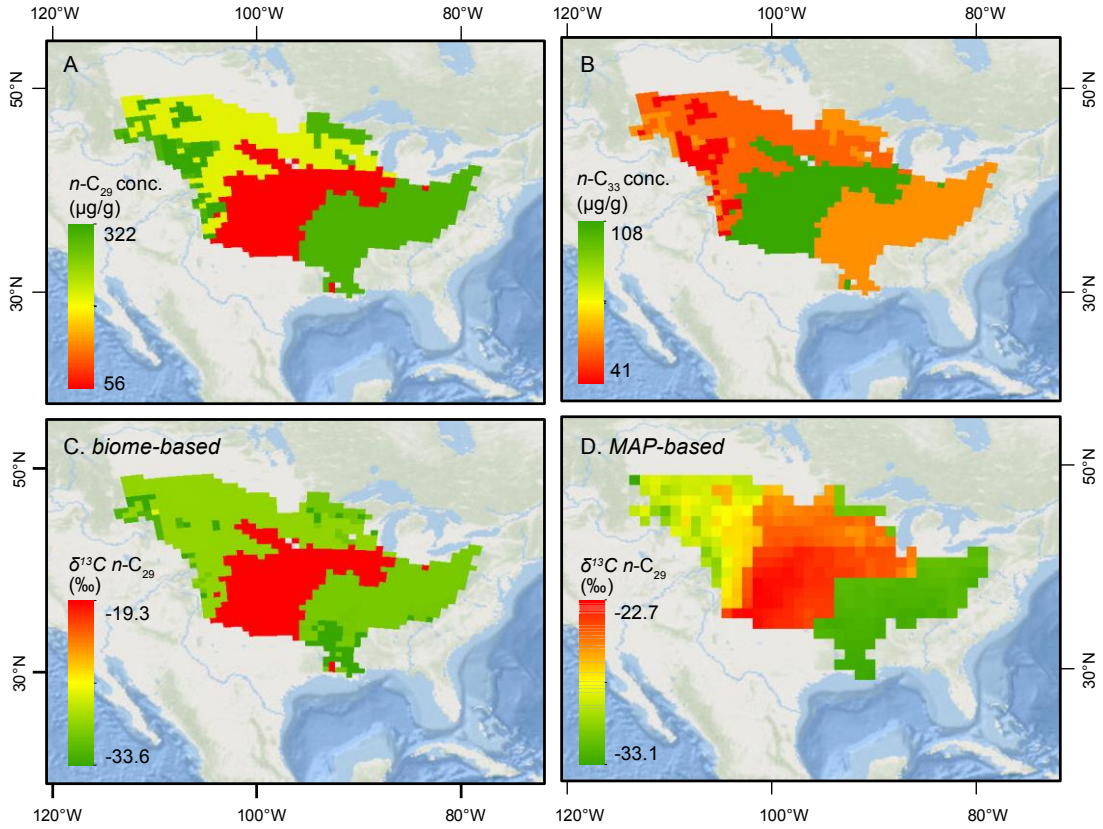

Figure 3. Maps showing spatial distribution of (A) average *n*-C_{29} concentration and (B) average *n*-C_{33} concentration (µg/g; Diefendorf and Freimuth, 2017), (C) *biome-based isoscape* of $\delta^{13}C_{C29}$ (‰), and (D) *MAP-based isoscape* of $\delta^{13}C_{C29}$ (‰).

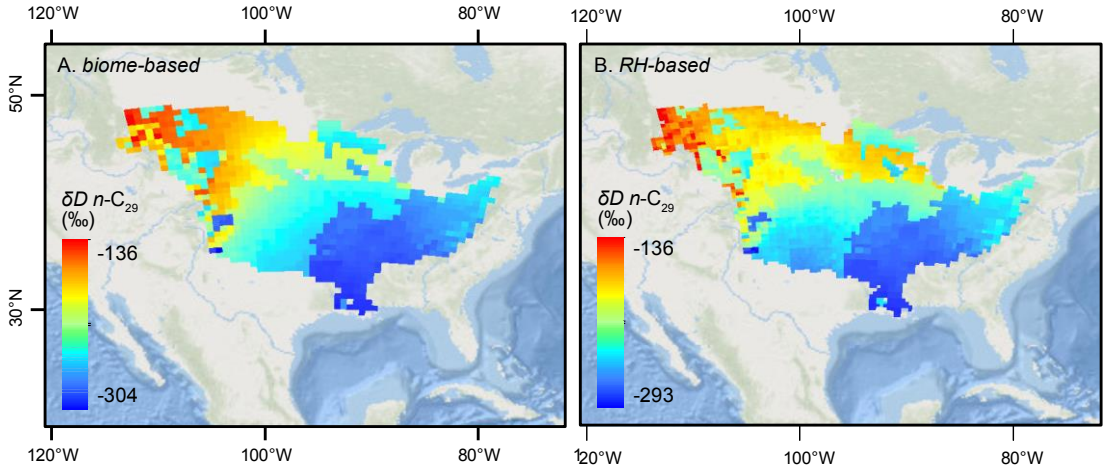

Figure 4. δD_{C29} isoscapes for the Mississippi River Basin estimated using modern 30-year average mean annual precipitation δD values and (A) ε_{app} values by biome and (B) ε_{app} values as a function of July relative humidity (RH) in grasslands (McInerney et al., 2011; Smith and Freeman, 2006).

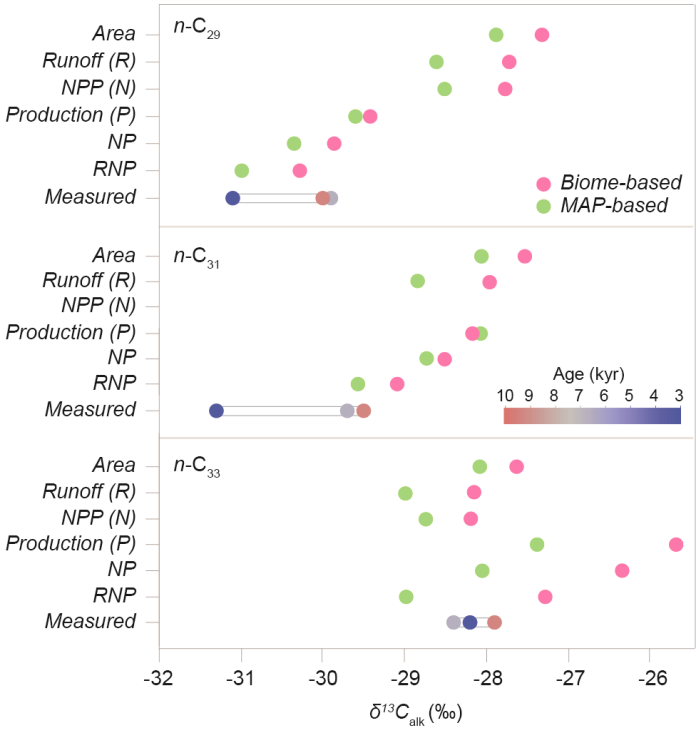

Figure 5. Modeled and measured $\delta^{13}C_{alk}$ values for *n*-C_{29}, *n*-C_{31} and *n*-C_{33} alkanes in the Mississippi River Basin (MRB). The modeled values are weighted by different climatic or ecologic parameters that may influence leaf wax integration and transport from the MRB to the Gulf of Mexico. The parameters are area, runoff (*R*), net primary productivity or NPP (*N*), leaf wax production (*P*), and their combinations (*NP* and *RNP models*). Green and pink dots indicate *MAP*- and *biome-based isoscapes*, respectively (see text for details). The three measured values correspond to the Holocene age sediment samples from the ODP 625B core in the northeastern Gulf of Mexico.

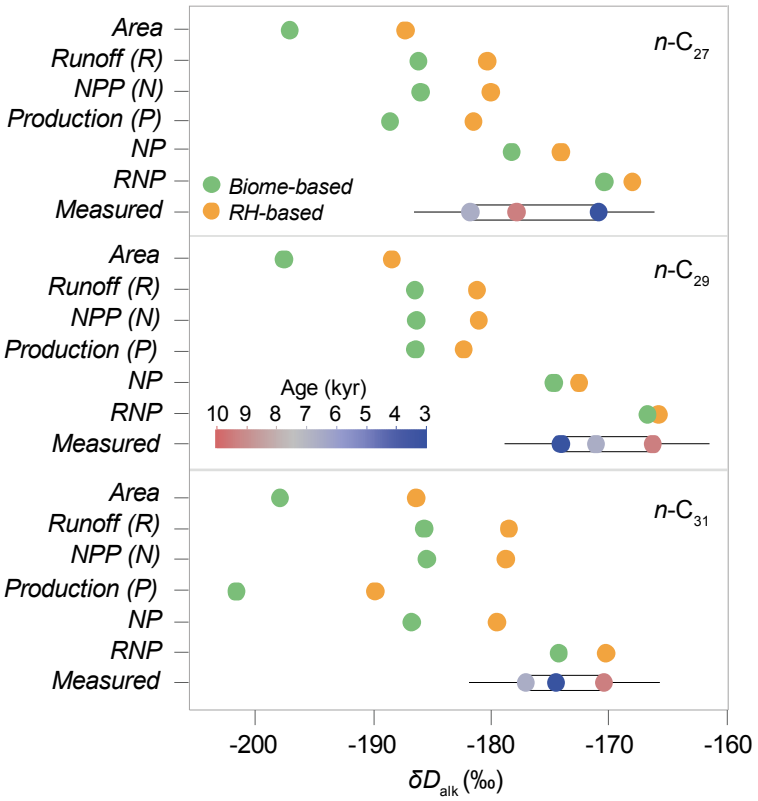

Figure 6. Modeled and measured δD_{alk} values for n-C_{27}, n-C_{29} and n-C_{31} alkanes in the Mississippi River Basin (MRB). The modeled values are weighted by different climatic or ecologic parameters that may influence leaf wax integration and transport from the MRB to the Gulf of Mexico. The parameters are area, runoff (*R*), net primary productivity or NPP (*N*), leaf wax production (*P*), and their combinations (*NP* and *RNP models*). Green and orange dots indicate *biome-* and *RH-based isoscapes*, respectively (see text for details). The three measured values correspond to the Holocene age sediment samples from the ODP 625B core in the northeastern Gulf of Mexico. Horizontal lines indicate analytical uncertainty (4‰).

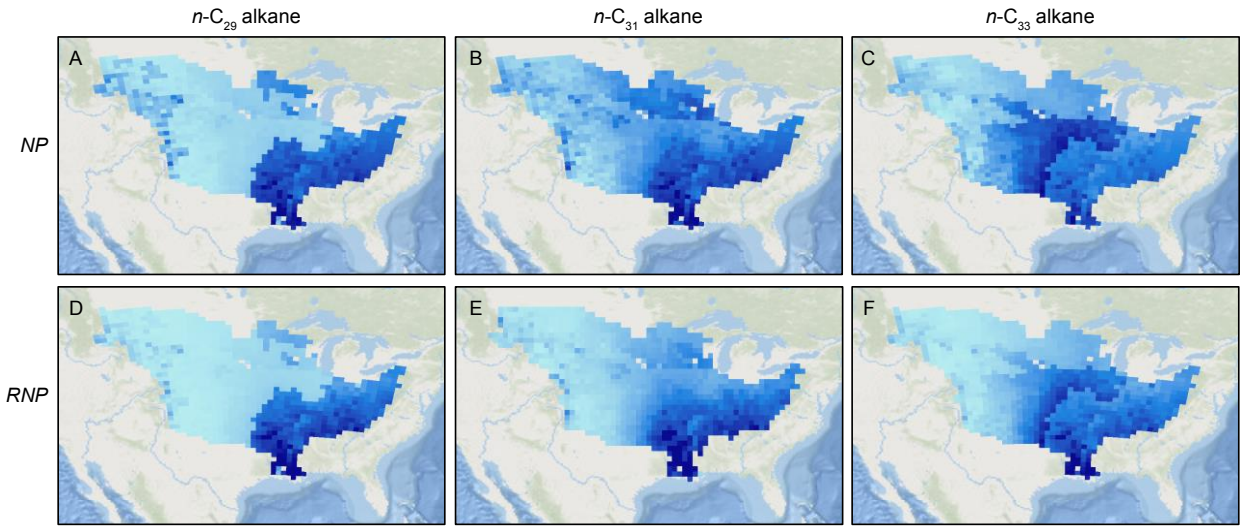

Figure 7. Maps showing modeled spatial contribution of leaf waxes from the Mississippi River Basin to the Gulf of Mexico (GOM) when climatic and ecologic parameters that may influence leaf wax integration and transport are weighted. Darker blue indicates regions with relatively higher leaf wax export to the GOM. The weighted parameters are runoff (R) net primary productivity (N), and leaf wax production (P). These parameters are combined to produce *NP* (A-C) and *RNP* (D-F) *models* for *n*-C_{29}, *n*-C_{31}, and *n*-C_{33} alkanes.

Table 1. A list of models in this study and their weighted parameters.

Linear mixing models and parameters weighted
Area
Runoff model
Net primary productivity model
Leaf wax production model
Net primary productivity + Production model (NP model)
Runoff + Net primary productivity + Production model (RNP model)

Table 2. Measured *n*-alkane carbon ($\delta^{13}C_{alk}$) and hydrogen (δD_{alk}) isotopic compositions in ODP 625B core sediment samples from the northeastern Gulf of Mexico and their depth (cm) and ^{14}C age (yr) measured in Limoges et al., (2014).

			$\delta^{13}C_{alk}$				δD_{alk}			
Core	**Depth (cm)**	**^{14}C age[A] (yr)**	***n*-C_{27}**	***n*-C_{29}**	***n*-C_{31}**	***n*-C_{33}**	***n*-C_{27}**	***n*-C_{29}**	***n*-C_{31}**	***n*-C_{33}**
100 625B	21-23	3,115	-28.7	-31.1	-31.3	-28.2	-170.9	-174.1	-174.5	-156.6
100 625B	57-59	6,645	-30.7	-29.9	-29.7	-28.4	-181.8	-171.1	-177.1	-166.8
100 625B	80-82	9,468	-29.6	-30.0	-29.5	-27.9	-177.8	-166.3	-170.4	-156.7
		Average	-29.7	-30.3	-30.2	-28.2	-176.8	-170.5	-174.0	-160.0
		1σ	1.0	0.7	1.0	0.3	5.5	3.9	3.3	5.9

[A]Limoges et al. (2014)

Table 3. Mississippi River Basin mean $\delta^{13}C_{alk}$ and δD_{alk} values for different approaches used to build the isoscapes (i.e. *biome-, MAP- and RH-based*), and weighted by climatic and ecologic parameters using linear mixing models.

Weighted parameters	$\delta^{13}C_{alk}$						δD_{alk}					
	Biome-based			*MAP-based*			*Biome-based*			*RH-based*		
	C_{29}	C_{31}	C_{33}	C_{29}	C_{31}	C_{33}	C_{27}	C_{29}	C_{31}	C_{27}	C_{29}	C_{31}
Area	-27.9	-28.1	-28.1	-27.3	-27.5	-27.6	-197.1	-197.6	-198.0	-187.3	-188.5	-186.4
Runoff (R)	-27.7	-28.0	-28.1	-28.6	-28.8	-29.0	-186.0	-186.4	-185.5	-180.0	-181.1	-178.8
NPP (N)	-27.8	-28.0	-28.2	-28.5	-28.7	-28.7	-186.2	-186.5	-185.7	-180.3	-181.2	-178.5
Production (P)	-29.4	-28.2	-25.7	-29.6	-28.1	-27.4	-188.6	-186.4	-201.7	-181.5	-182.3	-189.9
NP	-29.9	-28.5	-26.3	-30.4	-28.7	-28.1	-178.3	-174.7	-186.8	-174.1	-172.5	-179.5
RNP	-30.3	-29.1	-27.3	-31.0	-29.6	-29.0	-170.4	-166.7	-174.3	-168.0	-165.8	-170.3

Appendix

Table A1. Δ_{leaf} values for each biome used to create *n*-alkane carbon isoscapes in the Mississippi River Basin and their citations. Biome types are determined by Ramankutty and Foley (2010) with modifications.

Biome type	Abbreviation	Equivalent biome type	Δ_{leaf}	1σ	Δ_{leaf} Citations
Temperate Needleleaf Evergreeen Forest	TNEF	Evergreen Warm Moist Forest	22.5	1.6	Diefendorf et al., 2010
Temperate Deciduous Forest	TDF	Temperate Deciduous Forest	19.6	1.2	Diefendorf et al., 2010
Boreal Evergreen Forest	BEF	Cool Cold Evergreen Forest	21.3	1.0	Diefendorf et al., 2010
Boreal Deciduous Forest	BDF	Cool Cold Deciduous Forest	21.1		Diefendorf et al., 2010
Mixed Forest	MF	Mixed Forest	19.8	1.3	Diefendorf et al., 2010
Grassland/Steppe C3	C3 grassland	C3 grassland	17.4		Lloyd and Farquhar (1994)
Grassland/Steppe C4	C4 grassland	C4 grassland	3.5		Lloyd and Farquhar (1994)
Dense Shrubland	Shrubland	Shrubland	18.7	0.9	Lloyd and Farquhar (1994)
Open Shrubland	Shrubland	Shrubland	18.7	0.9	Lloyd and Farquhar (1994)
Tundra	Tundra	Tundra	16.1		Lloyd and Farquhar (1994)

Table A2. $\varepsilon_{alk\text{-}leaf}$ values and standard deviations for each biome used to estimate *n*-alkane carbon isoscapes in the Mississippi River Basin and their citations. Biome types are determined by Ramankutty and Foley (2010) with modifications.

Biome type	$\varepsilon_{C29\text{-}leaf}$	1σ	$\varepsilon_{C31\text{-}leaf}$	1σ	$\varepsilon_{C33\text{-}leaf}$	1σ	$\varepsilon_{alk\text{-}leaf}$ Citations
Temperate Needleleaf Evergreeen Forest	-4.6	2.2	-5.1	2.2	-5.8	1.8	Diefendorf and Freimuth 2017
Temperate Deciduous Forest	-4.6	2.2	-5.1	2.2	-5.8	1.8	Diefendorf and Freimuth 2017
Boreal Evergreen Forest	-4.6	2.2	-5.1	2.2	-5.8	1.8	Diefendorf and Freimuth 2017
Boreal Deciduous Forest	-4.6	2.2	-5.1	2.2	-5.8	1.8	Diefendorf and Freimuth 2017
Mixed Forest	-4.6	2.2	-5.1	2.2	-5.8	1.8	Diefendorf and Freimuth 2017
Grassland/Steppe C3	-6.0	2.0	-6.3	1.1	-6.3	1.2	Diefendorf and Freimuth 2017
Grassland/Steppe C4	-9.3	2.1	-9.0	1.9	-8.3	1.5	Diefendorf and Freimuth 2017
Dense Shrubland	-4.6	2.2	-5.1	2.2	-5.8	1.8	Diefendorf and Freimuth 2017
Open Shrubland	-4.6	2.2	-5.1	2.2	-5.8	1.8	Diefendorf and Freimuth 2017
Tundra	-4.6	2.2	-5.1	2.2	-5.8	1.8	Diefendorf and Freimuth 2017

Table A3. ε_{app} values and standard deviations for each biome used to estimate *n*-alkane hydrogen isoscapes in the Mississippi River Basin and their citations. Biome types are determined by Ramankutty and Foley (2010) with modifications.

Biome type	$\varepsilon_{C27\text{-}precip}$	1σ	$\varepsilon_{C29\text{-}precip}$	1σ	$\varepsilon_{C31\text{-}precip}$	1σ	ε_{app} Citations
Temperate Needleleaf Evergreeen Forest	-129.2	16.1	-130.4	13.2	-125.2	17.4	Hou et al 2007
Temperate Deciduous Forest	-129.2	16.1	-130.4	13.2	-125.2	17.4	Hou et al 2007
Boreal Evergreen Forest	-129.2	16.1	-130.4	13.2	-125.2	17.4	Hou et al 2007
Boreal Deciduous Forest	-129.2	16.1	-130.4	13.2	-125.2	17.4	Hou et al 2007
Mixed Forest	-129.2	16.1	-130.4	13.2	-125.2	17.4	Hou et al 2007
Grassland/Steppe C3	-178.4	16.9	-177.8	17.1	-184.1	17.7	Smith and Freeman (2006)
Grassland/Steppe C4	-157.0	9.1	-155.2	10.2	-157.9	9.1	Smith and Freeman (2006)
Dense Shrubland	-81.3	14.6	-92.7	19.5	-91.4	18.8	Liu et al. (2006)
Open Shrubland	-81.3	14.6	-92.7	19.5	-91.4	18.8	Liu et al. (2006)
Tundra	-129.2	16.1	-130.4	13.2	-125.2	17.4	Hou et al 2007

Table A4. *n*-Alkane concentrations (µg /g leaf) and standard deviations for each biome from *n*-C_{27} to *n*-C_{33} alkanes in the Mississippi River Basin and their citations.

	***n*-alkane concentrations (µg /g leaf)**								
Biome type	***n*-C_{27}**	**1σ**	***n*-C_{29}**	**1σ**	***n*-C_{31}**	**1σ**	***n*-C_{33}**	**1σ**	**Citations**
Temperate Needleleaf Evergreeen Forest	40	64	207	455	188	404	60	152	Diefendorf and Freimuth 2017
Temperate Deciduous Forest	40	64	207	455	188	404	60	152	Diefendorf and Freimuth 2017
Boreal Evergreen Forest	40	64	207	455	188	404	60	152	Diefendorf and Freimuth 2017
Boreal Deciduous Forest	40	64	207	455	188	404	60	152	Diefendorf and Freimuth 2017
Mixed Forest	40	64	207	455	188	404	60	152	Diefendorf and Freimuth 2017
Grassland/Steppe C3	18	15	81	84	242	353	54	82	Diefendorf and Freimuth 2017
Grassland/Steppe C4	39	56	56	48	159	173	108	122	Diefendorf and Freimuth 2017
Dense Shrubland	34	36	322	472	290	395	41	82	Diefendorf and Freimuth 2017
Open Shrubland	34	36	322	472	290	395	41	82	Diefendorf and Freimuth 2017
Tundra	18	15	81	84	242	353	54	82	Diefendorf and Freimuth 2017

References:

Aller, R.C., Blair, N.E., Brunskill, G.J., 2008. Early diagenetic cycling, incineration, and burial of sedimentary organic carbon in the central Gulf of Papua (Papua New Guinea). Journal of Geophysical Research: Earth Surface 113.

Bianchi, T.S., Filley, T., Dria, K., Hatcher, P.G., 2004. Temporal variability in sources of dissolved organic carbon in the lower Mississippi River. Geochimica et Cosmochimica Acta 68, 959-967.

Bird, M.I., Summons, R.E., Gagan, M.K., Roksandic, Z., Dowling, L., Head, J., Keith Fifield, L., Cresswell, R.G., Johnson, D.P., 1995. Terrestrial vegetation change inferred from *n*-alkane $\delta^{13}C$ analysis in the marine environment. Geochimica et Cosmochimica Acta 59, 2853-2857.

Blair, N.E., Aller, R.C., 2012. The fate of terrestrial organic carbon in the marine environment. Annual Review of Marine Science 4, 401-423.

Bowen, G., 2014. The Online Isotopes in Precipitation Calculator, version 2.2. 2015.

Bowen, G.J., Revenaugh, J., 2003. Interpolating the isotopic composition of modern meteoric precipitation. Water Resources Research 39.

Bowen, G.J., Wilkinson, B., 2002. Spatial distribution of $\delta^{18}O$ in meteoric precipitation. Geology 30, 315-318.

Broecker, W.S., Kennett, J.P., Flower, B.P., Teller, J.T., Trumbore, S., Bonani, G., Wolfli, W., 1989. Routing of meltwater from the Laurentide Ice Sheet during the Younger Dryas cold episode. Nature 341, 318-321.

Burnham, R.J., 1989. Relationships between standing vegetation and leaf litter in a paratropical forest: implications for paleobotany. Review of Palaeobotany and Palynology 58, 5-32.

Burnham, R.J., Johnson, S.Y., 1994. Paleoecological and floristic heterogeneity in the plant-fossil record: an analysis based on the Eocene of Washington. US Government Printing Office.

Carr, A.S., Boom, A., Chase, B.M., Meadows, M.E., Grimes, H.L., 2015. Holocene sea level and environmental change on the west coast of South Africa: evidence from plant biomarkers, stable isotopes and pollen. Journal of Paleolimnology 53, 415-432.

Cerling, T.E., Wynn, J.G., Andanje, S.A., Bird, M.I., 2011. Woody cover and hominin environments in the past 6million years. Nature (London) 476, 51-56.

Coplen, T.B., 2011. Guidelines and recommended terms for expression of stable-isotope-ratio and gas-ratio measurement results. Rapid Communications in Mass Spectrometry 25, 2538-2560.

Coplen, T.B., Brand, W.A., Gehre, M., Gröning, M., Meijer, H.A., Toman, B., Verkouteren, R.M., 2006. New guidelines for $\delta^{13}C$ measurements. Analytical Chemistry 78, 2439-2441.

Cotton, J.M., Cerling, T.E., Hoppe, K.A., Mosier, T.M., Still, C.J., 2016. Climate, CO_2, and the history of North American grasses since the Last Glacial Maximum. Science Advances 2.

Cramer, W., Kicklighter, D.W., Bondeau, A., Iii, B.M., Churkina, G., Nemry, B., Ruimy, A., Schloss, A.L., Intercomparison, T., Model, P.O.T.P.N., 1999. Comparing global models of terrestrial net primary productivity (NPP): overview and key results. Global change biology 5, 1-15.

Diefendorf, A.F., Freeman, K.H., Wing, S.L., Graham, H.V., 2011. Production of *n*-alkyl lipids in living plants and implications for the geologic past. Geochimica et Cosmochimica Acta 75, 7472-7485.

Diefendorf, A.F., Freimuth, E.J., 2017. Extracting the most from terrestrial plant-derived *n*-alkyl lipids and their carbon isotopes from the sedimentary record: A review. Organic Geochemistry 103, 1-21.

Diefendorf, A.F., Mueller, K.E., Wing, S.L., Koch, P.L., Freeman, K.H., 2010. Global patterns in leaf ^{13}C discrimination and implications for studies of past and future climate. Proceedings of the National Academy of Sciences 107, 5738-5743.

Domínguez, E., Heredia-Guerrero, J.A., Heredia, A., 2011. The biophysical design of plant cuticles: an overview. New Phytologist 189, 938-949.

Eglinton, G., Gonzalez, A.G., Hamilton, R.J., Raphael, R.A., 1962. Hydrocarbon constituents of the wax coatings of plant leaves: A taxonomic survey. Phytochemistry 1, 89-102.

Ellis, B., Johnson, K.R., 2013. Comparison of leaf samples from mapped tropical and temperate forests: Implications for interpretations of the diversity of fossil assemblages. Palaios 28, 163-177.

Feakins, S.J., Sessions, A.L., 2010. Controls on the D/H ratios of plant leaf waxes in an arid ecosystem. Geochimica et Cosmochimica Acta 74, 2128-2141.

Freeman, K.H., Colarusso, L.A., 2001. Molecular and isotopic records of C_4 grassland expansion in the late miocene. Geochimica et Cosmochimica Acta 65, 1439-1454.

Galy, V., Eglinton, T., France-Lanord, C., Sylva, S., 2011. The provenance of vegetation and environmental signatures encoded in vascular plant biomarkers carried by the Ganges–Brahmaputra rivers. Earth and Planetary Science Letters 304, 1-12.

Galy, V., France-Lanord, C., Lartiges, B., 2008. Loading and fate of particulate organic carbon from the Himalaya to the Ganga–Brahmaputra delta. Geochimica et Cosmochimica Acta 72, 1767-1787.

Garcin, Y., Schefuß, E., Schwab, V.F., Garreta, V., Gleixner, G., Vincens, A., Todou, G., Séné, O., Onana, J.-M., Achoundong, G., Sachse, D., 2014. Reconstructing C_3 and C_4 vegetation cover using *n*-alkane carbon isotope ratios in recent lake sediments from Cameroon, Western Central Africa. Geochimica et Cosmochimica Acta 142, 482-500.

Garzanti, E., Vezzoli, G., Andò, S., Lavé, J., Attal, M., France-Lanord, C., DeCelles, P., 2007. Quantifying sand provenance and erosion (Marsyandi River, Nepal Himalaya). Earth and Planetary Science Letters 258, 500-515.

Gat, J.R., 1996. Oxygen and hydrogen isotopes in the hydrologic cycle. Annual Review of Earth and Planetary Sciences 24, 225-262.

Goñi, M.A., Ruttenberg, K.C., Eglinton, T.I., 1997. Sources and contribution of terrigenous organic carbon to surface sediments in the Gulf of Mexico. Nature 389, 275-278.

Graham, H.V., 2014. Molecular and isotopic indicators of canopy closure in ancient forests and the effects of environmental gradients on leaf alkane expression. The Pennsylvania State University. pp. 1-206

Greenwood, D.R., 1991. The taphonomy of plant macrofossils, The processes of fossilization. Belhaven Press, London, pp. 141-169.

Harrington, J.A., Harman, J.R., 1991. Climate and vegetation in central North America: natural patterns and human alterations. Great Plains Quarterly, 103-112.

Hedges, J.I., Mayorga, E., Tsamakis, E., McClain, M.E., Aufdenkampe, A., Quay, P., Richey, J.E., Benner, R., Opsahl, S., Black, B., Pimentel, T., Quintanilla, J., Maurice, L., 2000. Organic matter in Bolivian

tributaries of the Amazon River: A comparison to the lower mainstream. Limnology and Oceanography 45, 1449-1466.

Hoffmann, B., Feakins, S.J., Bookhagen, B., Olen, S.M., Adhikari, D.P., Mainali, J., Sachse, D., 2016. Climatic and geomorphic drivers of plant organic matter transport in the Arun River, E Nepal. Earth and Planetary Science Letters 452, 104-114.

Hou, J., D'Andrea, W.J., Huang, Y., 2008. Can sedimentary leaf waxes record D/H ratios of continental precipitation? Field, model, and experimental assessments. Geochimica et Cosmochimica Acta 72, 3503-3517.

Hou, J., D'Andrea, W.J., MacDonald, D., Huang, Y., 2007a. Evidence for water use efficiency as an important factor in determining the δD values of tree leaf waxes. Organic Geochemistry 38, 1251-1255.

Hou, J., D'Andrea, W.J., MacDonald, D., Huang, Y., 2007b. Hydrogen isotopic variability in leaf waxes among terrestrial and aquatic plants around Blood Pond, Massachusetts (USA). Organic Geochemistry 38, 977-984.

Imhoff, M., Bounoua, L., Ricketts, T., Loucks, C., Harriss, R., Lawrence, W., 2004. Global patterns in net primary productivity. Data distributed by the Socioeconomic Data and Applications Center (SEDAC). http://sedac.ciesin.columbia.edu/es/hanpp.html.

Just, J., Schefuß, E., Kuhlmann, H., Stuut, J.-B.W., Pätzold, J., 2014. Climate induced sub-basin source-area shifts of Zambezi River sediments over the past 17 ka. Palaeogeography, Palaeoclimatology, Palaeoecology 410, 190-199.

Kammerer, J.C., 1987. Largest rivers in the United States. Available from books and open file report section, USGS Box 25425, Denver, CO 80225. Water resources investigations open file report 87-242, August 1987. 2 p, 1 fig, 1 tab, 1 ref.

Kaplan, J.O., Bigelow, N.H., Prentice, I.C., Harrison, S.P., Bartlein, P.J., Christensen, T., Cramer, W., Matveyeva, N., McGuire, A.D., Murray, D.F., 2003. Climate change and Arctic ecosystems: 2. Modeling, paleodata-model comparisons, and future projections. Journal of Geophysical Research:

Atmospheres 108.

Kirby, M.E., Feakins, S.J., Bonuso, N., Fantozzi, J.M., Hiner, C.A., 2013. Latest Pleistocene to Holocene hydroclimates from Lake Elsinore, California. Quaternary Science Reviews 76, 1-15.

Kunst, L., Samuels, A., Jetter, R., 2005. The plant cuticle: formation and structure of epidermal surfaces. Plant Lipids—Biology, Utilisation and Manipulation, D. Murphy, ed (Oxford, UK: Blackwell), 270-302.

Lieth, H., 1975. Primary productivity in ecosystems: comparative analysis of global patterns, Unifying concepts in ecology. Springer, pp. 67-88.

Limoges, A., de Vernal, A., Van Nieuwenhove, N., 2014. Long-term hydrological changes in the northeastern Gulf of Mexico (ODP-625B) during the Holocene and late Pleistocene inferred from organic-walled dinoflagellate cysts. Palaeogeography, Palaeoclimatology, Palaeoecology 414, 178-191.

Liu, W., Yang, H., Li, L., 2006. Hydrogen isotopic compositions of *n*-alkanes from terrestrial plants correlate with their ecological life forms. Oecologia 150, 330-338.

Lloyd, J., Farquhar, G.D., 1994. ^{13}C discrimination during CO_2 assimilation by the terrestrial biosphere. Oecologia 99, 201-215.

Magill, C.R., Ashley, G.M., Freeman, K.H., 2013. Ecosystem variability and early human habitats in eastern Africa. Proceedings of the National Academy of Sciences of the United States of America 110, 1167-1174.

Mayewski, P.A., Rohling, E.E., Stager, J.C., Karlén, W., Maasch, K.A., Meeker, L.D., Meyerson, E.A., Gasse, F., van Kreveld, S., Holmgren, K., 2004. Holocene climate variability. Quaternary research 62, 243-255.

McGuire, A.D., Melillo, J., Joyce, L., Kicklighter, D., Grace, A., Moore, B., Vorosmarty, C., 1992. Interactions between carbon and nitrogen dynamics in estimating net primary productivity for potential vegetation in North America. Global biogeochemical cycles 6, 101-124.

McInerney, F.A., Helliker, B.R., Freeman, K.H., 2011. Hydrogen isotope ratios of leaf wax *n*-alkanes in

grasses are insensitive to transpiration. Geochimica et Cosmochimica Acta 75, 541-554.

Pagani, M., Freeman, K.H., Arthur, M.A., 2000. Isotope analyses of molecular and total organic carbon from miocene sediments. Geochimica et Cosmochimica Acta 64, 37-49.

Parker, G.G., O'Neill, J.P., Higman, D., 1989. Vertical profile and canopy organization in a mixed deciduous forest. Plant Ecology 85, 1-11.

Pearson, A., Eglinton, T.I., 2000. The origin of *n*-alkanes in Santa Monica Basin surface sediment: a model based on compound-specific $\Delta^{14}C$ and $\delta^{13}C$ data. Organic Geochemistry 31, 1103-1116.

Polissar, P.J., D'Andrea, W.J., 2014. Uncertainty in paleohydrologic reconstructions from molecular δD values. Geochimica et Cosmochimica Acta 129, 146-156.

Polissar, P.J., Freeman, K.H., 2010. Effects of aridity and vegetation on plant-wax δD in modern lake sediments. Geochimica et Cosmochimica Acta 74, 5785-5797.

Ponton, C., West, A.J., Feakins, S.J., Galy, V., 2014. Leaf wax biomarkers in transit record river catchment composition. Geophysical Research Letters 41, 6420-6427.

Prentice, I., Harrison, S., Bartlein, P., 2011. Global vegetation and terrestrial carbon cycle changes after the last ice age. New Phytologist 189, 988-998.

Rabinowitz, P.D., Merrell, W.J., Garrison, L.E., Kidd, R.B., Garrison, E., 1985. Ocean Drilling Program Leg 100 report Northeastern Gulf of Mexico.

Ramankutty, N., Foley, J., 2010. ISLSCP II Potential Natural Vegetation Cover. ISLSCP Initiative II Collection, Data set, edited by: Hall, FG, Collatz, G., Meeson, B., Los, S., de Colstoun, B., and Landis, D., Oak Ridge National Laboratory Distributed Active Archive Center, Oak Ridge, TN, USA, doi 10.

Ramankutty, N., Foley, J.A., 1999. Estimating historical changes in global land cover: Croplands from 1700 to 1992. Global Biogeochemical Cycles 13, 997-1027.

Rommerskirchen, F., Plader, A., Eglinton, G., Chikaraishi, Y., Rullkötter, J., 2006. Chemotaxonomic significance of distribution and stable carbon isotopic composition of long-chain alkanes and alkan-1-ols in C_4 grass waxes. Organic Geochemistry 37, 1303-1332.

Sachse, D., Billault, I., Bowen, G.J., Chikaraishi, Y., Dawson, T.E., Feakins, S.J., Freeman, K.H., Magill,

C.R., McInerney, F.A., van der Meer, M.T.J., Polissar, P., Robins, R.J., Sachs, J.P., Schmidt, H.-L., Sessions, A.L., White, J.W.C., West, J.B., Kahmen, A., 2012. Molecular Paleohydrology: Interpreting the hydrogen-isotopic composition of lipid biomarkers from photosynthesizing organisms. Annual Review of Earth and Planetary Sciences 40, 221-249.

Saugier, B., Roy, J., Mooney, H.A., 2001. Estimations of global terrestrial productivity-23: Converging toward a single number?

Schefuß, E., Schouten, S., Schneider, R.R., 2005. Climatic controls on central African hydrology during the past 20,000 years. Nature 437, 1003-1006.

Seki, O., Nakatsuka, T., Shibata, H., Kawamura, K., 2010. A compound-specific *n*-alkane $\delta^{13}C$ and δD approach for assessing source and delivery processes of terrestrial organic matter within a forested watershed in northern Japan. Geochimica et Cosmochimica Acta 74, 599-613.

Smith, F.A., Freeman, K.H., 2006. Influence of physiology and climate on δD of leaf wax *n*-alkanes from C_3 and C_4 grasses. Geochimica et Cosmochimica Acta 70, 1172-1187.

Still, C.J., Berry, J.A., Collatz, G.J., DeFries, R.S., 2003. Global distribution of C_3 and C_4 vegetation: Carbon cycle implications. Global biogeochemical cycles 17, 6-1.

Suh Y.J., Diefendorf A.F., 2017. Seasonal and canopy height variation in *n*-alkanes and their carbon isotopes in a temperate forest. *Accepted*, Organic Geochemistry

Tao, S., Eglinton, T.I., Montluçon, D.B., McIntyre, C., Zhao, M., 2016. Diverse origins and pre-depositional histories of organic matter in contemporary Chinese marginal sea sediments. Geochimica et Cosmochimica Acta 191, 70-88.

Teller, J.T., 1990. Volume and routing of late-glacial runoff from the southern Laurentide Ice Sheet. Quaternary Research 34, 12-23.

Tipple, B.J., Meyers, S.R., Pagani, M., 2010. Carbon isotope ratio of Cenozoic CO_2: A comparative evaluation of available geochemical proxies. Paleoceanography 25.

Tipple, B.J., Pagani, M., 2010. A 35Myr North American leaf-wax compound-specific carbon and hydrogen isotope record: Implications for C_4 grasslands and hydrologic cycle dynamics. Earth and Planetary

Science Letters 299, 250-262.

Vogts, A., Moossen, H., Rommerskirchen, F., Rullkötter, J., 2009. Distribution patterns and stable carbon isotopic composition of alkanes and alkan-1-ols from plant waxes of African rain forest and savanna C_3 species. Organic Geochemistry 40, 1037-1054.

Watts, W.A., 1970. The full-glacial vegetation of Northwestern Georgia. Ecology 51, 17-33.

Wickert, A.D., 2016. Reconstruction of North American drainage basins and river discharge since the Last Glacial Maximum. Earth Surface Dynamics 4, 831.

Zhang, Y.K., Schilling, K.E., 2006. Increasing streamflow and baseflow in Mississippi River since the 1940s: Effect of land use change. Journal of Hydrology 324, 412-422.

Zhuang, G., Brandon, M.T., Pagani, M., Krishnan, S., 2014. Leaf wax stable isotopes from Northern Tibetan Plateau: Implications for uplift and climate since 15 Ma. Earth and Planetary Science Letters 390, 186-198.

Chapter 4: Paleohydrology and paleovegetation of the Mississippi River basin for the past ~150 kyr

ABSTRACT

Understanding past changes in water and vegetation, especially in drought sensitive regions such as the Great Plains of the central United States, is critical for anticipating future change. To this end, we reconstructed vegetation and hydrologic conditions in the Mississippi River Basin (MRB), which includes the Great Plains in the west to the temperate forests in the east, over the last ~150 kyr. Our focus includes Marine Isotope Stage 5e (MIS 5e; 130-115 kyr), which is thought to have been ~2°C warmer on average than today. We measured carbon ($\delta^{13}C_{wax}$) and hydrogen (δD_{wax}) stable isotope values of plant waxes (*n*-alkanes and *n*-alkanoic acids) as proxies for vegetation and hydrology, respectively, from the ODP 625B sediment core, which was collected near the MRB discharge area in the northeastern Gulf of Mexico (GOM). From long-chain *n*-alkanes (C_{33}), we find that percent C_4 (%C_4) did not vary much during the MIS 5e compared to the Holocene. Precipitation or runoff may have increased in southern forested areas during the MIS 5e than the Holocene. The results suggest that the spatial distribution of precipitation during the MIS 5e differed from the Holocene. This is due to increased summer insolation in low latitudes, leading to the expansion of Atlantic Warm Pool and northward migration of the Intertropical convergence zone. Increased northern extent of air masses from low latitudes may have shifted the mid-latitude Polar Front positions northward and increased GOM-derived precipitation over the southeastern MRB. At high latitudes, ice volume decreased and southward migration of Pacific and Arctic air masses may have diminished, bringing less precipitation over the northern Great Plains. After MIS 5e, aridity increased throughout MIS 5d and this drying persisted into MIS 5c. Since the MIS 5c to 5a, there is an increase in contribution of air masses from Pacific and Arctic, and concurrent decrease in C_4 grassland, which is similar to those in the Last Glacial. Towards the Holocene, there is an increase in warm GOM-derived precipitation, and C_4 grassland expansion. We observed a significant positive correlation in the

GOM sea surface temperature (SST) with average chain length ($r^2 = 0.65$, $p < 0.0001$) and *n*-alkane $\delta^{13}C$ values ($r^2 = 0.24$, $p < 0.05$) existed over the last 130 kyr. These correlations further suggest a link between low latitude heat and moisture transport to the continent and their influences on terrestrial plant composition in the MRB. This study illustrates changes in vegetation and hydrology in the MRB in response to changes in mid-latitude Polar Front positions as a result of global summer insolation and ice volume dynamics.

1. Introduction

The midcontinent North America (NA) is projected to experience severe and long-lasting droughts by the end of the 21st century under continued climate change (Cook et al., 2015; Hufkens et al., 2016; IPCC, 2014). Understanding changes in the water cycle and its influence on vegetation is important given the great socio-economic importance of the region. To place these future changes in context, this study aims to understand hydrologic and vegetation conditions in the midcontinental NA, specifically in the Mississippi River Basin (MRB) during the Last Interglacial (LIG) when global climate was warmer today (Barnola et al., 1991; Kukla et al., 2002; Martinson et al., 1987; Petit et al., 1999).

The LIG corresponds to Marine Isotope Stage (MIS) 5e and occurred between 130 to 115 kyr based on the high-resolution SPECMAP chronology (Martinson et al., 1987; Shackleton, 1969). MIS 5e is known as Eemian in Europe and Sangamonian in North America (Dahl-Jensen et al., 2013), designated after the first recognition of the warm period in Eem River deposits in the Netherlands (Harting, 1874) and the Sangamon Formation in Illinois (Leverett, 1898), respectively. Based on proxy reconstructions, the average global surface temperature during the MIS 5e was about 1.7°C higher on land and 0.8°C higher in the ocean compared to today (Otto-Bliesner et al., 2013). This global warming was driven by orbital forcing which increased insolation during boreal summer (Yin and Berger, 2012), resulting in "high" interglacial greenhouse gases around 280 ppmV (Fig. 2j; Loulergue et al., 2008; Siegenthaler et al., 2005), and lower global ice volume (Fig. 2i; Barnola et al., 1991; Kukla et al., 2002; Martinson et al., 1987; Petit et al., 1999).

In North America, sea surface temperature (SST) records indicate 2-5°C higher temperatures than the present (Fig. 2h; Herbert et al., 1995; Limoges et al., 2014; Mangelsdorf et al., 2000; Ziegler et al., 2008). Although not all proxies agree on the extent of SST increase, temperatures were all higher than the present. However, limited information exists as to the response of terrestrial hydrology and vegetation to

these increased temperatures, largely due to the paucity of terrestrial paleoclimate records from MIS 5e and much of the past 150 kyr. To complicate matters, model outputs contradict paleoclimate and paleovegetation records (Harrison et al., 1995; Epstein et al., 1997).

Past studies have recognized the value in characterizing LIG climate and vegetation in midcontinent NA. For example, physiologically simulated biomes were modelled using atmospheric general circulation models (Harrison et al., 1995). Under a warm summer climate scenario, a drier climate in midcontinent NA was suggested with an expansion of warm grasses and shrubs during the MIS 5e. This largely contrasts with proxy records. Montero-Serrano et al. (2011) suggested wetter conditions in midcontinent NA during the LIG than the Holocene based on geochemical and mineralogical characteristics in terrigenous sediments deposited in the northern GOM. The pollen records generally agree on dominant vegetation successions from evergreen conifers associated with Illinoian glaciation (MIS 6) to expansion of deciduous angiosperm trees and subsequent grassland expansion, and a return to conifer dominance during the Wisconsinan Glaciation (Curry and Baker, 2000; Grüger, 1972; King and Saunders, 1986). Some pollen studies suggest that the start of the Sangamonian was more consistent with today's climate and may have become more arid in mid-Sangamonian (Fig. 3d-3e; Grüger, 1972; Kapp and Gooding, 1964; Zhu and Baker, 1995). However, as with most paleosol records, the exact age of the sediments is not well-constrained, making correlation between the Sangamonian and MIS5e challenging (Curry and Baker, 2000; Fredlund and Jaumann, 1987; Grüger, 1972; Hall, 1981; Kapp, 1965; Kapp and Gooding, 1964; Ruhe et al., 1974; Swinehart, 1999). Additionally, without good age control, it is hard to identify gaps in these paleosol records.

The midcontinent NA receives moisture from four sources, namely GOM, Atlantic, Pacific, and Arctic derived air masses (Harrington and Harman, 1991). The temperature gradient in high and low latitudes determines the position of the mid-latitude Polar Front and strength of atmospheric circulation systems, such as the Bermuda High and the Westerlies that facilitate distribution and timing of precipitation in NA

(Harrington and Harman, 1991). At lower latitudes, increased temperatures during the MIS 5e would have expanded the Atlantic Warm Pool (AWP), and affected latitudinal position of the Intertropical Convergence Zone (ITCZ) (Fig 1; Limoges et al., 2014; Montero-Serrano et al., 2011; Ziegler et al., 2008). Migration of ITCZ regulates northward extension of warm Caribbean water into the GOM basin, and consequently affects sea surface temperature (SST) and ocean hydrology in GOM (Limoges et al., 2014). This ocean-atmospheric influence from low and high latitudes may shift source and contribution of moisture, and consequently affect terrestrial hydrology and vegetation in mid-continent NA.

In this study, we will provide evidence of moisture transport and vegetation shifts in MRB over the past ~150 kyr by using plant waxes and their carbon and hydrogen (δD_{wax}) isotopes ($\delta^{13}C_{wax}$) preserved in ODP 625B marine sediment core near the MR discharge area (Fig. 1), as proxies for paleovegetation and paleohydrology, respectively (Diefendorf and Freimuth, 2017; Freeman and Pancost, 2014; Sachse et al., 2012; Tipple and Pagani, 2010). Since we will be measuring the identical wax compounds to determine hydrology and vegetation, we can derive a more accurate paleo-record of the source region. Long-chain *n*-alkyl lipids are found in and on terrestrial plant leaf cuticle and consist of *n*-alkanes, *n*-alkanoic acids, *n*-alcohols, and wax esters (Eglinton and Hamilton, 1963; Eglinton and Hamilton, 1967). These waxes are transported via fluvial and aeolian processes and are preserved in terrestrial and marine sediments (Freeman and Colarusso, 2001; Pagani et al., 2000; Rieley et al., 1991). $\delta^{13}C_{wax}$ values reflect $\delta^{13}C$ values of the atmospheric CO_2 ($\delta^{13}C_{CO2}$), isotope fractionations during photosynthesis (Δ_{leaf}) and lipid biosynthesis ($\varepsilon_{alk\text{-}leaf}$). The strongest controls on net fractionation of carbon in plants are photosynthetic pathways and water availability. Plants using the C_3 photosynthetic pathway, including trees, shrubs, herbs, and cool growing season grasses have larger net fractionation, while C_4 pathway plants, mostly tropical/warm growing season grasses, have smaller net ^{13}C fractionation (Bi et al., 2005; Bush and McInerney, 2015; Chikaraishi and Naraoka, 2007; Collister et al., 1994; Diefendorf et al., 2011; Diefendorf and Freimuth, 2017; Garcin et al., 2014; Tipple and Pagani, 2010). Among C_3 plants, net fractionation also varies with water availability, showing highest correlation with mean annual

precipitation (MAP) over other climate parameters (Diefendorf et al., 2010). Moreover, C_4 grasses produce *n*-C_{33} alkanes in high abundance while C_3 trees produce higher concentration of *n*-C_{29} and *n*-C_{31} alkanes. δD_{wax} values, on the other hand, are highly correlated with regional precipitation (δD_p), as precipitation is the primary source of hydrogen for terrestrial plants (Sachse et al., 2012). δD_p values thus reflect precipitation sources and meterological processes, such as evaporation and condensation (Craig, 1961; Dansgaard, 1964; Gat, 1996). Therefore, sedimentary δD_{wax} values are increasingly used to reconstruct paleohydrologic change (Collins et al., 2013; Feakins et al., 2014; Garel et al., 2013; Pagani et al., 2006; Sessions et al., 2004; Tierney et al., 2008).

$\delta^{13}C_{wax}$ and δD_{wax} values in nearshore marine sediments are influenced by the complexities of vegetation and climate that are not uniform within source catchment areas and may also be influenced by taphonomic processes that favor wax from major wax producers, the upper canopy, and riparian zones (Diefendorf and Freimuth, 2017; Hoffmann et al., 2016; Suh and Diefendorf, 2017). To address these potential controls on the leaf wax isotopic signal preserved in downcore sediments, Chapter 3 used an isotope-enabled spatial modelling approach to identify key controls on leaf wax source and mixing within the MRB to better understand the signal preserved in nearshore marine cores, such as ODP site 625B. In Chapter 3, we found that leaf wax export was influenced by runoff and leaf wax productivity. Hence the leaf wax transport from forested areas in the MRB to the GOM was higher than from the grasslands. Leaf wax contribution also varied by chain length. As C_4 grasses produce higher concentration of *n*-C_{33} alkanes, grassland-derived *n*-alkane contribution was higher in *n*-C_{33} alkanes than in *n*-C_{29} or *n*-C_{31} alkanes.

As we partly understand leaf wax integration processes from the MRB to the GOM, we accounted for these factors into our interpretation. We minimized runoff and production bias in sedimentary leaf wax records by using *n*-C_{33} alkane $\delta^{13}C$ data to estimate grassland expansion and by calibrating to existing Last Glacial and current interglacial $\%C_4$ spatial data (Cotton et al., 2016; Ramankutty and Foley, 2010).

This is the first study to combine modern calibrations on spatial variations in leaf wax integration into leaf wax interpretations in marine sediments. Despite complications, we illustrate how to derive information about a poorly constrained area for important recent changes in paleovegetation and paleohydrology.

2. δD_p values reflect the precipitation source and distribution

Hydrogen isotopes of precipitation (δD_p) have a robust correlation with geographic or climatic parameters such as continentality, temperature (which changes with latitude and altitude), and humidity (Dansgaard, 1964; Yurtsever and Gat, 1981; Rozanski et al., 1993). The major controls on δD_p values in North America are latitude and elevation, although there are a few regions with notable effects from evaporation and distance from the coast (Fig. 2c). A few arid places in the MRB such as the western Great Plains may have D-enriched δD_p values. The northern states in the MRB may have lower δD_p values from Arctic and Pacific airmasses that rained out more deuterium while traveling over mountains in the western continent (Anderson, 2006). The Pacific and Arctic-derived air masses have a mean annual δD_p value of −125‰ (Bowen, 2014), which is distinct from the GOM and subtropical North Atlantic-derived moisture mean annual δD_p value (−10‰). Distribution of these air masses reflect the latitudinal position of the Polar Fronts which is intimately related to the strength of the Westerlies and Burmuda Highs. δD_p values in MRB primarily track precipitation source and distribution. The current mean annual δD_p value of the MRB is −47‰, and we can roughly estimate the contribution of each moisture source to the MRB using a simple mixing model. GOM/Atlantic air masses contribute 65% of the moisture, while a combined Pacific/Arctic source provides 35% of the precipitation in the MRB.

3. Modern vegetation and $\delta^{13}C_{alk}$ values in the MRB

MAP increases from west to east in MRB ranging from 140 mm to 2300 mm with a basin-wide average of 800 mm (Fig. 2a; http://prism.oregonstate.edu). There is a significant positive spatial correlation between MAT and MAP in MRB ($r^2 = 0.65$, $p < 0.05$). The mean annual temperature (MAT) normals in MRB varies from −4°C to 23°C (basin-wide mean = 11°C), with higher temperatures near the Gulf States and lower temperatures in the northwestern MRB (http://prism.oregonstate.edu). The regional climate of increasing moisture availability from west to east mirrors prairie-forest vegetation in MRB to some extent (Fig. 1; Harrington and Harman, 1991). There are grasslands in the west and deciduous and mixed forests in the east (Harrington and Harman, 1991). Based on potential natural vegetation cover under current climate condition without human activities, the MRB should consist of 55% grassland, 23% temperate deciduous forest, 6% temperate needleleaf evergreen forest, 6% mixed forest, 6% shrubland, 2% boreal evergreeen forest, and less than 1% of tundra (Fig. 1a; Ramankutty and Foley, 2010). When a temperature crossover approach was used to define C_3 and C_4 grassland composition (Still et al., 2003) in MRB, the overall 55% grassland cover was broken down into 26% C_3 grasses (in the north) and 29% C_4 grasses (in the south). Another study by Cotton et al. (2016) showed similar %C_4 for the mid-Holocene that 31% of vegetation in the MRB consisted of C_4 plants based on $\delta^{13}C$ values of bison and mammoth tissues. Figure 2b illustrates an isotope landscape model (i.e. isoscape) of $\delta^{13}C_{alk}$ values in the MRB based on carbon isotope fractionations during photosynthesis or Δ_{leaf} determined by MAP, and during lipid biosynthesis or $\varepsilon_{alk\text{-}leaf}$ by major plant types that dominate sedimentary records (See Chapter 3).

4. Site location and methods

4.1. The Mississippi River basin and ODP 625B core

The MRB is the largest drainage basin in North America with an area of 2,981,000 km^2 and an average annual discharge of ~17,000 m^3/s freshwater into the GOM (Kammerer, 1987). The waters are drained from rivers and tributaries between the Rocky and Appalachian Mountains, namely the St. Croix River, Wisconsin River, Rock River, Illinois River, Kaskaskia River, Ohio River, Minnesota River, Des Moines River, Missouri River, White River, Arkansas River, and Red River.

We used sediment samples from ODP 625B core retrieved from the northeastern GOM near the MR discharge point (Fig. 1; 28.83°N, 87.16°W) during the Ocean Drilling Program (ODP) Leg 100 in 1985 (Rabinowitz et al., 1985). The core site is located ~200 km east-southeast from the MR delta in 889 m of water depth. The entire 625B core is 231 m long and spans the Quaternary and Pliocene. Three radiocarbon dates from the upper 98 cm are Holocene in age and the rest of the sediment ages are constrained with an $\delta^{18}O$-based age model (Dowsett, 1999; Joyce et al., 1993; Joyce et al., 1990; Limoges et al., 2014). We studied upper sections that correspond to the last ~150 kyr with sampling done every 0.5 to 7 kyr within each marine isotope stages of 6, 5, 2, and 1, with a total sample number of 32. Sedimentation rates varied from 4 to 22 cm/ka, and were higher during the Last Glacial (18 to 22 cm/ka) than the other time periods (4 to 10 cm/ka).

The preservation of biomarkers in sediments is important for an accurate reconstruction of paleoclimate. The last deglaciation sediments from the Orca Basin in central GOM contained reworked terrestrial organic matter based on biomarkers and optical kerogen analyses (Meckler et al., 2008). Ages and diagenetical alteration of the organic matter tend to increase in finer-size particles or clay fractions, and

they can travel further offshore (Arnarson and Keil, 2001; Keil et al., 1998). ODP 625B core is located closer to the continent and may contain lesser amount of old organic matter than in the Orca Basin. Prior studies investigated ages and diagenetic alteration of organic matter in the lower MRB and sediments of the GOM (Goñi et al., 1997; Gordon and Goñi, 2004; Rosenheim et al., 2013; Wakeham et al., 2009). Radiocarbon (^{14}C) ages of long-chain fatty acids in lower MR and MR mouth ranged between 715 yr to 2,150 yr (Wakeham et al., 2009). Other studies also measured ^{14}C ages for particulate organic carbon (POC) from lower Mississippi-Atchafalaya River (MAR) system (Rosenheim et al., 2013) and near its outflow on the continental shelf (Goñi et al., 1997; Gordon and Goñi, 2004; Wakeham et al., 2009). In the lower MAR system, ^{14}C ages were younger than 2,000 year (Rosenheim et al., 2013), and on the continental shelf, the ages ranged between 1,070 and 6,770 year with an average of 2,310 year. Based on these prior studies, old organic matter input may be minor near the study site and may not largely affect the interpretation of 150 kyr record. We further analyzed carbon preference index (CPI) to indicate thermal maturity of the lipids.

4.2. Lipid extraction and separation

Sediment samples were freeze-dried and powered using a Spex ball mill. The powdered sediments (ca. 20 g) were extracted using an accelerated solvent extractor (ASE; Dionex 350) with dichloromethane (DCM)/methanol (MeOH) (2:1, v/v) at ~7.6 mpa (~1100 psi) and 100 ºC for three extraction cycles. The total lipid extract was then base saponified to cleave fatty esters with 2.5 ml of 0.5 N KOH in MeOH/H_2O (3:1, v/v) for 2 h at 75°C. After cooling the saponified lipid extract (SLE) to room temperature, ~3 ml of NaCl in water (5%, w/w) was added and was acidified by adding ~0.5 ml of 6 N HCl to a pH of ~1. The acidic solution was extracted using Hexanes/DCM (4:1, v/v). The saponified lipids were then neutralized with $NaHCO_3/H_2O$ (5%, w/w) and dried with Na_2SO_4. We separated the SLE into acid and neutral fractions with 0.5 g of aminopropyl (Supelco Supelclean LC-NH_2). The neutral fraction was eluted with 4

ml 2:1 DCM/IPA and acid fraction was eluted with 4 ml 4% formic acid in ethyl ether. The acid fraction was evaporated under a gentle stream of N_2 gas and methylated by adding ~1.5 ml of 95:5 MeOH/12 N HCl (v/v). The solution was heated at 70°C for 12 to 18 h, cooled, and water was added. Fatty acid methyl esters (FAMEs) were then extracted with hexanes.

4.3. Identification and quantification

n-Alkanes and FAMEs were analysed using an Agilent 7890A GC-MS and flame ion detection (FID) interfaced to an Agilent 5975C quadrupole mass selective detector (MSD) with electron-impact ionization (70 eV). Compounds were separated on a fused silica capillary column (Agilent J&W DB-5 ms; 30 m, 0.25 mm ID, 25-µm film thickness) and a 5 m guard column (Restek Rxi, 5 m, 0.32 mm) was used with helium as the carrier gas. The oven started at 60°C initially for 1 min and was increased to 320°C at 6°C/min, and a final hold of 15 min. The column effluent was split (1:1) between the FID and MSD with a 2-way splitter (Agilent G3180B) at a constant pressure (182 Pa). Compounds were identified using authentic standards, library databases (NIST 2008 and Wiley 2009), spectral library, and retention times.

Prior to quantification, all samples were diluted in hexanes with an internal standard, 1,1′-binaphthyl, at 25 µg/ml. The compound peak areas were normalized to those of 1,1′-binaphthyl and converted to concentrations using response curves of an in-house mixture of *n*-alkanes and FAMEs analysed at concentrations ranging from 0.5 to 100 µg/ml. Compound concentrations were normalized to the mass of dry sediment extracted. Precision and accuracy were determined by analyzing *n*-alkane and FAME standards at 25 µg/ml and were 0.85 µg/ml (1σ, n = 46) and -0.13 µg/ml (1σ, n = 46), respectively.

We characterized changes on average *n*-alkane chain length ($ACL_{25\text{-}35}$) from *n*-C_{25} to *n*-C_{35} using the following equation (Freeman and Pancost, 2014):

$$\mathrm{ACL}_{25-35} = \frac{(25\,C_{25} + 27\,C_{27} + 29\,C_{29} + 31\,C_{31} + 33\,C_{33} + 35\,C_{35})}{(C_{25} + C_{27} + C_{29} + C_{31} + C_{33} + C_{35})} \quad (1)$$

Carbon preference indices (CPI) were also measured to examine thermal maturity of the *n*-alkanes using the following equation by Bray and Evans (1961):

$$\mathrm{CPI} = 0.5\,[\frac{(C_{25} + C_{27} + C_{29} + C_{31} + C_{33})}{(C_{26} + C_{28} + C_{30} + C_{32} + C_{34})} + \frac{(C_{25} + C_{27} + C_{29} + C_{31} + C_{33})}{(C_{24} + C_{26} + C_{28} + C_{30} + C_{32})}] \quad (2)$$

4.4. Leaf wax compound-specific carbon and hydrogen isotope analysis

Prior to *n*-alkane $\delta^{13}C$ and δD analysis, hydrocarbons were separated into a saturated and unsaturated fraction by eluting with 4 ml hexanes and 4 ml ethyl acetate, respectively, using 5% silver nitrate impregnated silica gel. *n*-Alkanes were further separated from the unresolved complex mixture (UCM) by urea adduction. *n*-Alkanes and FAMEs were analyzed using Thermo Trace GC Ultra coupled to a Thermo Electron Delta V Advantage IRMS instrument, via an isolink combustion reactor for $\delta^{13}C$ at 1100°C and pyrolysis reactor for δD at 1420°C. GC conditions were similar to the above, but with a faster ramp rate (8°C/min). For FAME analysis, samples and standards were run with the backflush valve open to exclude high abundance compounds eluting before *n*-C_{22} alkanoic acid. The H_3^+ factor was tested daily and averaged 4.9 ppm mV^{-1} during the period of analysis. The $\delta^{13}C$ and δD values of the compounds were determined relative to a reference gas calibrated with Mix A5 standards (*n*-C_{16} to *n*-C_{30}; Arndt Schimmelmann, Indiana University) that was run every 5 to 10 samples (see Polissar and D'Andrea, 2014). $\delta^{13}C$ and δD values of the samples (SA) are reported in delta notation relative to the international standards VPDB and VSMOW/VSLAP, respectively (following Coplen 2006 and Coplen et al. 2011). Precision and accuracy for $\delta^{13}C$ analyses are 0.1 ‰ (n = 78) and −0.1‰ (n = 78), respectively. The mean analytical uncertainty was 5.1‰ (1σ, n = 12) for δD_{alk} samples and 4.2‰ (1σ, n = 15) for $\delta Dn\text{-}_{C28\ acid}$ samples. The δD value of the added methyl group was determined by mass balance equation of phthalic

acid of known δD composition (A. Schimmelmann, Indiana University) and derivatized methyl phthalate.

5. Results

5.1. Organic matter in the Mississippi River and Gulf of Mexico

CPI values indicate thermal maturity of the lipids. Larger CPI values (> 1) indicate a greater concentration of odd compared to even chain lengths, which is a characteristic distribution for terrestrial plant *n*-alkanes, while thermally matured rocks and oils have low CPI values (< 1) (Ishiwatari et al., 1977; Rushdi and Simoneit, 2002a, b). In this study, CPI values ranged from 2.6 to 6.1 (mean = 4.0, $\sigma = 0.7$, n = 36; Appendix Table A1). CPI values were slightly lower during the Last Glacial (3.1 ± 0.4), compared to the rest of the samples, but are not inconsistent with values commonly observed in sediments (Huang et al., 1997; Tipple and Pagani, 2010). For interglacial sediments, which are the focus of this study, CPI values were similar (t-test, $p > 0.05$) between the Holocene (4.1 ± 0.4) and MIS 5e (4.2 ± 0.5).

5.2. Plant wax concentrations and distributions

Long-chain *n*-alkane concentrations ranged from 2 ng/g to 360 ng/g and was generally lower during interglacials (ca. 100 ng/g for both *n*-C_{29} and *n*-C_{31}) and higher during the glacial (ca. 150-350 ng/g for both *n*-C_{29} and *n*-C_{31}; Fig. 3a, Table A2). MIS 5 is divided into five substages (5a to 5e), The lowest *n*-alkane concentrations was found in MIS 5d (*n*-C_{29} = 19.2 ng/g, *n*-C_{31} = 18.5 ng/g); the highest *n*-alkane concentrations (*n*-C_{29} = 359.9 ng/g, *n*-C_{31} = 328.7 ng/g) were during the last deglaciation (15.5 kyr).

$ACL_{25\text{-}35}$ values ranged from 29.0 to 30.2 (mean = 29.7, $1\sigma = 0.3$, n = 31), and was generally higher during interglacials (Holocene = 29.8 ± 0.2, MIS 5e = 30.0 ± 0.1, Fig. 3b and Table A1) and lower during

glacial periods (LGM = 29.2 ± 0.1). The average $ACL_{25\text{-}35}$ shift was the most prominent from the LGM to the Holocene (t-test, $p < 0.001$). However, late MIS 6 had $ACL_{25\text{-}35}$ values that were similar to those in the interglacial periods (difference = 0.2). MIS 5e (30.0) and 5c (30.1) had slightly higher mean $ACL_{25\text{-}35}$ values than the MIS 5d (29.8) and 5b (29.8). $ACL_{25\text{-}35}$ was statistically higher during MIS 5e (30.0 ± 0.1) than the Holocene (29.8 ± 0.1; t-test, $p < 0.03$).

5.3. Leaf wax $\delta^{13}C$ values

Terrestrial plants utilize atmospheric CO_2 as their source of carbon and, as such, plant $\delta^{13}C$ values reflect the $\delta^{13}C$ values of atmospheric CO_2 ($\delta^{13}C_{CO2}$), along with other factors that influence photosynthesis (e.g. Diefendorf and Freimuth, 2017; Farquhar et al., 1989; Freeman and Pancost, 2014). Because $\delta^{13}C_{CO2}$ changes over time, it should be considered when evaluating plant $\delta^{13}C$ values over time (Tipple et al., 2010). To assess changes in $\delta^{13}C_{CO2}$ for this study, we compiled $\delta^{13}C_{CO2}$ values for the past 150 kyr (Fig. 3k). For this period, we used the ice-core gas bubble records for the past 50 kyr (Elsig et al., 2009; Friedli et al., 1986; Leuenberger et al., 1992; Smith et al., 1999) and benthic foram-derived values for 50 to 150 kyr (Tipple et al., 2010). The $\delta^{13}C_{CO2}$ values in MIS 6 were between −8 to −7‰, and increased by ~1.5‰ in MIS 5e. Values remain roughly constant for the remaining interglacial at −6.5‰ before slightly decreasing from the LGM to late Holocene by 0.5 to 1‰. Although values change over our study interval by ~1.5‰, we choose not to apply a correction or to calculate fractionation factors. We made this decision based on several factors including 1) the lack of continuous record of $\delta^{13}C_{CO2}$ for the past 150 kyr, 2) the similarity in values for the past 120 kyr, and 3) modest change of ~1.5‰ from 150 kyr to 120 kyr relative to the range in our $\delta^{13}C_{wax}$ values. Below we comment on how changes in $\delta^{13}C_{CO2}$ could have influenced our results, especially at the transition from MIS 6 to 5e.

$\delta^{13}C_{alk}$ values ranged between −32.0‰ and −29.4‰ for *n*-C_{29}, −32.1‰ and −28.6‰ for *n*-C_{31}, and −31.3‰ and −26.7‰ for *n*-C_{33} (Fig. 3d). In general, interglacials had higher $\delta^{13}C_{alk}$ values, while glacial

periods had lower values in all *n*-alkane homologues (*n*-C_{29} to *n*-C_{33}). Temporal changes in $\delta^{13}C_{C33\ alk}$ values were slightly different from those in other homologues (*n*-C_{29} to *n*-C_{31}). For example, mean $\delta^{13}C_{C29\ alk}$ values increased from late MIS 6 (−31.8 ± 0.2‰) to MIS 5e (−30.8 ± 0.5‰), which then further increased in MIS 5d by ca. 1‰, recording the highest $\delta^{13}C_{alk}$ values over the last 150 kyr. The values remained similar in MIS 5c and then decreased during 5b and 5a by 0.3 to 2.3‰. $\delta^{13}C_{C33\ alk}$ values, on the other hand, varied between interstadials (5a and 5c) and stadials (5b and 5d). Average $\delta^{13}C_{C33\ alk}$ values were slightly lower during interstadials (MIS 5a = 29.5‰, 5c = −29.0‰, and 5e = −28.9‰), and higher during stadials (MIS 5b = −27.3‰ and 5d = −28.2‰). The LGM had relatively low $\delta^{13}C_{alk}$ values for all chain lengths (*n*-C_{29} = 31.5‰, *n*-C_{31} = 31.8‰, *n*-C_{33} = 31.0‰), and the values were ca. 1 to 3 ‰ significantly lower than the Holocene and MIS 5e in all chain lengths (i.e. *n*-C_{29} to *n*-C_{33}, t-test, $p < 0.05$). There was no significant difference in $\delta^{13}C_{alk}$ values between the Holocene and MIS 5e for *n*-C_{29} to *n*-C_{31} (t-test, $p > 0.05$). But for $\delta^{13}C_{C33\ alk}$ values, the Holocene had 0.7‰ higher values on average were (t-test, $p < 0.05$).

$\delta^{13}C$ values of *n*-C_{28} alkanoic acids ranged from −30.1‰ to −26.5‰ (Fig. 3e). Temporal variations in $\delta^{13}C_{C28\ acid}$ was in general similar to those in $\delta^{13}C_{alk}$ values. The LGM (29.9 ± 0.3‰) had significantly lower $\delta^{13}C_{C28\ acid}$ values compared to the interglacial periods (Holocene = −28.2 ± 0.9‰; MIS 5e = −27.8 ± 0.8‰; ANOVA, student's t-test, $p < 0.01$). However, between the two interglacials, no statistical difference was found (t-test, $p > 0.05$). *n*-C_{28} acid and *n*-C_{29} alkanes had an average offset ($\varepsilon_{alk\text{-}acid}$) of 2.3 ± 0.8‰, ranging from 1.1 to 4.7‰.

5.4. Changes in leaf wax contribution from C_4 plants

A simple linear mixing model with assigned $\delta^{13}C_{wax}$ end-member values is commonly used to reconstruct the relative contribution of C_3 and C_4 plants (Castaneda et al., 2009; Collins et al., 2011; Schefusz et al., 2003). However, $\delta^{13}C_{wax}$ values in sediments reflect not only C_4 plant contribution but also moisture

availability, the composition of the C_3 plant community, and variations in wax production among different plant groups (Garcin et al., 2014; Hoffmann et al., 2016; Seki et al., 2010; Tipple and Pagani, 2010). Therefore, a simple linear mixing model may not provide an accurate indicator of $\%C_4$ (Freeman and Pancost, 2014; Garcin et al., 2014). These complications have been addressed by using clever approaches. For example, Magill et al. (2013b) constructed a framework of ecologically relevant end member values for eastern African vegetation and made the important clarification that transitions from forests to woodlands are not a continuous linear gradient in $\delta^{13}C$ values. Uno et al. (2016) advanced this idea by using long-chain *n*-alkanes, like *n*-C_{31}, to calculate $\%C_4$ by recognizing that long-chain *n*-alkanes are more sensitive to C_4 grasses. In Chapter 3, we found that *n*-C_{31} alkanes are more sensitive to grasses than *n*-C_{29} alkanes, but was still underestimating C_4 grasses in the MRB. Angiosperm trees produce ca. 4 times more *n*-C_{29} alkanes than C_4 grasses on average, while C_4 grasses produce about twice as many *n*-C_{33} alkanes than C_3 trees (Diefendorf and Freimuth, 2017). *n*-C_{31} alkanes are produced by C_3 trees and C_4 grasses in a similar concentration, however C_3 grasses produce 30% and 50% more *n*-C_{31} alkanes than C_3 trees and C_4 grasses on average, respectively. C_3 grasses occupied ca. 26% of the MRB during the Holocene, and therefore the *n*-C_{31} contribution from C_3 plants in the MRB is anticipated to have been greater than that from C_4 plants. *n*-C_{33} alkanes in ODP 625B core, on the other hand, better represented $\%C_4$ in the MRB due to higher production by C_4 plants (Rommerskirchen et al., 2006; Vogts et al., 2009). We, therefore, utilize the $\delta^{13}C$ values of *n*-C_{29} and *n*-C_{31} alkanes as indicators of water availability (e.g. Diefendorf et al. 2010) and *n*-C_{33} as indicators of C_4 grasses (Diefendorf and Freimuth, 2017).

$\%C_4$ over time was calculated by calibrating $\delta^{13}C_{C33\ alk}$ values for the Holocene and LGM to the reconstructed $\%C_4$ values from the literature (Cotton et al., 2016; Ramankutty and Foley, 2010). Cotton et al. (2016) modelled spatial distribution of C_4 plants in NA for the mid-Holocene and LGM using classification and regression tree analysis based on $\delta^{13}C$ records of bison and mammoth tissues and their relationship with climatic variables. Using these isoscape maps, we estimated that $\%C_4$ in MRB during

the mid-Holocene and the LGM were 31.0% and 18.5%, respectively (Fig. 4c and Table A2). A temperature crossover approach (Still et al., 2003) on potential vegetation cover (Ramankutty and Foley, 2010) produced a similar $\%C_4$ of 29% in MRB for the Holocene. Using these calibrations, we estimate that $\%C_4$ ranged from 17% to 38% over the past 150 kyr. In late MIS 6, $\%C_4$ changed rapidly from 35% to 20%. Within MIS 5, average $\%C_4$ was slightly lower during interstadials (MIS 5a = 25%, 5c = 27%, and 5e = 28%) than stadials (MIS 5b = 35% and 5d = 31%) by 6% on average. The difference in $\%C_4$ between 5e and 5d is greater if we take into account slight decrease in $\delta^{13}C_{CO2}$ values during the MIS 5d (-6.7‰) and increase during the MIS 5e (-6.3‰) on average. Then, $\%C_4$ during the MIS 5e is 27% and 5d is 32%.

5.5. Leaf wax δD values

δD_{alk} values were generally higher during the interglacials (ca. −160‰ to −170‰) and lower during glacials (ca. −180‰ to −190‰, Fig. 3f and Table A3). However, the highest δD_{alk} values in the last 150 kyr occurred during the late MIS 6 (mean = −155.3‰). δD_{alk} values remained relatively consistent from MIS 6 to MIS 5d, and decreased from late MIS 5c to MIS 5a by ca. 30 to 40‰. δD_{alk} values were low during the LGM (ca. −190‰), and increased gradually towards the present by ca. 20-30‰. The δD_{alk} values for the Holocene were statistically higher than the LGM values (n-C_{29} t-test, $p < 0.001$; n-C_{31} t-test, $p < 0.004$; n-C_{33} t-test, $p < 0.043$). MIS 5e had higher average δD_{alk} values (n-C_{27} = −162.6‰, n-C_{29} = −163.6‰, n-C_{31} = −166.2‰, and n-C_{33} = −157.4‰) than the Holocene (n-C_{27} = −176.8‰, n-C_{29} = −170.5‰, n-C_{31} = −174.0‰, and n-C_{33} = −160.0‰). The offset between the two interglacials were statistically different only in n-C_{27} (t-test, $p < 0.033$), n-C_{29} (t-test, $p < 0.037$), and n-C_{31} (t-test, $p < 0.038$), and the average offset decreased with increasing chain length (average offset = 14.3‰ for C_{27}, 6.9‰ for n-C_{29}, 7.8‰ for n-C_{31}, and 1.6‰ for n-C_{33}).

$\delta D_{C28\ acid}$ values ranged from −168.7‰ to −115.4‰ (Fig. 3g and Table A3), and had a similar temporal

pattern to those in δD_{alk}. $\delta D_{C28\ acid}$ values were consistently high from MIS 6 to MIS 5b (a. −140‰ to −120‰), and dropped rapidly in MIS 5a to −165‰. The LGM values were similar to the MIS 5a and increased back to higher values toward the present. The LGM $\delta D_{C28\ acid}$ values (mean = −164.1‰) were statistically higher than the Holocene (- 136.4‰; t-test, $p < 0.003$) and MIS 5e (-130.5‰; t-test, $p < 0.001$), but the two interglacials had similar $\delta D_{C28\ acid}$ values.

6. Discussion

6.1. Paleovegetation and paleohydrology from the LGM to present

6.1.1 MRB paleovegetation from the LGM to present

During the Last Glacial, much of the northern parts of the MRB were covered by an ice sheet. Global mean temperatures at this time were ~4°C lower than today on land and ~2°C lower in the ocean (a. 2.5°C cooling in North Atlantic, Annan and Hargreaves, 2013; Waelbroeck et al., 2009). In eastern North America and the eastern MRB, open boreal woodlands and tundra were common along the ice margin (Jackson et al., 2000; Whitehead, 1973). Boreal and cool-temperate conifer forests extended as far south as 34°N (Watts, 1970). The lower Mississippi Valley was dominated by *Picea*, which co-existed with cool-temperate and temperate deciduous trees (Delcourt et al., 1980; Jackson and Givens, 1994; Royall et al., 1991). As climate ameliorates towards the Holocene, grasslands expanded, boreal and cool-temperate conifer forests migrated northward and temperate deciduous forest occupied much of the eastern MRB (Harrington and Harman, 1991). Changes in the distribution of C_3 and C_4 plants over the Last Glacial to the present in the MRB were primarily controlled by changes in growing temperature and mean amount and seasonality of precipitation (Cotton et al., 2016; Jackson et al., 2000; Prentice and Bartlein, 1991). However, direct evidence on the extent and timing of moisture source changes in terrestrial environment

and their roles in grassland expansion is limited. In this study, we provide the record of moisture transfer and terrestrial plant community shifts in the MRB using $\delta^{13}C_{alk}$ and δD_{alk} values in the ODP 625B.

Changes in $\delta^{13}C_{alk}$ values is primarily caused by C_3 and C_4 plant distribution and/or increased aridity in regions dominated by C_3 plants. From the LGM to the Holocene, C_4 grassland increased and forestland became drier since the LGM towards the present as indicated by $\delta^{13}C_{alk}$ increase in all *n*-alkane homologues by ca. 1 to 3‰ and $\delta^{13}C_{C28\ acid}$ values by ca. 2‰ (Fig. 3d and 4a-4b). Longer chains such as *n*-C_{33} or *n*-C_{35} are produced in high abundance by most C_4 grasses, some C_3 grasses, and forbs (Diefendorf and Freimuth, 2017; Garcin et al., 2014; Rommerskirchen et al., 2006; Vogts et al., 2009; Vogts et al., 2012). The ACL values during the Holocene were higher than the LGM, confirming C_4 grassland expansion (Fig. 3b-3c), which is similar to conclusions from prior studies (Cotton et al., 2016; Jackson et al., 2000; Prentice and Bartlein, 1991).

To understand the relationship between low latitude-derived heat and moisture on terrestrial vegetation (Harrington and Harman, 1991; Helfand and Schubert, 1995), we tested correlation between Mg/Ca-based SST variations in the GOM with $\delta^{13}C_{alk}$ values and ACL (Fig. 4). We observed a significant positive correlation between changes in ACL and GOM SST ($r^2 = 0.65$, $p < 0.0001$; Fig. 4a). This correlation illustrates far-reaching effects of low latitude-derived heat and moisture on the regional SST, and consequently affecting vegetation composition in the mid-latitude. The ITCZ, which is known to migrate on seasonal to orbital timescales in relation to summer insolation, may have shifted northward during the Holocene (Fig. 1; Limoges et al., 2014). In turn, this would have led to northward extension of warm seawaters from lower latitudes into the GOM, bringing warm, summer precipitation into the MRB, causing C_4 grassland expansion. We also found a positive relationship between SST and $\delta^{13}C_{C31}$ values (Fig. 4b; $r^2 = 0.24$, $p < 0.05$). The correlation was better from the Last glacial to the present ($r^2 = 0.45$, $p < 0.05$), and not significant during the MIS 5 ($p > 0.05$). During the MIS 5, when mean annual SST in the GOM was above 25°C, $\delta^{13}C_{alk}$ values ceased to increase; ACL values also remained consistent when SST

was above 27°C. This may be due to the plant community composition during the MIS 5 responding to regional hydrologic conditions that are not reflected in GOM SST variations.

6.1.2. MRB paleohydrology from the LGM to the present

δD_{wax} values reflect δD_p and apparent fractionation (ε_{app}) that occurs during lipid biosynthesis between plants source water (i.e. precipitation) and leaf waxes (Sachse et al., 2012). ε_{app} values vary by major plant types, for example, ca. −100 ± 19‰ for shrubland, ca. −120 ± 13‰ for C_3 trees, ca. −150 ± 10‰ for C_4 grassland, and ca. −170 ± 17‰ for C_3 grassland (Bi et al., 2005; Hou et al., 2007b; Liu et al., 2006; Sachse et al., 2006; Smith and Freeman, 2006). Shrublands occupy only 6% of the MRB biome for the current climate potential vegetation cover (Fig. 1), and their effects on δD_{wax} may be negligible. In arid environment and grasslands, Deuterium (D)-enrichment in leaf water occurs due to soil evaporation and/or leaf transpiration (Jackson et al., 1996; Feakins and Sessions, 2010; Kahmen et al., 2013a). However, prior studies based on sediment records along a wide climatic gradient found that this leaf water D-enrichment may counter the low ε_{app} values in grasslands, and therefore vegetation effects on δD_{wax} values are minor (Feakins and Sessions, 2010; Hou et al., 2008). The results from Chapter 3 suggested that vegetation effects in sediments are further reduced by taphonomic bias towards C_3 trees, whose ε_{app} values are not influenced by evapotranspiration (Garcin et al., 2014; Sachse et al., 2012; Seki et al., 2010). But leaf wax export and grassland composition changes across space and through time, and especially for *n*-C_{33} alkanes, a significant amount of them are sourced from grasslands. Therefore, we interpret δD_{wax} values mainly as changes in δD_p for *n*-C_{29} and *n*-C_{31}, and additionally as leaf wax sourcing and ε_{app} values for *n*-C_{33} alkanes. We will take advantage of distinct isotopic signatures between northwestern grasslands that have low δD_p and ε_{app} values and southeastern forestland with high δD_p and ε_{app} values.

n-C_{29} and *n*-C_{31} alkanes had very similar δD_{alk} patterns. During the LGM, average δD_{C29} value was −188

± 5‰, and −164 ± 4‰ for $\delta D_{C28\ acid}$, which is 28‰ lower than the Holocene (−136 ± 10‰). These lower LGM $\delta D_{C29\ alk}$ and $\delta D_{C28\ acid}$ values reflect an increase in contribution of the Pacific/Arctic air masses to the basin as ice sheets expanded in the NA. In low latitudes, relatively cooler SST may have compressed the ITCZ toward the equator and hence limited northward extension of warm air masses to higher latitudes (Chiang and Bitz, 2005). Relatively cool precipitation may have favored C_3 plant expansion, which is consistent with what we observed in $\delta^{13}C_{wax}$ values.

During the Holocene, the average δD_{C29} value was −170 ± 4‰, and this is ca. 18‰ higher than the LGM values (Fig. 3f). We interpret higher values during the Holocene as decreased contribution of precipitation from the Pacific/Arctic that possess lower δD_p values. Insolation increase and retreat of ice sheets at higher latitudes may have shifted the mid-latitude Polar Front position northward. In the tropics, global warming may have caused expansion of Atlantic Warm Pool (AWP) and northward shift in the ITCZ. This would have extended the warm Caribbean seawaters to the northern GOM and increased SST and changed hydrology (Limoges et al., 2014). Consequently, this may have pushed warm summer precipitation from the GOM into the MRB and increased C_4 grasslands as indicated by $\delta^{13}C_{alk}$ values.

6.2. MRB paleovegetation and paleohydrology from late MIS 6 to MIS 5a

6.2.1. MRB paleovegetation from late MIS 6 to MIS 5a

In the late MIS 6, $\delta^{13}C_{alk}$ values for *n*-C_{27} to *n*-C_{31} were similar to those in MIS 2; both reflect a cold glacial climate with C_3 tree dominance. Pollen records also suggest that late MIS 6 (150-130 kyr) was dominated by *Picea* and *Pinus* pollen in the Midwest (Fig. 4e; King and Saunders, 1986; Zhu and Baker, 1995). %C_4 cover (estimated using *n*-C_{33}) had a wider range of values from 20% to 35% during MIS 6, with an average of 30% (Fig. 4c). There are two potential explanations for the wide range and relatively high mean %C_4 during the late MIS 6: the climate may have begun to ameliorate or episodic runoff may

have occurred during deglaciation with increased meltwater discharge. Studies have reported a faster retreat of Laurentide ice sheets during the MIS 6 to 5, compared to the Last Glacial to the Holocene transition (Nürnberg et al., 2008; Ziegler et al., 2008), and we argue that both were likely.

During MIS 5, $\%C_4$ and water availability varied by substage. The average $\%C_4$ (as indicated by $\delta^{13}C_{C33}$) was 6% higher on average during stadials (MIS 5b = 35% and 5d = 31%) than interstadials (MIS 5a = 25%, 5c = 27%, and 5e = 28%). During MIS 5e, when global average temperature was warmer than today, the abundance of C_4 grasses (27%) was slightly lower than the Holocene (30%) with statistically significance when only the two time slices are compared (t-test, $p < 0.043$). However, when we compared means of $\%C_4$ for the entire 150 kyr record binned by MIS and substages, there was no statistical difference between the Holocene and substages from MIS 5e to 5b, suggesting that $\%C_4$ during the MIS 5e-5b were minor. We argue that these slight increases in average $\%C_4$ during stadials may be due to increase in leaf wax export from C_4 grasslands rather than the expansion of C_4 grasslands. With increase in Arctic/Pacific derived precipitation during cold stadials, precipitation may have increased in the Great Plains, facilitating leaf wax transport from the grasslands. This is further supported by lower ACL (i.e. expansion of trees) during the MIS 5 stadials than interstadials (Fig. 2; Table A1). As a whole basin, trees were still the major plant composition during the stadials. C_4 grassland distribution during the MIS 5 interstadials may have been similar to the Holocene. Epstein et al. (1997) used models to predict vegetation shift in the Great Plains with 2°C increase in mean annual temperature. They estimated that C_4 grasses would expand while C_3 grasses would decrease. However, we did not observe increases in C_4 grassland during the MIS 5e, when the average global temperature was 2°C higher than today. In the forests, moisture availability based on $\delta^{13}C_{C29}$ and $\delta^{13}C_{C31}$ values also did not vary between the two interglacials. We found higher ACL values during MIS 5 interstadials. Similar $\%C_4$ and higher ACL suggest that C_3 grasses and forbs may have increased during the MIS 5e and 5c. C_3 and C_4 grasses co-exist in the Great Plains, and C_3 grasses and forbs are favored in the early and late part of the growing season, when temperatures fall below the crossover temperature threshold (23°C; Still et al., 2003).

Precipitation and runoff in the Great Plains is higher during spring, and therefore, it is likely that C_3 plant waxes may have exported preferentially during the MIS 5e. Also, C_3 grasses may be favored over C_4 grasses, if winter precipitation increases (Epstein et al., 1997; Paruelo and Lauenroth, 1996). We will further discuss vegetation changes in relation to hydrologic conditions using δD_{wax} values in Section 6.2.2. interglacials.

MIS 5d could have been the driest period during the MIS 5 especially in the forestland based on *n*-C_{29} and *n*-C_{31} $\delta^{13}C_{alk}$ values, and this dry condition may have continued in MIS 5c (Fig. 4a). *n*-Alkane concentrations in the 625B core were the lowest during this period (Fig. 2a), which is also an indication of declined river discharge, resulting in lower transport of organic matter, including leaf waxes. Pollen data during middle Sangamonian in south-central Illinois also suggest an arid climate (Fig. 4e; Curry and Baker, 2000; Zhu and Baker, 1995), and this may correspond to MIS 5d and 5c. Since MIS 5b, grassland gradually decreased, which is coherent with the pollen record after the middle Sangamonian (Zhu and Baker, 1995). Since the late Sangamonian, conifers began to expand, and this may have been the MIS 5a when $\delta^{13}C_{alk}$ values were as low as the LGM.

6.2.2. MRB precipitation source changes from late MIS 6 to MIS 5a

δD_{alk} values during the late MIS 6 was unusually high (Fig. 3f). As high mean and range of $\delta^{13}C_{C33}$ values during the late MIS 6 suggested, the climate may have ameliorated due to earlier retreat of ice sheets and increased discharge during deglaciation (Nürnberg et al., 2008; Ziegler et al., 2008). High δD_{alk} values persisted throughout MIS 5e to 5c. During MIS 5e, average δD_{alk} values were higher than the Holocene (t-test, $p < 0.05$ for *n*-C_{27} and *n*-C_{31}; Table A8-A9). This may reflect decrease in contribution of precipitation from the Pacific/Arctic that has lower δD_p values. The leaf wax export from the southeastern forests that have higher δD_{alk} values than grasslands may have increased relatively to the GOM. With declined global ice sheets during the MIS 5e, moisture transport from higher latitudes may have diminished in the MRB.

In the tropics, the ITCZ may have shifted northward with increased warming, and moisture transport form the GOM may have intensified. The low latitude-derived warm air masses may have extended and thereby precipitation belt over the continent may have shifted northward.

Higher GOM-derived moisture transport to the MRB during the MIS 5e may have increased leaf wax transport from the southeastern forests to the GOM, suggesting that hydrologic conditions in the southeastern forests were not at least dry during the MIS 5e. This result is consistent with the hydrologic conditions inferred by $\delta^{13}C_{C29}$ and $\delta^{13}C_{C31}$ values that the forestlands in the MRB during the MIS 5e may have had similar hydrologic conditions to the Holocene. However, in grasslands, similar $\%C_4$ and slightly higher ACL suggested increased C_3 grasses and forbs during the MIS 5e. If winter precipitation significantly increased and caused expansion of C_4 grassland, δD_{alk} values should have decreased due to lower δD_p values in winter. We argue that the spring precipitation in the Great Plains may have dominated during the MIS 5e, exporting more C_3 grassland and forbs-derived *n*-alkanes to the GOM. During the MIS 5e, the mid-latitude Polar Front position may have shifted northward with increased warming.

It is also possible that the higher precipitation in southern MRB may have cooled surface temperature in the continents, reducing C_4 growth, as heat consumption for evaporation increases with higher precipitation rates. For example, in Eurasia, the positive temperature deviation decreased in mid-latitudes in warm periods in the past such as the Holocene optimum, Eocene optimum and Last Interglacial due to high precipitation rates in lower latitudes (Velichko et al., 1995; Velichko et al., 2008). It may also be plausible that winter precipitation could have increased episodically in southern MRB. The δD_p values in the southern MRB do not vary much seasonally (< 10‰), but given the data we have, we cannot determine the precipitation seasonality. Higher precipitation in Gulf States during winter with lower temperature anomalies near the GOM is a characteristic pattern of El Niño/Southern Oscillation (ENSO) events in NA (Kahya and Dracup, 1993; Piechota and Dracup, 1996; Ropelewski and Halpert, 1986).

ENSO corresponds to the departure from temperature and precipitation normals over the equatorial Pacific which has links to climatic anomalies in other parts of the world, including the U.S. (Halpert and Ropelewski, 1992; Walker and Bliss, 1932). The most consistent ENSO pattern in the U.S. is above normal precipitation in southern Gulf States during the winter. It has also been suggested that ENSO is related to stronger than normal Westerlies in the GOM bringing more frequent storms and precipitation (Ropelewski and Halpert, 1986). Increased δD_{alk} values during MIS 5e could be due to ENSO-like climate with increased GOM-derived moisture in winter, slightly reducing C_4 grasses and causing episodic runoff from Gulf States.

Overall, based on our $\delta^{13}C_{alk}$ and δD_{alk} results, it is most likely that the spatial distribution of precipitation during the MIS 5e differed from the Holocene, with lower precipitation in northwestern grasslands and higher in southeastern forestlands in the MRB. Detrital sources determined by clay minerals in sediments from the GOM also suggested that runoff from the western MRB may have been lower during MIS 5e than the Holocene (Montero-Serrano et al., 2011).

During the MIS 5d, aridity intensified compared to the MIS 5e based on high $\delta^{13}C_{alk}$ and δD_{alk} values (Fig. 3d and 3f). A slight expansion of global ice volume and reduction in summer insolation may have shifted the ITCZ towards the equator. With cooler SST in the GOM, the mid-latitude Polar Front position may have shifted southward, and moisture transport from the GOM to the continent may have reduced, making the southeastern forest drier. The southward migration of the Polar Front may have facilitated the delivery of moisture from the Pacific/Arctic to the grasslands, thereby resulting in grassland-derived leaf wax export to the sediments.

Hydrologic conditions may have been dry until the MIS 5c. Since MIS 5b, δD_{alk} values dropped as the Pacific/Arctic-derived precipitation sources may have increased, and began to transit to the glacial period. MIS 5a had average δD_{alk} values as low as the LGM. A significant positive correlation between δD_{alk}

values and the GOM SST was found (r^2 = 0.3 to 0.4, $p < 0.05$, Fig. 4d-4f), when MIS 6 samples are excluded, as this interval seem to be affected by increased runoff during deglaciation. This correlation confirms the broad link between sea-air circulation and terrestrial ecosystems as well as teleconnections between high to low latitudes that affect the mid-latitude Polar Front positions.

7. Conclusion

We provide a record of changes in the source and spatial distribution of terrestrial precipitation and vegetation composition in the MRB over the last ~150 kyr using leaf wax carbon and hydrogen isotopes preserved in ODP 625B core. The leaf wax isotope interpretation was refined by results from Chapter 3 on leaf wax sourcing in the 625B core, and vegetation records since the Last Glacial to the Holocene (Cotton et al., 2016). We used *n*-C_{33} alkanes for $\%C_4$ reconstructions, and *n*-C_{29} and *n*-C_{31} alkanes for moisture availability in forestland to minimize source bias. The LGM to the Holocene records were in good agreement with prior studies, indicating a transition from a cold, moist, C_3 tree dominated ecosystem to a warm, drier climate with grassland expansion. We compared hydrologic conditions during the MIS 5e and the Holocene to examine hydrologic response in the MRB to increased warming. We observed increase in C_3 grasses and forbs during the MIS 5e, and relative increase in precipitation in the southern MRB. The results also suggested that the MIS 5e precipitation patterns could have been somehow similar to modern ENSO events in the US. A relative precipitation increase in the south could have been due to northward migration of mid-latitude Polar Front position, leading to increase in GOM-derived precipitation. As summer insolation increased and global temperature rose during the MIS 5e, this expanded Atlantic Warm Pool, and migrated ITCZ northward, bringing warm Caribbean seawater into the GOM, transporting warm and humid moisture into the continent, and shifting the Polar Front position northward. During the MIS 5d, we observed drier-than-the-Holocene condition especially in forested areas due to lower moisture transport from the GOM to the MRB. Since MIS 5c to 5a, air mass contribution from the Pacific/Arctic began to increase, indicating the expansion of global ice volume and transition to the glacial climate. This is the first study to provide records of source and spatial pattern of precipitation and vegetation changes in the MRB within the MIS 5 and in comparison to the Holocene. The results of this study provide important insights into how global or regional temperature increase may influence atmospheric circulation, which determine the extent of air mass contribution and distribution in North America, and consequently terrestrial vegetation and hydrology.

Acknowledgement

We thank the Ministry of Oceans and Fisheries, South Korea (K-IODP) for funding this research. We also thank IODP for providing samples for this study.

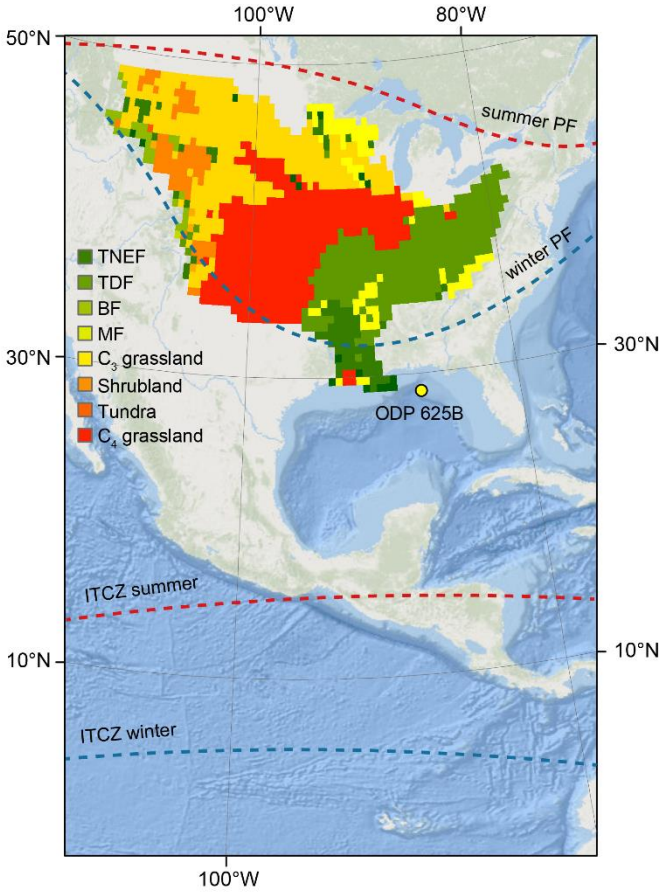

Figure 1. Spatial distribution of biomes in Mississippi River Basin for current climate without human activities (Ramankutty and Foley, 2010 with modification). Locations of Intertropical Convergence Zones (ITCZ) and Polar Front (PF) for summer and winter under modern climate. TNEF = Temperate Needleleaf Evergreen Forest; TDF = Temperat Deciduous Forest; BF = Boreal Forest; MF = Mixed Forest. Yellow dot indicates the location of ODP 625B core.

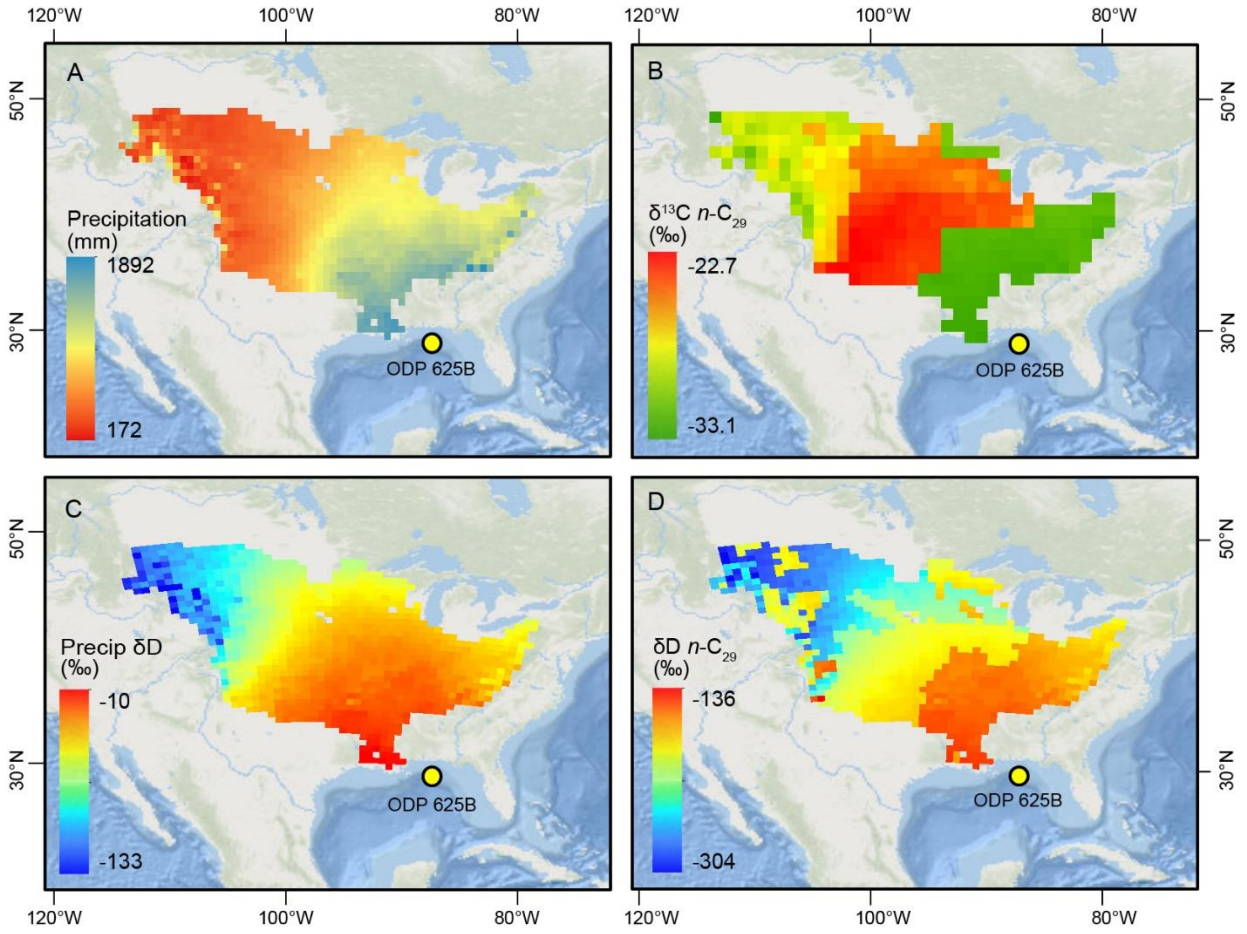

Figure 2. (a) 30-year average mean annual precipitation or MAP (mm; prism.oregonstate.edu), (b) $\delta^{13}C_{C29}$ values estimated based MAP and plant photosynthetic pathways, (c) 30-year average MAP δD values (Bowen, 2014) and (d) δD_{C29} values estimated based on biomes and plant photosynthetic pathways for the modern climate in the Mississippi River basin.

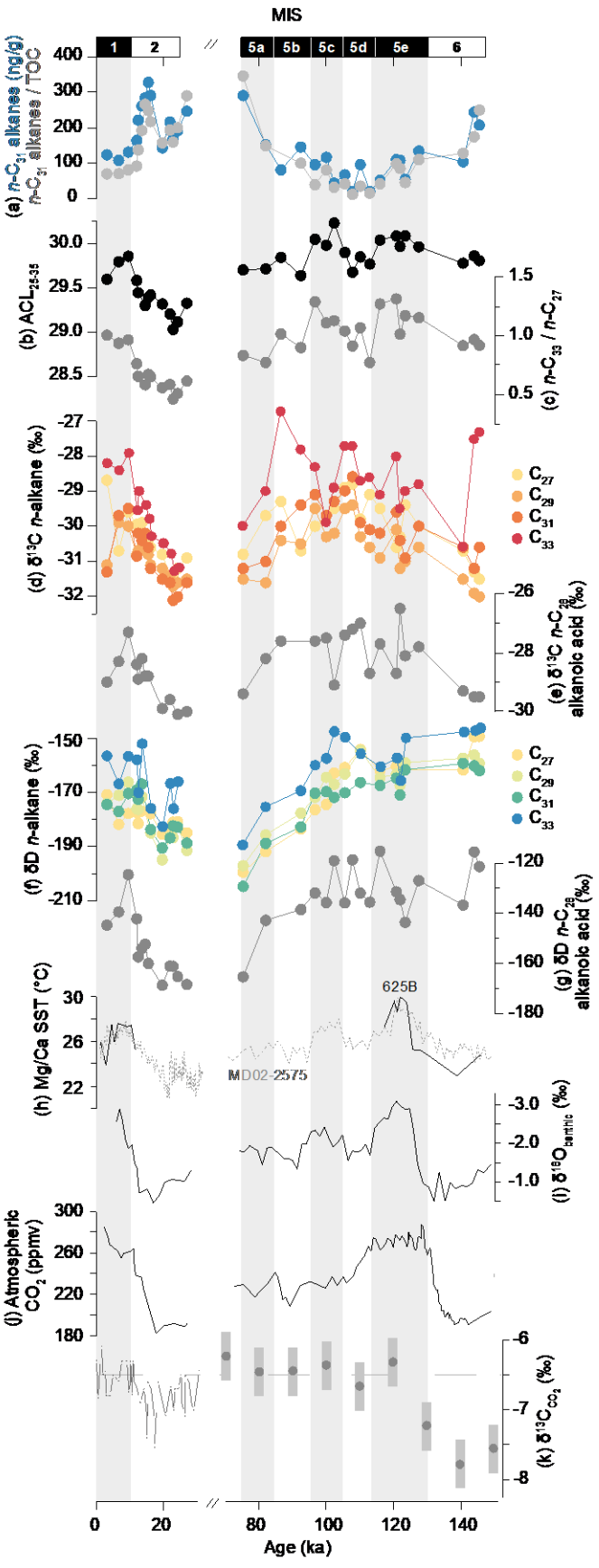

Figure 3. Temporal changes in (a) *n*-C_{31} alkane concentrations (ng/g; blue) and *n*-C_{31} alkane / TOC (gray), (b) average chain length, (c) *n*-C_{33} alkane / *n*-C_{27} alkane, (d) $\delta^{13}C_{alk}$ values (‰) for *n*-C_{27}, *n*-C_{29}, *n*-C_{31}, and *n*-C_{33}, (e) $\delta^{13}C$ *n*-C_{28} alkanoic acid (‰), (f) δD_{alk} (‰) for *n*-C_{27}, *n*-C_{29}, *n*-C_{31}, and *n*-C_{33}, (g) δD *n*-C_{28} alkanoic acid (‰), (h) Mg/Ca-based sea surface temperature (°C) from ODP 625B (Limoges et al., 2014) and MD02-2575 (Ziegler et al., 2008) from northeastern Gulf of Mexico, (i) low latitude $\delta^{18}O$ stack (Bassinot et al., 1994), (j) atmospheric CO_2 levels from the vostok ice core (Barnola et al., 1987) for the last 150 kyr, and (k) $\delta^{13}C_{CO2}$ variations based on ice core bubbles (dotted line) and benthic forams (circle) for the last 150 kyr. MIS = Marine Isotope Stages. Gray bars indicate interglacial (Holocene and MIS 5e) and interstadials (MIS 5a and 5c).

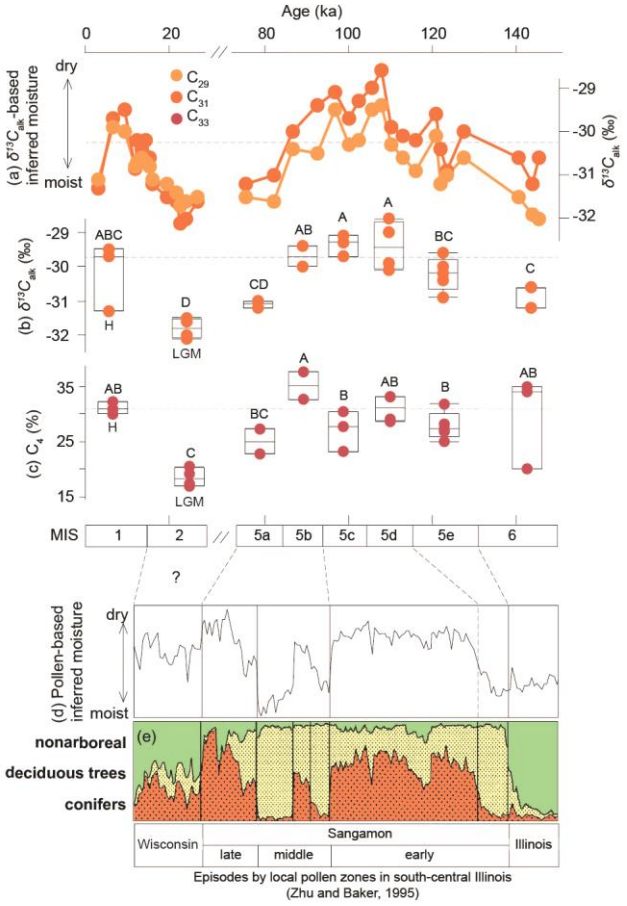

Figure 4. (a) *n*-C_{29} and *n*-C_{31} $\delta^{13}C_{alk}$-based inferred moisture availability for the last 150 kyr, (b) $\delta^{13}C_{C31}$ values and (c) $\%C_4$ calibrated to the known $\%C_4$ values in Cotton et al. (2016) binned by marine isotope stages (MIS 6 and 5), Last Glacial Maximum (LGM = 25-19 kyr), and Holocene (H = ~11 kyr) using ODP 625B core in northeastern Gulf of Mexico. (d) Pollen-based inferred moisture, and (e) pollen records from south-central Illinois (redrafted from Zhu and Baker, 1995) based on local pollen zones. Gray bars indicate interglacial (Holocene and MIS 5e) and interstadial (MIS 5c and 5a) periods. Different letters indicate significant differences among binned data (ANOVA, student's t-test, $p < 0.05$; Table A4-A7).

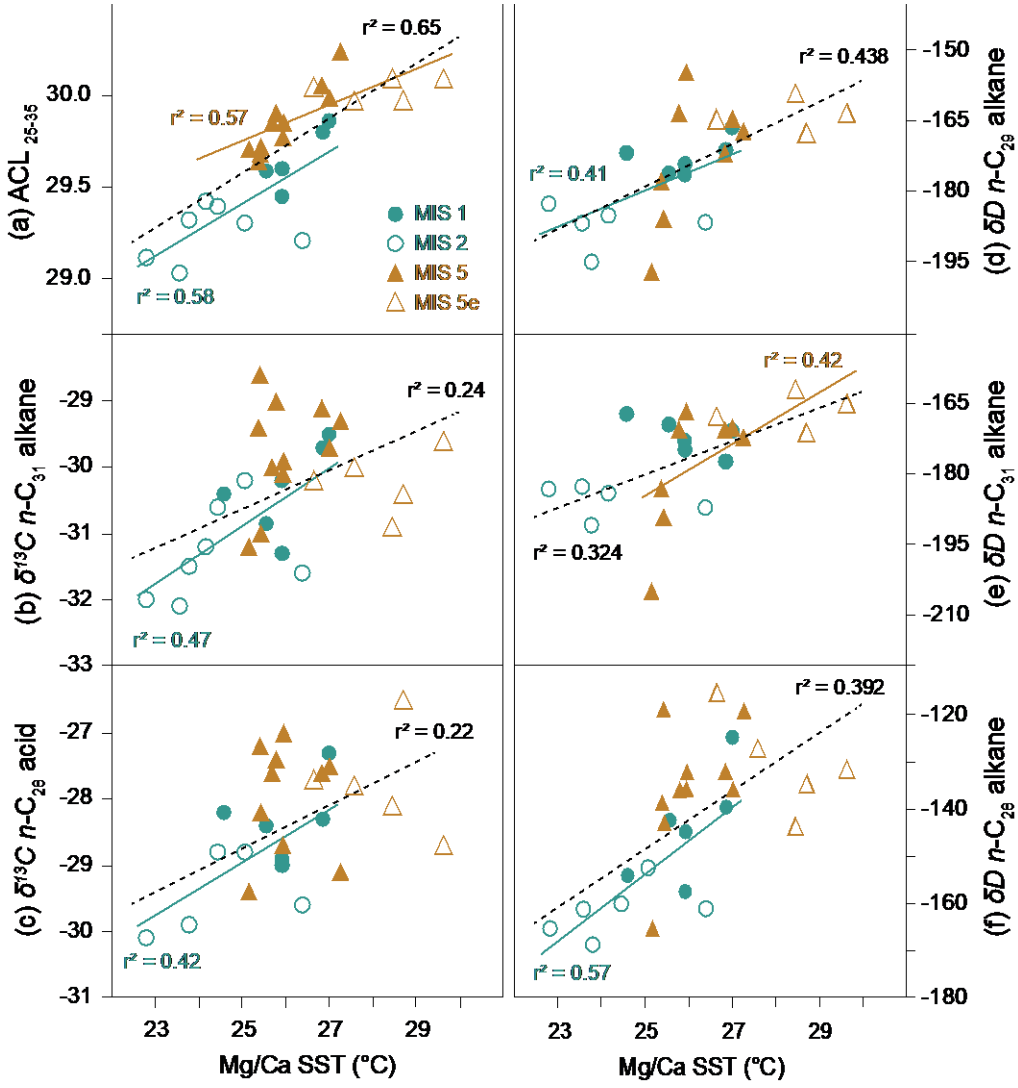

Figure 5. Relationship between Mg/Ca based sea surface temperature (SST, °C) from the northeastern Gulf of Mexico (Ziegler et al., 2008) and (a) average chain length (ACL_{25-35}), (b) $\delta^{13}C_{31\ alk}$ values, (c) $\delta^{13}C_{28\ alk}$ values, (d) $\delta D_{C29\ alk}$ values, (e) $\delta D_{C31\ alk}$ values, and (f) $\delta D_{C28\ acid}$ values in ODP 625B core for MIS 1 (closed circle), 2 (open circle), 5 (closed triangle), and 5e (open triangle). Green lines correspond to trendlines for MIS 1 and 2, orange lines are for MIS 5, while black dotted lines are for the all MIS 1, 2, and 5. Trendlines with significant r^2 values are reported ($p < 0.05$).

Appendix 1

Table A1. *N*-alkane concentrations (µg/g) for *n*-C25 to *n*-C35, average chain length (ACL), and carbon preference index CPI) in ODP 625B core sediment samples.

Sample	C25	C26	C27	C28	C29	C30	C31	C32	C33	C34	C35	ACL	CPI
100625B 1H 1W	36	22	54	24	93	25	124	16	55	0	0	29.6	3.7
100625B 1H 1W	25	17	51	18	101	19	108	11	48	5	12	29.8	4.3
100625B 1H 1W	32	19	57	23	117	22	131	15	55	6	19	29.9	4.3
100625B 1H 1W	51	30	95	33	169	27	164	10	73	6	18	29.6	4.7
100625B 1H 1W	80	42	143	47	243	42	221	22	94	10	25	29.4	4.4
100625B 1H 2W	110	68	160	67	256	65	262	58		33	41		
100625B 1H 2W	128	84	184	86	329	89	285	49	108	21	34	29.3	2.9
100625B 1H 2W	137	85	199	91	360	96	329	63	134	19	37	29.4	3.0
100625B 1H 2W	108	59	154	67	306	64	291	48	100	13	29	29.4	3.5
100625B 1H 2W	56	32	86	33	152	35	143	19	48	7	13	29.3	3.5
100625B 1H 3W	114	76	145	77	227	64	217	46	85	15	24	29.2	2.6
100625B 1H 3W	101	60	127	49	166	42	167	27	59	13	18	29.0	2.9
100625B 1H 3W	112	64	142	55	188	48	192	38	72	15	24	29.1	2.9
100625B 2H 4W	68	38	132	32	262	33	291	19	110	6	23	29.7	6.1
100625B 2H 4W	39	24	70	24	138	23	152	16	54	13	19	29.7	4.2
100625B 2H 4W	19	12	39	15	74	14	81	15	40	4	9	29.8	4.0
100625B 2H 5W	39	30	61	28	177	26	145	19	55	9	13	29.6	3.9
100625B 2H 5W	17	10	35	16	76	13	96	13	45	3	10	30.1	4.6
100625B 2H 5W	22	18	46	20	113	26	116	16	52	5	17	30.0	3.8
100625B 2H 5W	2	5	15	7	41	8	43	5	17	2	6	30.2	4.1
100625B 2H 5W	17	8	32	12	63	14	67	12	33	9	11	29.9	3.9
100625B 2H 5W	5	3	8	3	21	4	19	1	7	7	2	29.7	3.8
100625B 2H 5W	23	13	40	17	101	21	96	13	43	6	13	29.9	4.1
100625B 2H 5W	4	3	8	3	19	4	20	2	6	6	3	29.8	3.4
100625B 2H 5W	11	7	20	9	46	8	51	3	25	5	8	30.0	4.7
100625B 2H 6W	22	14	42	20	97	22	110	17	56	10	18	30.1	3.9
100625B 2H 6W	23	17	42	19	98	22	109	15	42	7	19	30.0	3.7
100625B 2H 6W	9	7	22	9	49	7	54	7	26	5	9	30.1	4.5
100625B 2H 6W	26	19	55	23	129	23	134	19	64	9	17	30.0	4.3
100625B 2H 6W	25	16	51	20	106	18	104	15	46	6	13	29.8	4.1
100625B 2H 6W	47	32	108	39	227	38	244	21	104	9	25	29.9	4.9
100625B 2H 6W	41	28	94	34	194	32.6	207	20	87	6	19	29.8	4.7

Table A2. Depth, sedimentation rates (cm/kyr), age (kyr), marine isotope stages (MIS), $\delta^{13}C_{leaf}$, $\delta^{13}C_{alk}$ values from *n*-C_{27} to *n*-C_{33}, %C_4 based on $\delta^{13}C_{C33,}$ and $\delta^{13}C_{C28\ acid}$ values in ODP 625B core sediment samples.

Sample	Depth (m)	Sed. Rates (cm/kyr)	Age (kyr)	MIS	$\delta^{13}C_{leaf}$	$\delta^{13}C_{C27}$	$\delta^{13}C_{C29}$	$\delta^{13}C_{C31}$	$\delta^{13}C_{C33}$	%C4	$\delta^{13}C_{C28\ acid}$
100625B 1H 1W	0.2		3.1	1	-22.2	-28.7	-31.1	-31.3	-28.2	30.9	-29.0
100625B 1H 1W	0.6	10.2	6.6	1	-22.4	-30.7	-29.9	-29.7	-28.4	30.0	-28.3
100625B 1H 1W	0.8	8.1	9.5	1	-21.7	-29.6	-30.0	-29.5	-27.9	32.2	-27.3
100625B 1H 1W	1.0	8.7	12.0	1	-23.4	-30.0	-30.8	-30.9	-29.6	24.8	-28.4
100625B 1H 1W	1.1	21.9	12.4	1	-24.9	-30.0	-30.7	-30.2	-29.0	27.3	-28.9
100625B 1H 2W	1.4	21.9	13.5	1	-25.2	-29.9	-30.6	-30.4	- -		-28.2
100625B 1H 2W	1.6	21.9	14.5	2	-25.4	-30.3	-30.7	-30.2	-29.4	25.5	-28.8
100625B 1H 2W	1.8	21.9	15.5	2	-25.7	-30.4	-30.8	-30.6	-29.8	23.7	-28.8
100625B 1H 2W	1.9	21.9	16.1	2	-25.4	-30.6	-31.1	-31.2	-30.3	21.4	-
100625B 1H 2W	2.7	21.9	19.6	2	-25.7	-30.8	-31.2	-31.5	-30.5	20.5	-29.9
100625B 1H 3W	3.2	21.9	21.9	2	-26.4	-31.4	-31.4	-31.6	-30.8	19.2	-29.6
100625B 1H 3W	3.4	21.9	22.8	2	-27.2	-31.4	-31.7	-32.1	-31.3	16.9	-
100625B 1H 3W	3.7	21.9	24.2	2	-26.5	-31.2	-31.6	-32.0	-31.2	17.4	-30.1
100625B 2H 4W	12.8	17.9	75.3	5a	-24.5	-30.8	-31.5	-31.2	-30.0	22.8	-29.4
100625B 2H 4W	13.3	7.1	82.1	5a	-22.8	-29.7	-31.6	-31.0	-29.0	27.3	-28.2
100625B 2H 4W	13.6	6.6	86.6	5b	-	-29.3	-30.4	-30.0	-26.7	37.6	-27.6
100625B 2H 5W	14.0	6.2	92.5	5b	-23.2	-30.7	-30.5	-29.4	-27.8	32.7	-
100625B 2H 5W	14.2	5.9	96.7	5c	-21.8	-30.0	-29.5	-29.1	-28.3	30.4	-27.6
100625B 2H 5W	14.4	5.7	100.1	5c	-22.5	-29.7	-30.3	-29.7	-29.9	23.2	-27.5
100625B 2H 5W	14.6	5.5	102.4	5c	-22.6	-29.5	-30.2	-29.3	-28.9	27.7	-29.1
100625B 2H 5W	14.7	5.4	105.6	5d	-22.9	-28.9	-29.5	-29.0	-27.7	33.1	-27.4
100625B 2H 5W	14.8	5.2	107.9	5d	-22.3	-28.8	-29.4	-28.6	-27.7	33.1	-27.2
100625B 2H 5W	15.0	5.1	110.2	5d	-28.5	-29.8	-30.3	-29.9	-28.7	28.6	-27.0
100625B 2H 5W	15.1	5.0	113.0	5d	-23.0	-29.1	-30.6	-30.1	-28.6	29.1	-28.7
100625B 2H 5W	15.3	4.9	116.1	5e	-22.6	-29.5	-30.9	-30.2	-29.1	26.8	-27.7
100625B 2H 6W	15.5	4.7	121.0	5e	-23.3	-30.6	-30.1	-29.6	-28.0	31.8	-28.7
100625B 2H 6W	15.5	4.6	122.0	5e	-23.6	-30.3	-31.2	-30.4	-29.5	25.0	-26.5
100625B 2H 6W	15.6	4.6	123.6	5e	-22.9	-29.4	-31.0	-30.9	-29.0	27.3	-28.1
100625B 2H 6W	15.8	4.5	127.6	5e	-24.0	-30.0	-30.6	-30.0	-28.8	28.2	-27.8
100625B 2H 6W	16.3	4.2	140.8	6	-23.8	-30.7	-31.5	-30.6	-30.6	20.1	-29.3
100625B 2H 6W	16.5	3.9	144.1	6	-23.6	-31.3	-31.9	-31.2	-27.5	34.0	-29.5
100625B 2H 6W	16.5	3.9	145.7	6	-23.1	-31.5	-32.0	-30.6	-27.3	34.9	-29.5

Table A3. δD_{alk} values from *n*-C_{27} to *n*-C_{33} and $\delta D_{C28\ acid}$ values in ODP 625B core sediment samples.

Sample	dD C27	dD C29	dD C31	dD C33	dD C28 FAME
100625B 1H 1W	-170.9	-174.1	-174.5	-156.6	-144.8
100625B 1H 1W	-181.8	-171.1	-177.1	-166.8	-139.6
100625B 1H 1W	-177.8	-166.3	-170.4	-156.7	-124.8
100625B 1H 1W	-177.5	-176.1	-169.2	-158.0	-142.3
100625B 1H 1W	-181.5	-176.2	-172.5	-170.0	-157.5
100625B 1H 2W	-176.9	-171.7	-166.9	-152.1	-154.0
100625B 1H 2W					-152.4
100625B 1H 2W					-160.0
100625B 1H 2W	-177.9	-185.0	-183.7	-175.9	
100625B 1H 2W	-185.5	-194.8	-190.5	-182.5	-168.7
100625B 1H 3W	-183.8	-186.5	-186.8	-166.7	-161.1
100625B 1H 3W	-181.0	-186.7	-182.3	-176.0	-161.2
100625B 1H 3W	-180.7	-182.5	-182.9	-166.1	-165.3
100625B 2H 4W	-199.4	-197.0	-204.7	-189.3	-165.3
100625B 2H 4W	-191.9	-185.7	-188.8	-175.3	-142.9
100625B 2H 4W					
100625B 2H 5W	-183.5	-177.7	-182.8	-169.4	-138.6
100625B 2H 5W	-176.4	-171.8	-170.3	-160.0	-132.1
100625B 2H 5W	-174.5	-164.5	-169.8	-157.5	-135.9
100625B 2H 5W	-162.9	-167.0	-171.9	-147.6	-119.3
100625B 2H 5W	-160.8	-163.2	-170.2	-149.7	-136.0
100625B 2H 5W					-118.9
100625B 2H 5W	-154.2	-154.6	-166.4	-155.8	-132.1
100625B 2H 5W					-135.8
100625B 2H 5W	-162.2	-164.6	-167.5	-160.6	-115.4
100625B 2H 6W	-160.4	-163.3	-164.8	-157.3	-131.6
100625B 2H 6W	-166.0	-167.5	-170.9	-165.7	-134.7
100625B 2H 6W	-161.7	-159.1	-161.7	-150.0	-143.7
100625B 2H 6W					-127.2
100625B 2H 6W	-161.7	-157.5	-159.4	-147.8	-136.9
100625B 2H 6W	-149.6	-156.3	-160.3	-147.3	-115.8
100625B 2H 6W	-149.4	-159.3	-162.0	-146.3	-121.7

We examined One-way ANOVA and student's t-test to compare of $\delta^{13}C_{C31}$, %C4 (based on $\delta^{13}C_{C33}$) and δD_{C31} values binned by marine isotope stages and major climatic periods (i.e. Holocene, LGM, MIS 5a to 5e, and MIS 6). One-way ANOVA had a p value of <.0001.

Table A4. Mean $\delta^{13}C_{C31}$ values and Student's t-test comparison.

Geologic periods	Mean δD_{alk}	*n*	Student's t
Holocene	-30.167	3	ABC
LGM	-31.800	4	D
MIS 5a	-31.100	2	CD
MIS 5b	-29.700	2	AB
MIS 5c	-29.367	3	A
MIS 5d	-29.400	4	AB
MIS 5e	-30.220	5	BC
Late MIS 6	-30.800	3	C

Table A5. p-value of each $\delta^{13}C_{C31}$ comparison by geologic periods

Level	Level	p-Value
MIS 5c	LGM	<.0001*
MIS 5d	LGM	<.0001*
MIS 5b	LGM	0.0003*
MIS 5c	MIS 5a	0.0026*
MIS 5d	MIS 5a	0.0020*
Holocene	LGM	0.0010*
MIS 5e	LGM	0.0004*
MIS 5c	MIS 6	0.0046*
MIS 5d	MIS 6	0.0034*
MIS 5b	MIS 5a	0.0189*
MIS 5b	MIS 6	0.0395*
MIS 6	LGM	0.0267*
Holocene	MIS 5a	0.0758
MIS 5e	MIS 5a	0.0685
MIS 5c	MIS 5e	0.0451*
MIS 5d	MIS 5e	0.0370*
MIS 5c	Holocene	0.0878
MIS 5d	Holocene	0.0809
MIS 5a	LGM	0.1537
Holocene	MIS 6	0.1700
MIS 5e	MIS 6	0.1606
MIS 5b	MIS 5e	0.2671
MIS 5b	Holocene	0.3587
MIS 5c	MIS 5b	0.5096
MIS 5d	MIS 5b	0.5313
MIS 6	MIS 5a	0.5524
Holocene	MIS 5e	0.8944
MIS 5c	MIS 5d	0.9368

Table A6. Mean $\%C_4$ and Student's t-test comparison.

Geologic periods	Mean $\%C_4$	*n*	Student's t
Holocene	31.010000	3	AB
LGM	18.495000	4	C
MIS 5a	25.015000	2	BC
MIS 5b	35.135000	2	A
MIS 5c	27.113333	3	B
MIS 5d	30.972500	4	AB
MIS 5e	27.802000	5	B
Late MIS 6	29.663333	3	AB

Table A7. *p*-value of each $\%C_4$ comparison by geologic periods

Level	Level	p-Value
5b	LGM	<.0001*
Holocene	LGM	0.0003*
5d	LGM	0.0001*
6	LGM	0.0009*
5b	5a	0.0128*
5e	LGM	0.0013*
5c	LGM	0.0064*
5b	5c	0.0274*
5b	5e	0.0278*
5a	LGM	0.0545
Holocene	5a	0.0896
5d	5a	0.0765
5b	6	0.1189
6	5a	0.1812
5b	5d	0.2057
5b	Holocene	0.2329
Holocene	5c	0.2088
5d	5c	0.1844
Holocene	5e	0.2457
5d	5e	0.2130
5e	5a	0.3749
6	5c	0.4048
5c	5a	0.5380
6	5e	0.4952
Holocene	6	0.6577
5d	6	0.6452
5e	5c	0.7996
Holocene	5d	0.9894

Table A8. Mean δD_{C31} values and Student's t-test comparison.

Geologic periods	Mean δD_{alk}	*n*	Student's t
Holocene	-174.0008	3	CD
LGM	-185.6297	4	E
MIS 5a	-196.7421	2	F
MIS 5b	-182.7834	1	DE
MIS 5c	-170.6528	3	BC
MIS 5d	-168.2873	2	ABC
MIS 5e	-166.2202	4	AB
Late MIS 6	-160.5553	3	A

Table A9. *p*-value of each δD_{C31} comparison by geologic periods

Level	Level	p-Value
MIS 6	MIS 5a	<.0001*
MIS 5e	MIS 5a	<.0001*
MIS 5d	MIS 5a	<.0001*
MIS 5c	MIS 5a	<.0001*
MIS 6	LGM	<.0001*
Holocene	MIS 5a	<.0001*
MIS 6	MIS 5b	0.0005*
MIS 5e	LGM	<.0001*
MIS 5d	LGM	0.0003*
MIS 5e	MIS 5b	0.0035*
MIS 5c	LGM	0.0004*
MIS 5d	MIS 5b	0.0143*
MIS 5b	MIS 5a	0.0176*
MIS 6	Holocene	0.0016*
MIS 5c	MIS 5b	0.0264*
Holocene	LGM	0.0029*
LGM	MIS 5a	0.0090*
MIS 6	MIS 5c	0.0112*
Holocene	MIS 5b	0.0941
MIS 5e	Holocene	0.0305*
MIS 6	MIS 5d	0.0653
MIS 5d	Holocene	0.1616
MIS 6	MIS 5e	0.1017
MIS 5e	MIS 5c	0.1921
MIS 5c	Holocene	0.3493
MIS 5b	LGM	0.5574
MIS 5d	MIS 5c	0.5504
MIS 5e	MIS 5d	0.5819

References

Anderson, R.C., 2006. Evolution and origin of the Central Grassland of North America: climate, fire, and mammalian grazers. The Journal of the Torrey Botanical Society 133, 626-647.

Annan, J.D., Hargreaves, J.C., 2013. A new global reconstruction of temperature changes at the Last Glacial Maximum. Clim. Past 9, 367-376.

Barnola, J., Raynaud, D., Lorius, C., Barkov, N., 1987. Historical carbon dioxide record from the Vostok ice core. Nature 329, 408-414.

Barnola, J.M., Pimienta, P., Raynaud, D., Korotkevich, Y.S., 1991. CO_2-climate relationship as deduced from the Vostok ice core: a re-examination based on new measurements and on a re-evaluation of the air dating. Tellus B 43, 83-90.

Bassinot, F.C., Labeyrie, L.D., Vincent, E., Quidelleur, X., Shackleton, N.J., Lancelot, Y., 1994. The astronomical theory of climate and the age of the Brunhes-Matuyama magnetic reversal. Earth and Planetary Science Letters 126, 91-108.

Bi, X., Sheng, G., Liu, X., Li, C., Fu, J., 2005. Molecular and carbon and hydrogen isotopic composition of *n*-alkanes in plant leaf waxes. Org. Geochem. 36, 1405-1417.

Bianchi, T.S., Filley, T., Dria, K., Hatcher, P.G., 2004. Temporal variability in sources of dissolved organic carbon in the lower Mississippi River. Geochimica et Cosmochimica Acta 68, 959-967.

Bianchi, T.S., Mitra, S., McKee, B.A., 2002. Sources of terrestrially-derived organic carbon in lower Mississippi River and Louisiana shelf sediments: implications for differential sedimentation and transport at the coastal margin. Marine Chemistry 77, 211-223.

Bowen, G., 2014. The Online Isotopes in Precipitation Calculator, version 2.2. 2015.

Bray, E., Evans, E., 1961. Distribution of n-paraffins as a clue to recognition of source beds. Geochimica et Cosmochimica Acta 22, 2-15.

Bush, R.T., McInerney, F.A., 2015. Influence of temperature and C_4 abundance on *n*-alkane chain length distributions across the central USA. Organic Geochemistry 79, 65-73.

Castaneda, I.S., Mulitza, S., Schefuss, E., Lopes dos Santos, R.A., Sinninghe Damste, J.S., Schouten, S.,

2009. Wet phases in the Sahara/Sahel region and human migration patterns in North Africa. Proceedings of the National Academy of Sciences of the United States of America 106, 20159-20163.

Chiang, J.C., Bitz, C.M., 2005. Influence of high latitude ice cover on the marine Intertropical Convergence Zone. Climate Dynamics 25, 477-496.

Chikaraishi, Y., Naraoka, H., 2007. $\delta^{13}C$ and δD relationships among three *n*-alkyl compound classes (*n*-alkanoic acid, *n*-alkane and *n*-alkanol) of terrestrial higher plants. Org. Geochem. 38, 198-215.

Collins, J.A., Schefuß, E., Heslop, D., Mulitza, S., Prange, M., Zabel, M., Tjallingii, R., Dokken, T.M., Huang, E., Mackensen, A., 2011. Interhemispheric symmetry of the tropical African rainbelt over the past 23,000 years. Nature Geoscience 4, 42-45.

Collins, J.A., Schefuß, E., Mulitza, S., Prange, M., Werner, M., Tharammal, T., Paul, A., Wefer, G., 2013. Estimating the hydrogen isotopic composition of past precipitation using leaf-waxes from western Africa. Quaternary Science Reviews 65, 88-101.

Collister, J.W., Rieley, G., Stern, B., Eglinton, G., Fry, B., 1994. Compound-specific $\delta^{13}C$ analyses of leaf lipids from plants with differing carbon dioxide metabolisms. Organic Geochemistry 21, 619-627.

Cook, B.I., Ault, T.R., Smerdon, J.E., 2015. Unprecedented 21st century drought risk in the American Southwest and Central Plains. Science Advances 1, e1400082.

Cotton, J.M., Cerling, T.E., Hoppe, K.A., Mosier, T.M., Still, C.J., 2016. Climate, CO_2, and the history of North American grasses since the Last Glacial Maximum. Science Advances 2.

Craig, H., 1961. Isotopic variations in meteoric waters. Science, 1702-1703.

Curry, B.B., Baker, R.G., 2000. Palaeohydrology, vegetation, and climate since the late Illinois Episode (~ 130 ka) in south-central Illinois. Palaeogeography, Palaeoclimatology, Palaeoecology 155, 59-81.

Dahl-Jensen, D., Albert, M., Aldahan, A., Azuma, N., Balslev-Clausen, D., Baumgartner, M., Berggren, A.-M., Bigler, M., Binder, T., Blunier, T., 2013. Eemian interglacial reconstructed from a Greenland folded ice core. Nature 493, 489-494.

Dansgaard, W., 1964. Stable isotopes in precipitation. Tellus A 16.

Delcourt, P.A., Delcourt, H.R., Brister, R.C., Lackey, L.E., 1980. Quaternary vegetation history of the

Mississippi embayment. Quaternary Research 13, 111-132.

Diefendorf, A.F., Freeman, K.H., Wing, S.L., Graham, H.V., 2011. Production of *n*-alkyl lipids in living plants and implications for the geologic past. Geochim. Cosmochim. Acta 75, 7472-7485.

Diefendorf, A.F., Freimuth, E.J., 2017. Extracting the most from terrestrial plant-derived *n*-alkyl lipids and their carbon isotopes from the sedimentary record: A review. Organic Geochemistry 103, 1-21.

Diefendorf, A.F., Mueller, K.E., Wing, S.L., Koch, P.L., Freeman, K.H., 2010. Global patterns in leaf ^{13}C discrimination and implications for studies of past and future climate. Proceedings of the National Academy of Sciences 107, 5738-5743.

Dowsett, H.J., 1999. Sediment color and reflectance record from Ocean Drilling Program Hole 625B, Gulf of Mexico (marine isotope stage 5 interval). US Dept. of the Interior, US Geological Survey.

Eglinton, G., Hamilton, R., 1963. The distribution of alkanes. Chemical plant taxonomy 187, 217.

Eglinton, G., Hamilton, R.J., 1967. Leaf epicuticular waxes. Science 156, 1322-1335.

Elsig, J., Schmitt, J., Leuenberger, D., Schneider, R., Eyer, M., Leuenberger, M., Joos, F., Fischer, H., Stocker, T.F., 2009. Stable isotope constraints on Holocene carbon cycle changes from an Antarctic ice core. Nature 461, 507-510.

Epstein, H.E., Lauenroth, W.K., Burke, I.C., Coffin, D.P., 1997. Productivity patterns of C_3 and C_4 functional types in the U.S. Great Plains. Ecology 78, 722-731.

Farquhar, G.D., Ehleringer, J.R., Hubick, K.T., 1989. Carbon isotope discrimination and photosynthesis. Annual review of plant biology 40, 503-537.

Feakins, S.J., Kirby, M.E., Cheetham, M.I., Ibarra, Y., Zimmerman, S.R., 2014. Fluctuation in leaf wax D/H ratio from a southern California lake records significant variability in isotopes in precipitation during the late Holocene. Organic Geochemistry 66, 48-59.

Feakins, S.J., Sessions, A.L., 2010. Controls on the D/H ratios of plant leaf waxes in an arid ecosystem. Geochimica et Cosmochimica Acta 74, 2128-2141.

Fredlund, G.G., Jaumann, P.J., 1987. Late Quaternary palynological and paleobotanical records from the central Great Plains. Quaternary Environments of Kansas, 167-178.

Freeman, K.H., Colarusso, L.A., 2001. Molecular and isotopic records of C_4 grassland expansion in the late Miocene. Geochimica et Cosmochimica Acta 65, 1439-1454.

Freeman, K.H., Pancost, R.D., 2014. Biomarkers for Terrestrial Plants and Climate. 395-416.

Friedli, H., Lötscher, H., Oeschger, H., Siegenthaler, U., Stauffer, B., 1986. Ice core record of the $^{13}C/^{12}C$ ratio of atmospheric CO_2 in the past two centuries. Nature 324, 237-238.

Garcin, Y., Schefuß, E., Schwab, V.F., Garreta, V., Gleixner, G., Vincens, A., Todou, G., Séné, O., Onana, J.-M., Achoundong, G., Sachse, D., 2014. Reconstructing C_3 and C_4 vegetation cover using *n*-alkane carbon isotope ratios in recent lake sediments from Cameroon, Western Central Africa. Geochimica et Cosmochimica Acta 142, 482-500.

Garel, S., Schnyder, J., Jacob, J., Dupuis, C., Boussafir, M., Le Milbeau, C., Storme, J.-Y., Iakovleva, A.I., Yans, J., Baudin, F., Fléhoc, C., Quesnel, F., 2013. Paleohydrological and paleoenvironmental changes recorded in terrestrial sediments of the Paleocene–Eocene boundary (Normandy, France). Palaeogeography, Palaeoclimatology, Palaeoecology 376, 184-199.

Gat, J.R., 1996. Oxygen and hydrogen isotopes in the hydrologic cycle. Annual Review of Earth and Planetary Sciences 24, 225-262.

Gordon, E.S., Goñi, M.A., 2003. Sources and distribution of terrigenous organic matter delivered by the Atchafalaya River to sediments in the northern Gulf of Mexico. Geochimica et Cosmochimica Acta 67, 2359-2375.

Grüger, E., 1972. Late Quaternary vegetation development in south-central Illinois. Quaternary Research 2, 217IN213-231IN214.

Hall, S.A., 1981. Deteriorated pollen grains and the interpretation of Quaternary pollen diagrams. Review of Palaeobotany and Palynology 32, 193-206.

Halpert, M.S., Ropelewski, C.F., 1992. Surface temperature patterns associated with the Southern Oscillation. Journal of Climate 5, 577-593.

Harrington, J.A., Harman, J.R., 1991. Climate and vegetation in central North America: natural patterns and human alterations. Great Plains Quarterly, 103-112.

Harrison, S.P., Kutzbach, J.E., Prentice, I.C., Behling, P.J., Sykes, M.T., 1995. The response of Northern Hemisphere extratropical climate and vegetation to orbitally induced changes in insolation during the Last Interglaciation. Quaternary Research 43, 174-184.

Harting, P., 1874. De bodem van het Eemdal. Versl. Kon. Ak. V. Wet., Afd. N, II, deel 8, 282-290.

Helfand, H.M., Schubert, S.D., 1995. Climatology of the simulated Great Plains low-level jet and its contribution to the continental moisture budget of the United States. Journal of Climate 8, 784-806.

Herbert, T.D., Yasuda, M., Burnett, C., 1995. 19. Glacial–Interglacial sea-surface temperature record inferred from Alkenone unsaturation indices, Site 893, Santa Barbara Basin, Proceedings of the Ocean Drilling Program, Scientific Results.

Hoffmann, B., Feakins, S.J., Bookhagen, B., Olen, S.M., Adhikari, D.P., Mainali, J., Sachse, D., 2016. Climatic and geomorphic drivers of plant organic matter transport in the Arun River, E Nepal. Earth and Planetary Science Letters 452, 104-114.

Hou, J., D'Andrea, W.J., Huang, Y., 2008. Can sedimentary leaf waxes record D/H ratios of continental precipitation? Field, model, and experimental assessments. Geochimica et Cosmochimica Acta 72, 3503-3517.

Hou, J., D'Andrea, W.J., MacDonald, D., Huang, Y., 2007. Hydrogen isotopic variability in leaf waxes among terrestrial and aquatic plants around Blood Pond, Massachusetts (USA). Organic Geochemistry 38, 977-984.

Huang, Y., Eglinton, G., Ineson, P., Latter, P.M., Bol, R., Harkness, D.D., 1997. Absence of carbon isotope fractionation of individual *n*-alkanes in a 23-year field decomposition experiment with Calluna vulgaris. Organic Geochemistry 26, 497-501.

Hufkens, K., Keenan, T.F., Flanagan, L.B., Scott, R.L., Bernacchi, C.J., Joo, E., Brunsell, N.A., Verfaillie, J., Richardson, A.D., 2016. Productivity of North American grasslands is increased under future climate scenarios despite rising aridity. Nature Clim. Change 6, 710-714.

IPCC, 2014. Climate Change 2014: Impacts, Adaptation, and Vulnerability. Part A: Global and Sectoral Aspects. Contribution of Working Group II to the Fifth Assessment Report of the Intergovernmental

Panel on Climate Change [Field, C.B., V.R. Barros, D.J. Dokken, K.J. Mach, M.D. Mastrandrea, T.E. Bilir, M. Chatterjee, K.L. Ebi, Y.O. Estrada, R.C. Genova, B. Girma, E.S. Kissel, A.N. Levy, S. MacCracken, P.R. Mastrandrea, and L.L. White (eds.)]. Cambridge University Press, Cambridge, United Kingdom and New York, NY, USA.

Ishiwatari, R., Ishiwatari, M., Rohrback, B.G., Kaplan, I.R., 1977. Thermal alteration experiments on organic matter from recent marine sediments in relation to petroleum genesis. Geochimica et Cosmochimica Acta 41, 815-828.

Jackson, R.B., Canadell, J., Ehleringer, J.R., Mooney, H.A., Sala, O.E., Schulze, E.D., 1996. A global analysis of root distributions for terrestrial biomes. Oecologia 108, 389-411.

Jackson, S.T., Givens, C.R., 1994. Late Wisconsinan vegetation and environment of the Tunica Hills Region, Louisiana/Mississippi. Quaternary Research 41, 316-325.

Jackson, S.T., Webb, R.S., Anderson, K.H., Overpeck, J.T., Webb Iii, T., Williams, J.W., Hansen, B.C.S., 2000. Vegetation and environment in Eastern North America during the Last Glacial Maximum. Quaternary Science Reviews 19, 489-508.

Joyce, J.E., Tjaisma, L.R., Prutzman, J.M., 1993. North American glacial meltwater history for the past 2.3 my: Oxygen isotope evidence from the Gulf of Mexico. Geology 21, 483-486.

Joyce, J.E., Tjalsma, L.R.C., Prutzman, J.M., 1990. High-resolution planktic stable isotope record and spectral analysis for the last 5.35 M.Y.: Ocean Drilling Program Site 625 northeast Gulf of Mexico. Paleoceanography 5, 507-529.

Kahmen, A., Hoffmann, B., Schefuß, E., Arndt, S.K., Cernusak, L.A., West, J.B., Sachse, D., 2013a. Leaf water deuterium enrichment shapes leaf wax *n*-alkane δD values of angiosperm plants II: Observational evidence and global implications. Geochimica et Cosmochimica Acta 111, 50-63.

Kahya, E., Dracup, J.A., 1993. US streamflow patterns in relation to the El Niño/Southern Oscillation. Water Resources Research 29, 2491-2503.

Kammerer, J.C., 1987. Largest rivers in the United States. Available from Books and Open File Report Section, USGS Box 25425, Denver, CO 80225. Water Resources Investigations Open File Report 87-

242, August 1987. 2 p, 1 fig, 1 tab, 1 ref.

Kapp, R.O., 1965. Illinoian and Sangamon vegetation in southwestern Kansas and adjacent Oklahoma.

Kapp, R.O., Gooding, A.M., 1964. Pleistocene Vegetational Studies in the Whitewater Basin, Southeastern Indiana. The Journal of Geology 72, 307-326.

King, J.E., Saunders, J.J., 1986. Geochelone in Illinois and the Illinoian-Sangamonian vegetation of the type region. Quaternary Research 25, 89-99.

Kukla, G.J., Bender, M.L., de Beaulieu, J.L., Bond, G., Broecker, W.S., Cleveringa, P., Gavin, J.E., Herbert, T.D., Imbrie, J., Jouzel, J., Keigwin, L.D., Knudsen, K.L., McManus, J.F., Merkt, J., Muhs, D.R., Müller, H., Poore, R.Z., Porter, S.C., Seret, G., Shackleton, N.J., Turner, C., Tzedakis, P.C., Winograd, I.J., 2002. Last interglacial climates. Quaternary Research 58, 2-13.

Leuenberger, M., Siegenthaler, U., Langway, C., 1992. Carbon isotope composition of atmospheric CO_2 during the last ice age from an Antarctic ice core. Nature 357, 488-490.

Leverett, F., 1898. The weathered zone (Sangamon) between the Iowan loess and Illinoian till sheet. The Journal of Geology 6, 171-181.

Limoges, A., de Vernal, A., Van Nieuwenhove, N., 2014. Long-term hydrological changes in the northeastern Gulf of Mexico (ODP-625B) during the Holocene and late Pleistocene inferred from organic-walled dinoflagellate cysts. Palaeogeography, Palaeoclimatology, Palaeoecology 414, 178-191.

Liu, W., Yang, H., Li, L., 2006. Hydrogen isotopic compositions of *n*-alkanes from terrestrial plants correlate with their ecological life forms. Oecologia 150, 330-338.

Loulergue, L., Schilt, A., Spahni, R., Masson-Delmotte, V., Blunier, T., Lemieux, B., Barnola, J.-M., Raynaud, D., Stocker, T.F., Chappellaz, J., 2008. Orbital and millennial-scale features of atmospheric CH_4 over the past 800,000 years. Nature 453, 383-386.

Magill, C.R., Ashley, G.M., Freeman, K.H., 2013. Ecosystem variability and early human habitats in eastern Africa. Proceedings of the National Academy of Sciences of the United States of America 110, 1167-1174.

Mangelsdorf, K., Güntner, U., Rullkötter, J., 2000. Climatic and oceanographic variations on the California continental margin during the last 160 kyr. Organic Geochemistry 31, 829-846.

Martinson, D.G., Pisias, N.G., Hays, J.D., Imbrie, J., Moore, T.C., Shackleton, N.J., 1987. Age dating and the orbital theory of the ice ages: Development of a high-resolution 0 to 300,000-year chronostratigraphy. Quaternary Research 27, 1-29.

Montero-Serrano, J.-C., Bout-Roumazeilles, V., Carlson, A.E., Tribovillard, N., Bory, A., Meunier, G., Sionneau, T., Flower, B.P., Martinez, P., Billy, I., Riboulleau, A., 2011. Contrasting rainfall patterns over North America during the Holocene and Last Interglacial as recorded by sediments of the northern Gulf of Mexico. Geophysical Research Letters 38, n/a-n/a.

Nürnberg, D., Ziegler, M., Karas, C., Tiedemann, R., Schmidt, M.W., 2008. Interacting Loop Current variability and Mississippi River discharge over the past 400 kyr. Earth and Planetary Science Letters 272, 278-289.

Otto-Bliesner, B.L., Rosenbloom, N., Stone, E.J., McKay, N.P., Lunt, D.J., Brady, E.C., Overpeck, J.T., 2013. How warm was the last interglacial? New model–data comparisons. Philosophical Transactions of the Royal Society of London A: Mathematical, Physical and Engineering Sciences 371, 20130097.

Pagani, M., Freeman, K.H., Arthur, M.A., 2000. Isotope analyses of molecular and total organic carbon from miocene sediments. Geochimica et Cosmochimica Acta 64, 37-49.

Pagani, M., Pedentchouk, N., Huber, M., Sluijs, A., Schouten, S., Brinkhuis, H., Sinninghe Damsté, J.S., Dickens, G.R., Expedition, S., Backman, J., Clemens, S., Cronin, T., Eynaud, F., Gattacceca, J., Jakobsson, M., Jordan, R., Kaminski, M., King, J., Koc, N., Martinez, N.C., McInroy, D., Moore Jr, T.C., O'Regan, M., Onodera, J., Pälike, H., Rea, B., Rio, D., Sakamoto, T., Smith, D.C., St John, K.E.K., Suto, I., Suzuki, N., Takahashi, K., Watanabe, M., Yamamoto, M., 2006. Arctic hydrology during global warming at the Palaeocene/Eocene thermal maximum. Nature 442, 671-675.

Petit, J.R., Jouzel, J., Raynaud, D., Barkov, N.I., Barnola, J.M., Basile, I., Bender, M., Chappellaz, J., Davis, M., Delaygue, G., Delmotte, M., Kotlyakov, V.M., Legrand, M., Lipenkov, V.Y., Lorius, C., Pepin, L., Ritz, C., Saltzman, E., Stievenard, M., 1999. Climate and atmospheric history of the past

420,000 years from the Vostok ice core, Antarctica. Nature 399, 429-436.

Piechota, T.C., Dracup, J.A., 1996. Drought and regional hydrologic variation in the United States: Associations with the El Niño-Southern Oscillation. Water Resources Research 32, 1359-1373.

Polissar, P.J., D'Andrea, W.J., 2014. Uncertainty in paleohydrologic reconstructions from molecular *δD* values. Geochimica et Cosmochimica Acta 129, 146-156.

Prentice, I.C., Bartlein, 1991. Vegetation and climate change in eastern North America since the last glacial maximum. Ecology (Durham) 72, 2038.

Rabinowitz, P.D., Merrell, W.J., Garrison, L.E., Kidd, R.B., Garrison, E., 1985. OCEAN DRILLING PROGRAM LEG 100 REPORT NORTHEASTERN GULF OF MEXICO.

Ramankutty, N., Foley, J., 2010. ISLSCP II Potential Natural Vegetation Cover. ISLSCP Initiative II Collection, Data set, edited by: Hall, FG, Collatz, G., Meeson, B., Los, S., de Colstoun, B., and Landis, D., Oak Ridge National Laboratory Distributed Active Archive Center, Oak Ridge, TN, USA, doi 10.

Rieley, G., Collier, R.J., Jones, D.M., Eglinton, G., Eakin, P.A., Fallick, A.E., 1991. Sources of sedimentary lipids deduced from stable carbon-isotope analyses of individual compounds. Nature 352, 425-427.

Rommerskirchen, F., Plader, A., Eglinton, G., Chikaraishi, Y., Rullkötter, J., 2006. Chemotaxonomic significance of distribution and stable carbon isotopic composition of long-chain alkanes and alkan-1-ols in C4 grass waxes. Organic Geochemistry 37, 1303-1332.

Ropelewski, C.F., Halpert, M.S., 1986. North American precipitation and temperature patterns associated with the El Niño/Southern Oscillation (ENSO). Monthly Weather Review 114, 2352-2362.

Royall, P.D., Delcourt, P.A., Delcourt, H.R., 1991. Late Quaternary paleoecology and paleoenvironments of the Central Mississippi Alluvial Valley. GSA Bulletin 103, 157-170.

Ruhe, R.V., Hall, R.D., Canepa, A.P., 1974. Sangamon paleosols of southwestern Indiana, U.S.A. Geoderma 12, 191-200.

Rushdi, A.I., Simoneit, B.R.T., 2002a. Hydrothermal alteration of organic matter in sediments of the

Northeastern Pacific Ocean: Part 1. Middle Valley, Juan de Fuca Ridge. Applied Geochemistry 17, 1401-1428.

Rushdi, A.I., Simoneit, B.R.T., 2002b. Hydrothermal alteration of organic matter in sediments of the Northeastern Pacific Ocean: Part 2. Escanaba Trough, Gorda Ridge. Applied Geochemistry 17, 1467-1494.

Sachse, D., Billault, I., Bowen, G.J., Chikaraishi, Y., Dawson, T.E., Feakins, S.J., Freeman, K.H., Magill, C.R., McInerney, F.A., van der Meer, M.T.J., Polissar, P., Robins, R.J., Sachs, J.P., Schmidt, H.-L., Sessions, A.L., White, J.W.C., West, J.B., Kahmen, A., 2012. Molecular paleohydrology: Interpreting the hydrogen-isotopic composition of lipid biomarkers from photosynthesizing organisms. Annu. Rev. Earth Planet. Sci. 40, 221-249.

Sachse, D., Radke, J., Gleixner, G., 2006. *δD* values of individual *n*-alkanes from terrestrial plants along a climatic gradient – Implications for the sedimentary biomarker record. Org. Geochem. 37, 469-483.

Schefusz, E., Schouten, S., Jansen, J.H.F., Sinninghe Damste, J.S., 2003. African vegetation controlled by tropical sea surface temperatures in the mid-Pleistocene period. Nature 422, 418-421.

Seki, O., Nakatsuka, T., Shibata, H., Kawamura, K., 2010. A compound-specific *n*-alkane $\delta^{13}C$ and *δD* approach for assessing source and delivery processes of terrestrial organic matter within a forested watershed in northern Japan. Geochimica et Cosmochimica Acta 74, 599-613.

Sessions, A.L., Sylva, S.P., Summons, R.E., Hayes, J.M., 2004. Isotopic exchange of carbon-bound hydrogen over geologic timescales. Geochimica et Cosmochimica Acta 68, 1545-1559.

Shackleton, N.J., 1969. The Last Interglacial in the Marine and Terrestrial Records. Proceedings of the Royal Society of London. Series B, Biological Sciences 174, 135-154.

Siegenthaler, U., Stocker, T.F., Monnin, E., Lüthi, D., Schwander, J., Stauffer, B., Raynaud, D., Barnola, J.-M., Fischer, H., Masson-Delmotte, V., 2005. Stable carbon cycle–climate relationship during the late Pleistocene. Science 310, 1313-1317.

Smith, F.A., Freeman, K.H., 2006. Influence of physiology and climate on *δD* of leaf wax n-alkanes from C3 and C4 grasses. Geochimica et Cosmochimica Acta 70, 1172-1187.

Smith, H.J., Fischer, H., Wahlen, M., Mastroianni, D., Deck, B., 1999. Dual modes of the carbon cycle since the Last Glacial Maximum. Nature 400, 248.

Still, C.J., Berry, J.A., Collatz, G.J., DeFries, R.S., 2003. Global distribution of C3 and C4 vegetation: Carbon cycle implications. Global biogeochemical cycles 17, 6-1.

Suh Y.J., Diefendorf A.F., 2017. Seasonal and canopy height variation in *n*-alkanes and their carbon isotopes in a temperate forest. *Accepted*, Organic Geochemistry

Swinehart, J.B., 1999. 200,000 years of climate change recorded in eolian sediments of the High Plains of eastern Colorado and western Nebraska. Colorado and Adjacent Areas 1, 71.

Tierney, J.E., Russell, J.M., Huang, Y., Damsté, J.S.S., Hopmans, E.C., Cohen, A.S., 2008. Northern hemisphere controls on tropical southeast African climate during the past 60,000 years. Science 322, 252-255.

Tipple, B.J., Meyers, S.R., Pagani, M., 2010. Carbon isotope ratio of Cenozoic CO2: A comparative evaluation of available geochemical proxies. Paleoceanography 25.

Tipple, B.J., Pagani, M., 2010. A 35Myr North American leaf-wax compound-specific carbon and hydrogen isotope record: Implications for C4 grasslands and hydrologic cycle dynamics. Earth and Planetary Science Letters 299, 250-262.

Uno, K.T., Polissar, P.J., Kahle, E., Feibel, C., Harmand, S., Roche, H., 2016. A Pleistocene palaeovegetation record from plant wax biomarkers from the Nachukui Formation, West Turkana, Kenya. Phil. Trans. R. Soc. B 371, 20150235.

Velichko, A., Borisova, O., Svetlitskaya, T., 1995. The climate of the ice-free Earth (quantitative reconstructions for the Eocene optimum). Izvestiya Akademii Nauk SSSR, Geographical Series 1, 31-42.

Velichko, A.A., Borisova, O.K., Zelikson, E.M., 2008. Paradoxes of the Last Interglacial climate: reconstruction of the northern Eurasia climate based on palaeofloristic data. Boreas 37, 1-19.

Vogts, A., Moossen, H., Rommerskirchen, F., Rullkötter, J., 2009. Distribution patterns and stable carbon isotopic composition of alkanes and alkan-1-ols from plant waxes of African rain forest and savanna

C_3 species. Org. Geochem. 40, 1037-1054.

Vogts, A., Schefuß, E., Badewien, T., Rullkötter, J., 2012. n-Alkane parameters from a deep sea sediment transect off southwest Africa reflect continental vegetation and climate conditions. Organic Geochemistry 47, 109-119.

Waelbroeck, C., Paul, A., Kucera, M., Rosell-Melé, A., Weinelt, M., Schneider, R., Mix, A.C., Abelmann, A., Armand, L., Bard, E., 2009. Constraints on the magnitude and patterns of ocean cooling at the Last Glacial Maximum. Nature Geoscience 2, 127.

Walker, G.T., Bliss, E., 1932. World weather. V. Mem. Roy. Meteor. Soc. 4, 53-84.

Watts, W.A., 1970. The Full-Glacial Vegetation of Northwestern Georgia. Ecology 51, 17-33.

Whitehead, D.R., 1973. Late-Wisconsin vegetational changes in unglaciated Eastern North America. Quaternary Research 3, 621-631.

Zhu, H., Baker, R.G., 1995. Vegetation and climate of the last glacial-interglacial cycle in southern Illinois, USA. J Paleolimnol 14, 337-354.

Ziegler, M., Nürnberg, D., Karas, C., Tiedemann, R., Lourens, L.J., 2008. Persistent summer expansion of the Atlantic Warm Pool during glacial abrupt cold events. Nature Geoscience 1, 601-605.

Chapter 5: Conclusions

One powerful way to understand carbon and water cycle changes in the past is to utilize terrestrial plant biomarkers and their carbon and hydrogen isotopes preserved in geologic sediments. However, accurate interpretation of this proxy is limited by poor knowledge about forest-level *n*-alkane $\delta^{13}C$ ($\delta^{13}C_{alk}$) variations as well as basin-level integration processes that affect the resulting sedimentary leaf wax records. In this dissertation, I specifically improved understanding of temporal and canopy variation in $\delta^{13}C_{alk}$ values within a temperate forest and controls on leaf wax integration from a catchment with dynamic climate and vegetation to marine sediments via fluvial systems. Then I utilized some of the knowledge gained from these studies to resolve paleovegetation and paleohydrologic questions about the Mississippi River Basin during the last 150 kyr. I have specifically made contributions towards understanding: (1) timing and magnitude of variations in *n*-alkane production and carbon isotope fractionation during lipid biosynthesis ($\varepsilon_{alk\text{-}leaf}$) over the growing season and across the canopy, (2) how runoff, net primary productivity (NPP), distance from the source, and wax production control leaf wax integration and transport from the Mississippi River Basin (MRB) to the Gulf of Mexico (GOM), and (3) changes in precipitation source and distribution in the MRB over the last 150 kyr and their effects on terrestrial vegetation composition. Below, I present conclusions drawn from this dissertation.

First, carbon isotope fractionation during photosynthesis ($\varepsilon_{leaf\text{-}CO2}$) and $\delta^{13}C_{alk}$ values changed as buds developed into fully mature leaves. These changes most likely reflect a shift in the source of carbon from stored reserves to recently photosynthesized carbon. $\delta^{13}C_{alk}$ values stabilized in the mature leaf stage when specific leaf area also stabilized and average chain length started to increase. This suggests that $\delta^{13}C_{leaf}$ and $\delta^{13}C_{alk}$ values reflect environment and plant physiologic conditions during leaf development, but that these values remain largely consistent once the leaf has matured. Across the canopy, $\varepsilon_{alk\text{-}leaf}$ values did not vary in relation to height. However, we observed large changes in the concentration of leaf waxes within the canopy. The uppermost canopy leaves had up to 8 times higher *n*-alkane concentrations than

observed in the lower canopy. We speculate that leaves have higher *n*-alkane concentrations in the uppermost canopy in response to high light intensity, to limit water loss in the most photosynthetically active leaves, and possibly due to decreased leaf damage. This has important implications for interpreting leaf wax isotopic compositions in sedimentary deposits. Given that the upper canopy has higher biomass and *n*-alkane concentrations, the *n*-alkanes of leaf litter are likely biased towards upper canopy leaves.

Second, based on linear mixing models, we found that runoff, NPP, distance and wax production controls leaf wax integration and transport from the MRB catchment to GOM sediments. Leaf wax export was higher from southeastern forested regions because runoff, NPP, proximity and wax production were generally higher than the grasslands, at least for *n*-C_{29} and *n*-C_{31} alkanes. *n*-C_{33} alkanes integrated C_4 grassland-derived leaf waxes better than *n*-C_{29} and *n*-C_{31} alkanes due to higher production of *n*-C_{33} alkanes in C_4 grasses. We compared the modeled values to measured values in GOM sediments. Models that combine leaf wax biomass and runoff predicted values similar to measured values, confirming that the combination of runoff, productivity and distance may influence leaf wax integration into marine sediments. I also found that vegetation effects on ε_{app} values are reduced not only due to the canceling of low ε_{app} values by leaf water D-enrichment, but also to integration bias towards C_3 angiosperm trees in the southeastern MRB. I therefore conclude that runoff, productivity (i.e. NPP and wax production) and distance should be taken into account when interpreting leaf wax isotope records in sedimentary records with high fluvial influence.

Third, during the MIS 5e when average global temperature was warmer than present, we observed an increase in precipitation in southeastern forestlands compared to the Holocene. This spatial variation in precipitation was most likely due to northward migration of mid-latitude Polar Front position. As summer insolation increased and global temperature rose during the MIS 5e, this expanded Atlantic Warm Pool in the tropics, and migrated Intertropical Convergence zone northward, bringing warm Caribbean Seawater into the GOM, transporting warm and humid moisture into the continent. At high latitudes, as ice sheets

retreated, southward migration of Arctic airmasses diminished bringing less precipitation to the MRB. During the MIS 5d and 5c, we observed drier-than-the-Holocene conditions. The results of this study provide important insights into how global or regional temperature increase may influence atmospheric circulation, which determine the extent of air mass contribution and distribution in North America, and consequently terrestrial vegetation and hydrology.

Collectively, this dissertation improves interpretation and application of leaf wax isotopic compositions in geologic sediments by resolving uncertainties that are critical for deriving accurate ecological and hydrologic information using this proxy. My results will help fill the gap between modern and geologic leaf waxes by understanding the processes from production to transportation and burial. Improving such proxies is essential for understanding the evolution of Earth's climate system and assessing current and future global changes, as well as global carbon and water cycling from primary production to geologic preservation.